UNIVERSITY OF CALIFORNIA SAN DIEGO

Superenhancer-activation of KLHDC8A Drives Glioma Ciliation and Hedgehog Signaling

A Dissertation submitted in partial satisfaction of the requirements
for the degree Doctor of Philosophy

in

Biomedical Sciences

by

Derrick Lee

Committee in charge:

Professor David Cheresh, Chair
Professor Jeremy Rich, Co-Chair
Professor Hannah Carter
Professor Frank Furnari
Professor Christopher Glass
Professor Tannishtha Reya

2022

The Dissertation of Derrick Lee is approved, and it is acceptable in quality and form for publication on microfilm and electronically.

University of California San Diego

2022

DEDICATION

To:

My mother, Hui-Chen Chiu, my father, Bernard Wai-Shing Lee, and my sister, En-Tsai Lee, who's support, encouragement, and sacrifice have allowed me to be who I am.

To my girlfriend, Xue Wang, who's love and smiles led me through the darkness.

TABLE OF CONTENTS

LIST OF FIGURES

LIST OF TABLES

LIST OF ABBREVIATIONS

TMZ	Temozolomide
TTF	Tumor treating field
TERT	Telomerase reverse transcriptase
IDH	Isocitrate dehydrogenase
ecDNA	Extrachromosomal DNA
α-KG	α-ketoglutarate
2-HG	R-2-hydroxyglutarate
TET2	Tet methylcytosine dioxygenase 2
G-CIMP	Glioma CpG Island Methylation phenotype
GSC	Glioblastoma stem cells
H3K9me3	Histone 3 lysine 9 trimethylation
ChIP	Chromatin immunoprecipitation
m6A	N^6-methyladenosine
YTHDF2	YTH domain-containing family protein 2
A-to-I	Adenosine-to-inosine
PI3K	PhosphoInositol-3 kinase
CSC	Cancer stem cell
PDGF	Platelet-derived growth factor
METTL3	Methyltransferase-like 3
OPTN	Modification of optineurin
DGC	Differentiated glioma cell
BDNFB	Brain-derived neurotrophic factor

HIF	Hypoxia-induced factor
VEGFA	Vascular endothelial growth factor A
OPC	Oligodendrocyte precursor cells
KLHDC8A	Kelch domain containing 8A
CCT	Chaperonin containing tailless complex polypeptide 1
CDC	Ciliary dissociation complex
PDAC	Pancreatic ductal adenocarcinoma
BCC	Basal cell Carcinomas
INTU	Inturned
PL4	Polo-like kinase 4
HH	Hedgehog
PTCH	Patched
SMO	Smoothened
SUFU	Suppressor of fuse
GLI	Glioma-associated oncogene
SHH	Sonic Hedgehog
IHH	Indian Hedgehog
DHH	Desert Hedgehog
GPCRs	G-protein-coupled receptors
H3K27ac	Histone 3 lysine 27 acetylation
TCGA	The Cancer Genome Atlas
CGGA	Chinese Glioma Genome Atlas
ELDA	Extreme limiting dilution assay

PARP1	poly(ADP-ribose)polymerase-1
NSC	Neural stem cell
NPC	Neural progenitor cell
NM	Nonmalignant neural cell
DEPMAP	The Cancer Dependency Map
BRD4	Bromodomain Containing 4
RNA-seq	RNA sequencing
GSEA	Gene set enrichment analysis
ssGSEA	Single-sample gene set enrichment analysis
Ac-tubulin	Acetylated-α-tubulin
BioGRID	Biological General Repository for Interaction Datasets
CTRP	The Cancer Therapeutics Response Portal
CCLE	Cancer Cell Line Encyclopedia
AUC	Area under curve
IGF1R	Insulin-like growth factor 1 receptor
BBSome	Bardet-Biedl syndrome protein complex
αTAT1	α-tubulin acetyltransferase
RIPA	Radio-Immunoprecipitation assay
BCA	Bicinchoninic acid
PVDF	Polyvinylidene difluoride
HOMER	Hypergeometric Optimization of Motif EnRichment
GEO	Gene expression Omnibus
NSG	NOD.Cg-*Prkdc*^{scid} *Il2rg*^{tm1Wjl}/SzJ

SSET	Serial section electron tomography
BET	Bromo- and extra-terminal domain

ACKNOWLEDGMENTS

I would like to thank my thesis advisor Jeremy Rich for allowing me to join his group and work alongside so many incredible lab members, as well as for providing extremely valuable input and suggestions. He granted me the freedom to explore my own ideas and guided me in the process of my Ph.D. both scientifically and intellectually. I have grown and learned so much over the years and become an independent researcher because of his exceptional guidance.

I would like to thank my thesis committee members, Drs David Cheresh, Tannishtha Reya, Hannah Carter, Christopher Glass, and Frank Furnari, for all their guidance and support. I have presented both of my projects to them during our thesis meetings. Both projects were difficult, and I always felt challenged in every meeting. However, their instruction and guidance were invaluable to getting me to this point.

I also want to recognize the tremendous contributions from former and current lab members for providing technical support, scientific discussion, constructive criticism, and friendship. Many of us hang out every week and have become good friends. My Ph.D. life was never boring and tedious with you guys being with me. I hope we will meet again somewhere in the future.

I would like to thank my family, my parents, and my sister, for supporting me in pursuing a Ph.D. degree abroad. We have not gathered together for almost three years due to the COVID situation, and I can't wait to visit you all in Taiwan after graduation. Thank you for all the support, sacrifices, and commitment you made toward my growth. I could have never achieved my goals and become who I am without you.

Special thanks to my best friend, Juan Hernandez. I still remember the first time we talked during the recruitment weekend back in 2017. We became best friends after school started. We

have been through the hardest times together. You were always there to listen to my complaints when I was depressed. I am truly glad to have a friend like you.

Lastly, I would like to thank my girlfriend, Xue Wang. Moving to Pittsburgh and having a long distance relationship wasn't what I expected, but we still managed to see each other routinely even when we were 2,500 miles away. I couldn't have finished my project on time and survived in Pittsburgh without your encouragement and support. You have given me a reason to look forward to every day.

Chapter 3 contains data of the material that has been submitted for publication as it may appear in the Journal of Clinical Investigation, 2022; Derrick Lee, Ryan C. Gimple, Xujia Wu, Briana C. Prager, Zhixin Qiu, Qiulian Wu, Vikas Daggubati, Aruljothi Mariappan, Jay Gopalakrishnan, Matthew R. Sarkisian, David R. Raleigh, Jeremy N. Rich. The dissertation author was the primary researcher and author of this paper. This work was supported by National Institutes of Health: Derrick Lee, CA243296; Briana C. Prager, CA217066; Ryan C. Gimple, CA217065; David R. Raleigh, HD106238, CA251221, CA262311; Jeremy N. Rich, P30 CA047904, CA238662, CA197718, NS103434.

Chapter 4 contains data of the material that has been submitted for publication as it may appear in the Journal of Clinical Investigation, 2022; Derrick Lee, Ryan C. Gimple, Xujia Wu, Briana C. Prager, Zhixin Qiu, Qiulian Wu, Vikas Daggubati, Aruljothi Mariappan, Jay Gopalakrishnan, Matthew R. Sarkisian, David R. Raleigh, Jeremy N. Rich. The dissertation author was the primary researcher and author of this paper. This work was supported by National Institutes of Health: Derrick Lee, CA243296; Briana C. Prager, CA217066; Ryan C. Gimple, CA217065; David R. Raleigh, HD106238, CA251221, CA262311; Jeremy N. Rich, P30 CA047904, CA238662, CA197718, NS103434.

Chapter 5 contains unpublished materials that may or may not appear in future publications. The dissertation author solely completed all the work presented in chapter 5. This work was supported by National Institutes of Health: Derrick Lee, CA243296; Briana C. Prager, CA217066; Ryan C. Gimple, CA217065; David R. Raleigh, HD106238, CA251221, CA262311; Jeremy N. Rich, P30 CA047904, CA238662, CA197718, NS103434.

VITA

Education

2022 Doctor of Philosophy, Biomedical Sciences, University of California San Diego

2014 Master of Science, Biochemical Science and Technology, National Taiwan University

2012 Bachelor of Science, Biochemical Science and Technology, National Taiwan University

Publications

Lee D, Gimple RC, Prager BC, Qiu Z, Wu Q, Daggubati V, Gopalakrishnan J, Raleigh DR, Rich JN. Superenhancer-activation of KLHDC8A Drives Glioma Ciliation and Hedgehog Signaling. J Clin Invest. Under revision.

Lv D, Gimple RC, Zhong C, Wu Q, Yang K, Prager BC, Godugu B, Qiu Z, Zhao L, Zhang G, Dixit D, **Lee D**, Shen JZ, Li X, Xie Q, Wang X, Agnihotri S, Rich JN. PDGF signaling inhibits mitophagy in glioblastoma stem cells through N6-methyladenosine. Dev Cell. 2022 Jun 20;57(12):1466-1481.e6.

Dixit D, Prager BC, Gimple RC, Miller TE, Wu Q, Yomtoubian S, Kidwell RL, Lv D, Zhao L, Qiu Z, Zhang G, **Lee D**, Park DE, Wechsler-Reya RJ, Wang X, Bao S, Rich JN. Glioblastoma stem cells reprogram chromatin in vivo to generate selective therapeutic dependencies on DPY30 and phosphodiesterases. Sci Transl Med. 2022 Jan 5;14(626):eabf3917.

Prager BC, Vasudevan HN, Dixit D, Bernatchez JA, Wu Q, Wallace LC, Bhargava S, **Lee D**, King BH, Morton AR, Gimple RC, Pekmezci M, Zhu Z, Siqueira-Neto JL, Wang X, Xie Q, Chen C, Barnett GH, Vogelbaum MA, Mack SC, Chavez L, Perry A, Raleigh DR, Rich JN. The Meningioma Enhancer Landscape Delineates Novel Subgroups and Drives Druggable Dependencies. Cancer Discov. 2020 Nov;10(11):1722-1741.

Tang M, Xie Q, Gimple RC, Zhong Z, Tam T, Tian J, Kidwell RL, Wu Q, Prager BC, Qiu Z, Yu A, Zhu Z, Mesci P, Jing H, Schimelman J, Wang P, **Lee D**, Lorenzini MH, Dixit D, Zhao L, Bhargava S, Miller TE, Wan X, Tang J, Sun B, Cravatt BF, Muotri AR, Chen S, Rich JN. Three-dimensional bioprinted glioblastoma microenvironments model cellular dependencies and immune interactions. Cell Res. 2020 Oct;30(10):833-853.

Gimple RC, Kidwell RL, Kim LJY, Sun T, Gromovsky AD, Wu Q, Wolf M, Lv D, Bhargava S, Jiang L, Prager BC, Wang X, Ye Q, Zhu Z, Zhang G, Dong Z, Zhao L, **Lee D**, Bi J, Sloan AE, Mischel PS, Brown JM, Cang H, Huan T, Mack SC, Xie Q, Rich JN. Glioma Stem Cell-Specific Superenhancer Promotes Polyunsaturated Fatty-Acid Synthesis to Support EGFR Signaling. Cancer Discov. 2019 Sep;9(9):1248-1267.

Awards and Honors

Outstanding teaching award, National Taiwan University, August 2014

Ruth L. Kirschstein Individual Predoctoral NRSA Recipient, NCI, July 2018

ABSTRACT OF THE DISSERTATION

Superenhancer-activation of KLHDC8A Drives Glioma Ciliation and Hedgehog Signaling

by

Derrick Lee

Doctor of Philosophy in Biomedical Sciences
University of California San Diego, 2022
Professor David Cheresh, Chair
Professor Jeremy Rich, Co-Chair

Glioblastoma ranks among the most aggressive and lethal of all human cancers. Self-renewing, highly tumorigenic glioblastoma stem cells (GSCs) contribute to therapeutic resistance and maintain cellular heterogeneity. Here, we interrogated superenhancer landscapes of primary glioblastoma specimens and patient-derived GSCs, revealing a kelch domain-containing gene (KLHDC8A) with a previously unknown function as an epigenetically-driven oncogene. Targeting

KLHDC8A decreased GSC proliferation and self-renewal, induced apoptosis, and impaired in vivo tumor growth. Transcription factor control circuitry analyses revealed that the master transcriptional regulator SOX2 stimulated KLHDC8A expression. Mechanistically, KLHDC8A bound Chaperonin-Containing TCP1 (CCT) to promote assembly of primary cilia to activate Hedgehog signaling. KLHDC8A expression correlated with Aurora B/C Kinase inhibitor activity, which induced primary cilia and Hedgehog signaling. Combinatorial targeting of Aurora B/C Kinase and Hedgehog displayed augmented benefit against GSC proliferation. Collectively, superenhancer-based discovery revealed KLHDC8A as a novel molecular target of cancer stem cells that promotes ciliogenesis to activate the Hedgehog pathway, offering insights into therapeutic vulnerabilities for glioblastoma treatment.

Chapter 1

Introduction of glioblastoma and glioblastoma stem cells (GSCs)

CHAPTER 1

1.1 Glioblastoma overview and genetic alterations

Glioblastoma is the most common and aggressive primary brain tumor and one of the most lethal cancers among all human cancers, accounting for 80% of intrinsic malignant tumors in the central nervous system (1). It is estimated that around 250,000 people worldwide are diagnosed with glioblastoma annually, and 13,000 Americans are expected to receive a glioblastoma diagnosis in 2022. Standard-of-care includes maximal surgical resection followed by radiation and/or chemoradiation with the oral methylator, temozolomide (TMZ), and adjuvant TMZ (2). Additional FDA-approved treatments, such as TTF (Tumor Treating Fields, Optune®) (3) and angiogenesis inhibitors, bevacizumab (Avastin®) (4, 5), have offered only modest benefits. The median survival rate of glioblastoma patients is less than 15 months, and the 5-year survival rate remains below 5% despite all the available treatment modalities (6). The most frequently mutated gene locus in glioblastoma is the promoter region of telomerase reverse transcriptase (TERT), which is found in >70% of cases of Isocitrate dehydrogenase (IDH) wild-type glioblastoma. The most common mutation sites on the TERT promoter are C228T and C250T, which lead to upregulation of TERT expression, telomere lengthening, and infinite proliferation of tumor cells (7). EGFR amplification is another common genetic alteration in glioblastoma. It is estimated that approximately 60% of glioblastomas harbor an EGFR amplification. In addition to wild-type EGFR amplification, the EGFRVIII variant, which results from in-frame deletion of exons 2-7, is found in approximately 25% of IDH wide-type glioblastoma and in 50% of glioblastoma patients with EGFR amplification. EGFRVIII loses the ability to bind ligands and is constitutively active. Given the high prevalence of EGFR amplifications and mutations, two therapeutic approaches, including monoclonal antibodies and small molecule inhibitors against EGFR or EGFRVIII, have

been developed. However, both approaches have failed to demonstrate clinical efficacy in clinical trials of patients with glioblastoma. The aneuploidy of chromosomes 7 and 10 is the most common chromosome alteration in around 80% of glioblastoma patients (8, 9). Chromosome 7 amplification and chromosome 10 deletion lead to EGFR amplification and PTEN loss in primary glioblastoma. Chromothripsis, characterized by massive chromosome shattering and chromosomal rearrangements, is observed in more than 50% of glioblastoma patients and contributes to the amplification of oncogenes and inactivation of tumor suppressors (10). The amplification of oncogenes also results from the presence of extrachromosomal DNA (ecDNA) in the cells (11). These ecDNAs often carry multiple copies of oncogenes, such as MYC, EGFR, and MET, and are also able to propagate and be maintained in daughter tumor cells and patient-derived xenografts (11, 12). Another striking and common genetic alteration that distinguishes glioblastoma and low-grade gliomas from other cancer types is IDH mutations (13). IDH1 and 2 are essential enzymes that catalyze the conversion of isocitrate to α-ketoglutarate (α-KG) in the tricarboxylic acid (TCA) cycle, and neomorphic mutations in IDH1 (R132) or IDH2 (R172) result in neo-function of catalyzing α-ketoglutarate (α-KG) into R-2-hydroxyglutarate (2-HG), which is a potent inhibitor of α-ketoglutarate-dependent dioxygenase, including tet methylcytosine dioxygenase 2 (TET2) and histone demethylases (14). Inhibition of α-KG-dependent dioxygenases induces epigenetic modifications, such as DNA hypermethylation and increased histone tail methylation, and promotes tumor growth (14). However, IDH-mutant glioblastoma is clinically and genetically distinct and is associated with better prognosis compared to IDH-wild-type glioblastoma. Although many genetic alterations are glioblastoma-specific, genetic mutations in common oncogenes (PIK3CA, PIK3R1, and PTPRD) and tumor suppressors (RB1, TP53, and NF1) also contribute to the progression and malignancy of glioblastoma (14).

1.2 Epigenetic alterations in glioblastoma

Although cancer has traditionally been viewed as a disease process based exclusively on genetic aberrations, increasing evidence has demonstrated that epigenetic alterations contribute to the pathogenesis and progression of many types of cancer. Epigenetics is the study of how cells control gene expression through mechanisms, such as DNA modifications, histone modifications, and RNA modifications, without affecting the DNA sequence. As we mentioned earlier, IDH mutations are found in a subset of glioblastoma patients, associated with a widespread DNA hypermethylation that defines the Glioma CpG Island Methylation phenotype (G-CIMP) and is associated with better prognosis compared to IDH wild-type glioblastoma (15).

In addition to the canonical DNA methylation at the Cytosine C5, N6-methyladenine (N^6-mA) DNA modifications, which were originally thought to exist only in bacteria (16) and a limited number of eukaryotes (17, 18), but not in mammals, has been demonstrated to occur in embryonic stem cells (19) and glioblastoma, specifically in glioblastoma stem cells (GSCs) (20). N^6-mA DNA modification is preferentially upregulated in GSCs and primary glioblastoma cultures compared to astrocytes and is enriched in heterochromatin regions marked by histone 3 lysine 9 trimethylation (H3K9me3), where tumor suppressor genes such as CDKN3, RASSF2, and AKAP6 are located. Further investigation demonstrated that DNA demethylase ALKBH1 regulates the dynamics of N6-mA DNA modification and is critical for GSC maintenance (20). Alterations in histone modifications, for example Histone 3 lysine 27 acetylation, which marks active enhancer regions, have been found in multiple brain cancers, such as ependymoma and meningioma. H3K27ac chromatin immunoprecipitation (ChIP) combined with deep sequencing on patient-derived ependymoma and meningioma tumor cells has identified superenhancer-associated genes that define tumor states and transcriptional networks. Targeting superenhancer-associated genes

impaired tumor proliferation (21, 22), suggesting that interrogation of superehanacers will help us understand glioblastoma biology and uncover targetable therapeutic vulnerabilities. Dixit et al. identified the histone 3 lysine 4 trimethylation regulator DPY30, which promotes angiogenesis and hypoxia pathways in intracranial glioblastoma xenografts, as a therapeutic dependency in vivo (23).

N^6-methyladenosine (m6A) mRNA modification, regulated by RNA methyltransferases METTL3 and METTL14 and demethylases ALKBH5 and FTO, is commonly dysregulated in glioblastoma. For example, YTH domain-containing family protein 2 (YTHDF2), an m6A reader, promotes GSC growth and angiogenesis by interacting and stabilizing MYC and VEGF mRNA transcripts (24). Zhang et al. demonstrated that GSCs preferentially upregulated m6A RNA demethylase ALKBH5 to support GSC proliferation by demethylating FOXM1 transcripts. Moreover, alterations of m6A RNA modifications in glioblastoma by overexpression of METTL3 and METTL14 or inhibition of FTO led to the loss of stemness and downregulation of genes essential for glioblastoma propagation (25). Another RNA modification, adenosine-to-inosine (A-to-I) RNA editing, also has implications in glioblastoma biology. Upregulation of ADAR1, an adenosine deaminase, is observed in GSCs compared to neural stem cells. Targeting ADAR1 expression using Tyk2 inhibitors led to downregulation of ADAR1, ganglioside metabolism, and impaired cell proliferation and in vivo tumor initiation capacity.

Aberrant expression and activation of chromatin remodelers and transcriptional machinery also drive glioblastoma cell growth through altering the epigenetic landscape and gene expression. Qiu et al. demonstrated that the master transcription factor YY1 is preferentially upregulated in GSCs compared to differentiated glioma cells and neural stem cells. YY1 interacts with the

transcription elongation complex and regulates m6A RNA modification through upregulation of METTL3 and YTHDF2 expression (26).

1.3 Intratumoral heterogeneity

Glioblastoma can be classified into three molecular subtypes—proneural, mesenchymal, and classical—based on their unique transcriptional profiles. The three molecular subtypes are defined by aberrant expressions of EGFR (Classical), NF1 (Mesenchymal), and PDGFRA/TP53/IDH1 (Proneural) and are associated with distinct patient prognosis and responses to standard treatments (27). The Mesenchymal subtype is associated with highly angiogenic, invasive, and aggressive phenotypes and is correlated with poor patient prognosis compared to Classical and Proneural subtypes. Each tumor subtype preferentially localizes to different regions of the brain, with Mesenchymal subtype tumors localizing to hypoxic, necrotic, and microvascular proliferation areas, and Classical subtype tumors to vascular and invasive regions (28). Therefore, genomic studies using a single regional biopsy from a patient may fail to comprehensively capture the spatial heterogeneity of glioblastoma. Furthermore, recent technological advances, including scRNA-seq, reveal high intratumoral heterogeneity with the presence of multiple subtypes and "hybrid" subtypes that express two molecular modules within a tumor (29). Intratumor heterogeneity promotes therapeutic resistance, as the possibility of having resistant clones increases, and this eventually leads to inevitable recurrence. Reinartz et al. demonstrate that multiple molecular subclones coexist within a single tumor, with each subclone having distinct genetic identities and different drug-response profiles (30). This observation is further supported by another study by Szerlip et al. that dual pharmacological inhibition of EGFR and PDGFR, which are heterogeneously amplified in different glioblastoma cell populations, completely abrogated the activation of downstream PhosphoInositol-3 kinase (PI3K) and cell growth when compared to inhibition of EGFR or PDGFR alone (31), suggesting that the development of combinatorial therapies targeting multiple molecular subclones is needed in order to eliminate

multiple subtypes and achieve prolonged patient survival. Using a single cell-derived clonal analysis, Meyer et al. show that TMZ-resistant clones already preexist in untreated glioblastoma tissues, which may explain the failure of conventional therapy (32). Ravi et al. utilized a spatially resolved multi-omics approach, including transcriptomics, metabolomics, and proteomics, to decipher the intra- and intertumoral heterogeneity, which are shaped by the bidirectional interactions between tumor cells and the microenvironment, such as hypoxia and immune cells. In addition to intratumoral heterogeneity, subtype conversions often occur during recurrence due to changes in tumor microenvironments and responses to therapeutic intervention. Alterations in environmental conditions, for example, metabolic changes and immune stress, promote bidirectional transition of glioblastoma subtypes, showing the dynamic adaption and plasticity of glioblastoma tissues in response to environmental cues (33). Additionally, subtype conversions from proneural to mesenchymal subtypes were observed in recurrence tumors induced by radiotherapy in a TNFα /NFκB-driven manner. Higher expression of Mesenchymal signatures, including the cancer stem cell marker CD44 and genes downstream of NFκB, are correlated with poor patient prognosis and radioresistance (34).

1.4 Glioblastoma stem cells (GSCs)

As one of the most lethal human cancers, the current therapy options for glioblastoma are only palliative. One of the major contributions to intratumoral heterogeneity, therapeutic resistance, and poor prognosis is the presence of glioblastoma stem cells (GSCs) within the tumor. GSCs have been demonstrated to promote therapeutic resistance to chemotherapy or radiotherapy by activating DNA damage checkpoints and supporting angiogenesis, invasion, and recurrence following treatment therapy. The current cancer stem cell (CSC) hypothesis describes the cellular hierarchies and cell-state plasticity that govern tumor cell growth, maintenance, recurrence, and resistance to current therapies. GSCs are at the apex of the cellular developmental hierarchy and contribute to primary tumor formation and reconstitution of entire tumors after treatment therapy by giving rise to a more differentiated progeny. Although the functional importance of GSCs has been well-characterized in glioblastoma, these models have been questioned by the lack of unifying GSC markers or isolation methods. Several cell surface markers, including CD133, CD44, and CD15, have been used to isolate and enrich GSC populations from glioblastoma tissues. Additionally, sustained self-renewal, sphere formation, and anchorage-independent growth are key characteristics of GSCs. Therefore, neurosphere formation assay, in which cells are cultured in non-adherent and serum-free conditions, is another method to isolate GSCs from primary glioblastoma tissues. However, no single markers or isolation methods can comprehensively capture the heterogeneity of GSCs and model the interaction between GSCs and other non-neoplastic cells, including endothelial cells, immune cells, and differentiated glioma cells.

Despite the controversies regarding GSC models in the field, GSCs have been functionally defined in our system or by other groups by their abilities of persistent cell proliferation, sustained self-renewal, and tumor initiation *in vivo*. *In vivo* studies support the current hypothesis of the

existence of GSCs, which express stemness molecules and form orthotopic xenograft or serial xenograft when intracranially injected into mouse brains. Furthermore, the states of GSCs are not static. Molecular profiling of the glioblastoma tissues using scRNA-seq (SMART-seq2) identified intra- and inter-tumoral heterogeneity and the plasticity of GSCs. GSCs can be defined as one of four main cellular states—Astrocytic like-cells, Oligodendrocytic precursor like-cells, Mesenchymal like-cells, and Neural progenitor like-cells—based on their distinct genetic perturbations, with relatively rarer populations of GSCs expressing two molecular modules classified into "hybrid" states (35). Each subtype is able to initiate tumors in mice, indicating the *in vivo* tumor capacity of these cells. Moreover, the tumors derived from each subtype possess the four main states similar to their original tumors, demonstrating the plasticity of GSCs (35). Along with this study, another report revealed that GSC states can be described in a single proneural-mesenchymal axis, and targeting two GSC phenotypes simultaneously using FDA-approved drugs synergistically inhibits tumor growth compared to targeting only one GSC phenotype (36). Using single-cell ATAC-seq, Guilhamon et al. identified three GSC states—Reactive, Constructive, and Invasive—which are defined by their unique expression of essential transcription factors and signatures. For example, the Reactive state of GSCs relies on transcription factor SP1 and TERT expressions, and the Constructive state of GSCs is dependent on the expression of OLIG2—a known stemness marker—AHR, and ASCL1. Therefore, targeting the molecular dependencies in all three subtypes using combinatorial treatment strategies may be required to completely eliminate GSCs in tumors (37). Garofano et al. proposed a new classification using a pathway-based approach and classified GSCs into four stable cellular states—Mitochondrial, Glycolytic/lurimetabolic, Neuronal, and Proliferative/progenitor—with each subtype associated with different metabolic states, clinical outcomes, and sensitivity to different pathway inhibitors

(38). Leveraging a novel genetically engineered mouse model, Schmitt et al. observed a dynamic interconversion between Proneural and Mesenchymal states. Contrary to other studies that Proneural and Mesenchymal subtypes are two distinct cell identities, Schmitt et al. argued that the Proneural state is an entity driven by cell-intrinsic mechanisms, and the Mesenchymal state is driven by microenvironmental, genetic, and pharmacologic insults (39). While these studies provided insight into the heterogeneity, plasticity, and classification of GSCs, the questions regarding which systems are the best to capture all the molecular and clinical features of GSCs and whether this knowledge can be translated into clinical practice still remain to be answered.

GSCs are dependent on core stem cell pathways shared by non-neoplastic stem cells, including Notch, Wnt, and Sonic hedgehog pathways, to promote stemness, proliferation, and suppressed apoptosis. GSCs additionally utilize other oncogenic signalings that cooperate with stem cell pathways, essential transcription factors, and extracellular signals to promote self-renewal, survival, therapeutic resistance, plasticity, and adaptability to different microenvironments. For example, Notch signaling is highly expressed in GSCs, and the Notch ligand is expressed in the surrounding vessels (40), which enhances the stemness phenotype, cell growth, invasiveness (41), dormancy escape, and therapeutic resistance of GSCs (42). Furthermore, Notch signaling induces the transdifferentiation of GSCs to vascular lineages, such as endothelial cells and pericytes, to support neo-angiogenesis. Inhibition of Notch signaling using gamma-secretase inhibitor or Notch1 silencing suppressed GSC growth and angiogenesis (43). Wnt-β-Catenin signaling is another core stem signaling pathway that has been implicated in GSC biology and promotes self-renewal (44), angiogenesis (45), invasion (46), epithelial to mesenchymal transition, migration, and invasion through the interaction between β-Catenin and cadherin and through the crosstalk with EGFR signaling (47). Overexpression of EGFR mutants or the

constitutively active form of EGFR, EGFRVIII, promotes multiple aspects of GSC biology, including proliferation, invasiveness, survival, and resistance to therapies, through alteration of epigenome (48) and metabolic states (49). Lv et al. demonstrated that Platelet-derived growth factor (PDGF) signaling activation promoted the upregulation of methyltransferase-like 3 (METTL3) and the subsequent N6-methyladenosine (m6A) modification of optineurin (OPTN), which resulted in suppressed mitophagy and enhanced GSC proliferation. Treating GSCs with METTL3 inhibitor in combination with PDGFR or mitophagy inhibitor synergized to kill GSCs, serving as a new therapeutic approach to target GSCs (50). Other signaling pathways, such as Sonic Hedgehog (51) and TGF-β (52), also support GSC tumorigenicity.

1.5 GSCs and the tumor microenvironment

Glioblastomas are a complex tumor ecosystem, which is composed of malignant and non-malignant cells, including GSCs, differentiated glioma cells (DGC), endothelial cells, astrocytes, immune cells, and other cells. The interaction between GSCs and other cell types via interconnected microtubules in the tumor microenvironment provide essential cues that promote plasticity, proliferation, and radioresistance of GSCs (53). Our lab has demonstrated that the bidirectional interaction between GSCs and DGCs promotes GSC growth via brain-derived neurotrophic factor (BDNF)-NTRK2 paracrine signaling (54). Astrocytes have been recently demonstrated to be involved in regulating the cell states of glioblastoma cells. Single glioblastoma cells without any connection to other cell types showed increased cell invasion. After cell invasion, glioblastoma cell connection to astrocytes induced subtype transition from OPC/NPC to MES via interconnected microtubules (55). Astrocytes support GSC growth via supplementation with essential nutrients, such as glutamine (56) and cholesterol (57), and via providing pro-invasive and pro-proliferative signals (58). Oxygen limitation, also known as hypoxia, is a key hallmark of glioblastoma. To overcome tumor hypoxia, GSCs preferentially upregulate Hypoxia-induced factors 1α and 2α (HIF1α and HIF2α) to promote stemness, angiogenesis (59), and autophagy (60) as well as to survive in a nutrient-deficient environment. Furthermore, GSCs secrete pro-angiogenic factor Vascular endothelial growth factor A (VEGFA) (61) or directly differentiate into endothelial cells (62) and pericytes (63) to support angiogenesis and supply oxygen and nutrients.

1.6 Cell-of-origin

It is noteworthy that the term "glioblastoma stem cells" does not imply or describe the cell-of-origin. GSCs could derive from normal stem cells residing in the brain through acquiring genetic mutations promoting proliferation, migration, and invasion. On the other hand, it is possible that more differentiated neoplastic cells accumulate genetic perturbations that promote stem-like properties and malignant transformation of these cells. The astrocyte-like neural stem cells (NPCs) in the subventricular zone frequently harbor driver mutations in glioblastoma tissues and acquire the ability to migrate to distinct regions in the brain and initiate tumor formation (64). These observations support the cancer stem cell hypothesis that a small population of normal stem cells in the subventricular zone acquires genetic mutations that promote the tumorigenicity of these cells and eventually give rise to GSCs. On the other hand, genomic deletion of p53 and NF1 in mice or overexpression of the active forms of Ras and AKT in NSC-derived astrocytes is sufficient to induce malignant brain cancer (65, 66). Others contend that oligodendrocyte precursor cells (OPCs) are the cell of origin for GSCs. Introducing oncogenic mutations to OPCs consistently gives rise to glioblastoma, but not in NPCs or other NPC-derived lineages. Stem-like populations enriched with radial glia-like signatures contribute to the invasiveness of GSCs and the heterogeneity of GSCs and more differentiated progeny within the tumor (67). Therefore, GSCs could arise from either NSCs, OPCs, or more differentiated progeny that have acquired mutations promoting stem-like properties and uncontrolled proliferation.

Chapter 2

Introduction of KLHDC8A, primary cilia, and Hedgehog signaling

CHAPTER 2

2.1 Kelch domain containing 8A (KLHDC8A)

KLHDC8A is a 350-amino acid protein that belongs to the kelch repeat superfamily. The kelch repeat superfamily members function through binding to their unique interaction partners and regulate many cellular processes, including signal transduction (68), transcription (69), DNA repair (70), and protein homeostasis (71). KLHDC8A consists of 7 tandem kelch repeats, which form a beta-propeller tertiary structure known to mediate protein-protein interactions. Current understanding of the physiological and pathological functions of KLHDC8A remains unclear. KLHDC8A was first identified in glioblastoma cells that escaped from the treatment of EGFR inhibitors. Escaped tumor cells lost the expression of EGFRVIII, a constitutively active form of EGFR. However, several downstream effectors of EGFR signaling, including AKT, ERK, and p38 MAPK remain active even in the absence of EGFRVIII. Moreover, targeting KLHDC8A in escaper cells inhibited the *in vivo* tumor formation capacity of tumor cells, suggesting that KLHDC8A may orchestrate alternative compensatory pathways to maintain aggressiveness in the event of EGFRVIII silencing (72). Xiaolong Zhu et al. reported that KLHDC8A promotes glioblastoma cell proliferation, migration, and invasion by mediating the expression of apoptosis, cell cycle, and migration-related proteins and activating common oncogenic pathways. Lactate and glucose promote the expression of KLHDC8A in a concentration-dependent manner. However, the detailed mechanisms of how KLHDC8A promotes glioblastoma cell growth remain an area of investigation (73). Based on the protein structure of KLHDC8A, it is likely to mediate protein-protein interactions and act as an activator, inhibitor, or adaptor protein. From the analysis of a biomedical interaction repository named BioGRID, KLHDC8A interacts with the catalytic subunit of Protein phosphatase 2 and all the subunits of Chaperonin containing tailless complex

polypeptide 1 (CCT), suggesting that KLHDC8A may regulate the activity and function of Protein phosphatase 2 and may be involved in facilitating its protein folding through interacting with CCT. While KLHDC8A is predicted to be a cytoplasmic protein, nuclear localization signals were found in its sequence, suggesting that KLHDC8A may be able to shuttle between the nucleus and cytoplasm. In the next chapter, we will discuss the upstream regulatory mechanisms and downstream molecular functions of KLHDC8A.

2.2 Primary cilia

A primary cilium is a non-motile microtubule-based cell surface protrusion that extends from a microtubule-organizing center called the basal body, which is derived from the mother centriole and provides an anchor for the main structure called an axoneme. The axoneme of primary cilia consists of a ring of 9 microtubule doublets and anchors to the basal body (74). The microtubule doublets of the axoneme consist of an A-tubule and B-tubule (75), which both consist of an assembly of alpha- and beta-tubulin heterodimers. The microtubules within primary cilia are long-lived and stable compared to the highly dynamic microtubules in the cytoplasm. Several tubulin post-translational modifications, including acetylation, polyglutamylation, and detyrosination, contribute to the stability of microtubules and primary cilia structure (76). Most human cells display one primary cilium per cell except hematopoietic cells, which are devoid of this structure, and olfactory receptor cells, which possess around 10-30 cilia. Primary cilia are key signaling hubs for numerous extracellular signaling pathways, such as Hedgehog, GPCR, and WNT signaling, and function as the cellular antennas that sense the optical, chemical, and mechanical signals from the environment in cell-type specific and context-dependent manners (77). The embedding of these transmembrane receptors allows primary cilia to react to signals derived from other cells or tissue microenvironments. The well-known receptor localized on primary cilia is the receptor of Hedgehog, Wnt, PDGF, and Notch signaling. Hedgehog signaling is the most characterized signaling on primary cilia and is essential for embryonic development and stem cell maintenance. Cilia ablation via deleting IFT88 and KIF3, which are both critical in ciliogenesis, resulted in the downregulation of Hedgehog signaling and reduced proliferation of ciliated basal cell carcinomas (78). Several Wnt signaling components have been found in primary cilia, including β-catenin and glycogen synthase kinase-3β, Frizzled3, and Dischevelled2.

Genomic knockout of KIF3 led to reduced β-catenin activity and inactivation of the Wnt pathway in mouse fibroblasts and mouse embryonic stem cells (79). Primary cilia have been tightly linked to cell cycle phases. The assembly, disassembly, and length of primary cilia are tightly controlled by kinases and proteins in a cell cycle-dependent manner. Primary cilia are found in the G0 (quiescent) or G1 (proliferating) phases of the cell cycle. In proliferating cells, primary cilia extend away from a cell during the post-mitotic G1 phase and remain present in the S/G2 phases. Upon entry into the late G2 phase, cilia disassembly occurs. The basal body, which is derived from the mother centriole, needs to be released from primary cilia to form the centrosome and mitotic spindle before mitosis (74). Given that primary cilia play an essential role in transducing signals from extracellular environments, defects in primary cilia formation lead to a group of disorders generally called ciliopathies.

2.3 Primary cilia in cancers

The role of primary cilia in cancers is still under investigation. The loss of primary cilia in neoplastic cells was observed in a variety of cancer types, including pancreatic, renal, breast, prostate, and melanoma cancers (77, 80). Genetic mutations in ciliary-associated genes or upregulation of the ciliary dissociation complex (CDC) contribute to the loss of primary cilia. Given that primary cilia are only present in G1, S, and early G2 phases, it remains unclear whether the low frequencies of ciliated cells are due to the rapid proliferation of tumor cells or if only a subset of populations within tumors are able to form primary cilia. In another study, primary cilia were found in approximately 25% of tumor cells from patients with pancreatic ductal adenocarcinoma (PDAC) and were associated with a higher rate of metastasis and poor patient prognosis (81). Further investigation on PDAC and breast cancer cells demonstrated that primary cilia-positive cells expressed high levels of Ki67, a proliferation marker, suggesting that the presence of primary cilia was not affected by cell cycle progression and the rate of proliferation (82, 83). In thyroid cancer, genetic disruption of essential cilia components ablated primary cilia formation and induced mitochondrial-dependent apoptosis (84). Ciliogenesis has also been linked to cell cycle-regulators, such as Aurora kinase A, a serine/threonine kinase that regulates G2/M progression. The activation of Aurora kinase A triggers reabsorption of primary cilia to ensure proper cell cycle progression. Chefetz et al. demonstrated that the localization of Aurora kinase A on the centrosome was associated with the downregulation of primary cilia formation and decreased Hedgehog signaling activation in epithelial ovarian cancer stem cells (85). Elevated Aurora kinase A expression driven by beta-catenin activation drives cilia disassembly in renal cancers (86). Wong et al. revealed that in basal cell carcinomas (BCC), a large proportion of patient-derived BCC cells display primary cilia. Depleting the essential components of primary

cilia resulted in two opposite results in SHH-dependent tumors. In tumors that are driven by overactivation of SMO, ablation of primary cilia led to suppressed cell proliferation, while the proliferation rate was significantly increased in the tumors induced by overactivation of Gli2, suggesting that primary cilia have dual and opposite roles in SHH-dependent BCC in a context-dependent manner (78). Yang et al. further described the detailed mechanisms of elevated ciliogenesis in BCC. The higher frequency of ciliated cells, increased proliferation, and activation of hedgehog signaling were caused by elevated expression of Inturned (INTU), an essential effector which promotes intraflagellar transport within primary cilia and downstream hedgehog pathway activation (87). In melanoma, cilliogenesis is associated with the early stages of disease and is inhibited in more advanced and metastatic melanomas (88). The downregulation of primary cilia during melanoma development was driven by elevated expression of polo-like kinase 4 (PL4) (89), a centriole duplication regulator, and the methyltransferase EZH2, which inhibited the transcription of ciliary genes (90). Taking all this evidence together, primary cilia may promote or suppress tumorigenesis in a context-dependent manner. Future studies are still required to decipher the roles of primary cilia in cancers.

2.4 Primary cilia in brain cancers

Almost all normal human cells, including cells in the brain, are ciliated. Primary cilia play a pivotal role in maintaining the stem and progenitor populations in the brain by organizing and activating the extracellular signaling pathways that promote stem-like proliferation (91, 92), suggesting that primary cilia may potentially promote the growth of glioblastoma cells, especially GSCs. Therefore, the first compelling question for understanding the role of primary cilia in glioblastoma is to ask the percentage of all glioblastoma cells that are ciliated. Sarkisian et al. have examined the frequency of ciliated cells in 20 glioblastoma tissues and revealed that approximately 1~25% of cells in primary tissues display primary cilia (93). No cilia or extremely low percentages of ciliated cells were observed in commonly used glioblastoma cell lines, including U87MG, U251MG, and U373MG (94). However, the DNA profiles of these cell lines are different from their original tumors, and the origins of these cell lines are unknown. On the other hand, 10~30% of glioblastoma cells derived from patient-derived xenografts display cilia with normal ciliary ultrastructure (93, 95). In stem-like populations, Goranci-Buzhala et al. demonstrated that approximately 20% of OPC-like GSCs are ciliated, while MES-like, AC-like, and NPC-like GSCs display a lower frequency of ciliated cells. Inhibition of NEK2 promotes ciliogenesis in OPC-like GSCs and triggers the differentiation of GSCs (96). However, NEK2 is a known cell cycle kinase, which promotes cell cycle G2/M transition. It is possible that inhibition of NEK2 triggered cell cycle arrest at the G2 phase, in which primary cilia are still present, and that the differentiation of GSCs was solely driven by NEK2 inhibition and was independent of ciliogenesis. It remains unclear which cell types have primary cilia and if primary cilia promotes or suppresses tumorigenesis in glioblastoma.

In medulloblastoma, primary cilia have dual and opposite roles in promoting tumorigenesis. Inhibition of ciliogenesis suppressed tumors driven by a constitutively active SMO or promoted tumors expressing constitutively active Gli2, suggesting that the role of primary cilia in medulloblastoma is determined by the initiating oncogenic events (97). Furthermore, primary cilia are abundant in Wnt- and Sonic hedgehog-dependent medulloblastoma but are absent in other molecular group subtypes. Disruption of ciliogenesis in Wnt-dependent medulloblastoma led to the inactivation of Wnt-driven downstream signaling pathways and subsequent reduced cell proliferation (98).

2.5 Primary cilia and therapeutic resistance

Primary cilia have been linked to enhanced therapeutic resistance in multiple cancers, including glioblastoma. Depletion of PCM1 or KIF3A in glioblastoma cells suppressed primary cilia formation and induced resistance to TMZ (95). On the other hand, Tumor Treating Fields, Optune®, treatment suppressed cillogenesis in glioblastoma cells and enhanced TMZ-induced cell death (99). Moreover, inhibition of ciliogenesis via IFT88 knockdown or treatment with chloral hydrate led to impaired autophagy and DNA damage repair and sensitized glioblastoma cells to TMZ and irradiation (100).

In other cancer types, primary cilia promote therapeutic resistance to multiple kinase inhibitors, including Hedgehog, EGFR, and MEK inhibitors as well as chemotherapy agents, with increased cilia frequency and length associated with higher levels of resistance (101). Aurora kinase A inhibition restored primary cilia formation in the stem-like populations of ependymoma and sensitized cancer cells to Hedgehog pathway inhibitors (102). The loss of primary cilia rendered medulloblastoma cells resistant to Hedgehog pathway inhibitors and led to a persister state (103).

2.6 Hedgehog signaling overview

The Hedgehog signaling pathway is an evolutionarily conserved pathway that was first discovered in *Drosophila melanogaster* (D. melanogaster) in 1980 (104). Hedgehog signaling plays a critical role in embryonic development and adult tissue maintenance, including stem cell differentiation, maintenance, and proliferation (105). Dysregulation of Hedgehog signaling often leads to a number of birth defects and the transformation of normal cells to neoplastic cells. The main components of Hedgehog signaling are comprised of Hedgehog proteins (HH), the Hedgehog receptors Patched (PTCH), Smoothened (SMO), and suppressor of fuse (SUFU); and the downstream transcription factor glioma-associated oncogene (GLI). Three mammalian Hedgehog proteins—Sonic Hedgehog (SHH), Indian Hedgehog (IHH), and Desert Hedgehog (DHH)—have been identified. The functions of these three Hedgehog proteins are similar in their physiological effect but differ in their roles in embryonic development due to differential and spatial expression. PTCH is the transmembrane receptor that binds to Hedgehog proteins, with Patched1 (PTCH1) expressed in mesenchymal cells and Patched2 (PTCH2) expressed in squamous cells, basal cells, melanocytes, and gonad cells. Both PTCH receptors have been shown to interact with all three Hedgehog proteins. In the absence of Hedgehog proteins, PTCHs act as repressors that bind to SMO and prevent SMO from activating Gli proteins. SMO is another transmembrane protein structurally similar to the G-protein-coupled receptors (GPCRs). SMO is sequestered from primary cilia when it binds to PTCH but is constitutively active and acts as a activator of the Hedgehog pathway upon the binding of hedgehog proteins to PTCH. The downstream transcription factor Gli was first identified in glioblastoma because of its elevated expression and gene amplification in glioblastoma tissues. Three mammalian Gli proteins have been identified, with Gli1 and Gli2 being transcriptional activators in response to Hedgehog signals and Gli3 acting as a transcriptional

repressor. In the absence of Hedgehog proteins, PTCH binds to SMO, which prevents SMO from accumulating in primary cilia. In the cytoplasm, the SUFU interacts with GLI proteins and prevents them from translocating to the nucleus. When Hedgehog proteins bind to PTCH, PTCH loses the ability to interact with SMO. SMO translocates to primary cilia and triggers the dissociation of SUFU and Gli. Gli proteins are then activated and enter the nucleus, where they drive the expression of genes that mediate embryonic development or promote cancer stem cell maintenance. Several Hedgehog pathway genes have been identified and play important roles in the cell cycle (CCND1, CCND2 and CCNE1), apoptosis (BCL2), oncogene expression (MYCN and FOXM1), and angiogenesis (VEGFA).

In addition to the canonical hedgehog signaling, which is mediated by the SHH-PTCH-SMO axis and is typically found in normal cells and ciliated tumor cells, recent studies have shown that Hedgehog signaling is abnormally activated in several types of cancer through PTCH- and SMO-independent mechanisms. These non-canonical mechanisms are involved in alteration of Gli protein expression or activity through other signaling pathways, including RAS-RAF-MEK-ERK, PI3K-AKT-mTOR, TGF-β, and AMPK signaling.

2.7 Hedgehog signaling in cancers

Given the pivotal roles of Hedgehog signaling in embryonic development and stem cell maintenance, it is not surprising that abnormal activation of the Hedgehog pathway promotes tumorigenesis of cancer cells, especially cancer stem cells. Dysregulation of Hedgehog signaling has been observed in both solid and liquid cancers, such as medulloblastoma, glioma, breast, basal cell carcinoma, pancreatic, ovarian, and leukemia (106-109). For instance, misregulation of Hedgehog signaling, such as that caused by inactivating mutations in PTCH1 and activating mutations in SMO, which account for 85% and 10% of BCCs, drives tumorigenesis and shapes the tumor microenvironment (110). In addition to tumor cells, the massive secretion of Hedgehog proteins from malignant tumors dampens the antitumor properties of T cells through upregulation of IL4, the key Th2 cytokine (111). Inhibition of hedgehog signaling by overexpression of the repressor form of Gli2 increased T cell activation and promoted the proliferation of mature T cells (112). Medulloblastoma, an aggressive malignant brain tumor predominantly present in children, is another cancer type that exhibits abnormal activation of hedgehog signaling. It is estimated that over one-third of Medulloblastoma cases are caused by mutations of hedgehog components similar to BCC (113). PTCH1 inactivating mutations, SMO activating mutations, and SUFU loss-of-function mutations account for 45%, 14%, and 14% of the total cases, respectively (114). Aberrant Hedgehog pathway activation is also reported to promote the stemness of cancer stem cells, enhance chemoresistance, and cause the recurrence of myeloid and other types of leukemia (115-117).

2.8 Clinical and therapeutic implications

The Hedgehog pathway has been studied extensively, and this knowledge has been translated into the development of Hedgehog pathway inhibitors. These inhibitors were designed to target several components of the Hedgehog pathway, including Hedgehog proteins, SMO, and Gli1. Most current efforts are focused on the development of SMO inhibitors, including Cyclopamine, Saridegib, Sonidegib, Glasdegib, and Vismodegib (118). Cyclopamine belongs to the family of natural steroidal alkaloids and was the first SMO antagonist developed for targeting Hedgehog signaling. Cyclopamine has very high affinity and is currently under investigation for Hedgehog-driven cancers. It has shown pre-clinical efficacy in inhibiting tumor growth and extending the life span of mice bearing xenograft tumors. However, its low solubility, poor pharmacokinetics, and severe side effects, including weight loss and mortality, hinder its potential in clinical use (119). Among other SMO inhibitors, Vismodegib and Sonidegib have been approved by the FDA for the use of treating basal cell carcinoma, medulloblastoma, and leukemia (119). Vismodegib is the first compound approved for the treatment of basal cell carcinoma. However, it displayed low clinical efficacy and several side effects, such as fatigue, hypocalcemia, and atrial fibrillation, in phase II trials (120). Sonidegib is the most successful FDA-approved drug in the treatment of basal cell carcinoma and medulloblastoma, with fewer side effects, better pharmacokinetics, and greater therapeutic efficacy compared to Vismodegib (121). Although Sonidegib has greater potential in treating tumors driven by the activation of SMO, mutations in the drug-binding pockets of SMO, which abolish the binding of Sonidegib and Vismodegib, lead to enhanced resistance of tumors to these inhibitors (122). Therefore, other strategies for targeting Hedgehog signaling are under investigation. Several Gli1 inhibitors, such as GANT-56, GANT-61, and arsenic trioxide, have been developed, and they inhibit Gli1 transcriptional activity by

interfering its DNA binding ability (123), serving as an alternative approach for targeting SMO-mutant canonical hedgehog signaling or noncanonical hedgehog signaling. Furthermore, BET inhibitors have been demonstrated to inhibit the expression of Gli and its downstream target genes and suppress the tumor proliferation of medulloblastoma and basal cell carcinoma (124). However, some patients develop therapeutic resistance to these inhibitors, which eventually leads to recurrence. Future studies are required to uncover new mechanisms and drug targets.

Chapter 3

Superenhancer screen identified a GSC vulnerability

CHAPTER 3

Superenhancer-activation of KLHDC8A Drives Glioma Ciliation and Hedgehog Signaling

Derrick Lee[1,2,3], Ryan C. Gimple[3,4], Xujia Wu[1,2], Briana C. Prager[3,5], Zhixin Qiu[1-3], Qiulian Wu[1-3], Vikas Daggubati[6,7], Aruljothi Mariappan[8], Jay Gopalakrishnan[8], Matthew R. Sarkisian[9,10], David R. Raleigh[6,7,*,#], Jeremy N. Rich[1,3,11,*,#]

1. UPMC Hillman Cancer Center, Pittsburgh, PA, USA.
2. Department of Medicine, University of Pittsburgh, Pittsburgh, PA, USA.
3. Division of Regenerative Medicine, Department of Medicine, University of California, San Diego, La Jolla, CA, USA.
4. Department of Pathology, Care Western Reserve University, Cleveland, OH, USA.
5. Cleveland Clinic Lerner College of Medicine, Cleveland, OH, USA.
6. Department of Radiation Oncology, University of California, San Francisco, USA.
7. Department of Neurological Surgery, University of California San Francisco, San Francisco, CA, USA.
8. Institute of Human Genetics, University Hospital Düsseldorf, Heinrich-Heine-Universität, Universitätsstr. 1, 40225 Düsseldorf, Germany.
9. Department of Neuroscience, McKnight Brain Institute, University of Florida, Gainesville, FL, USA
10. Preston A. Wells, Jr. Center for Brain Tumor Therapy, University of Florida, Gainesville, FL, USA
11. Department of Neurology, University of Pittsburgh, Pittsburgh, PA, USA.

*, These authors contributed equally.

#, Correspondence:

Jeremy N. Rich: Mailing address: 5150 Centre Avenue, UPMC Cancer Pavilion, Room 549, Pittsburgh, PA, 15232; Telephone: 412-623-3364; Email: drjeremyrich@gmail.com

David R. Raleigh: Mailing address: 505 Parnassus Ave, San Francisco, CA 94143

Phone: 415-353-7175; Email: david.raleigh@ucsf.edu

Keywords: glioblastoma, glioblastoma stem cell, cancer stem cell, KLHDC8A, Hedgehog, Sonic Hedgehog, Primary cilia, Aurora kinase, superenhancer

Conflict-of-interest statement: The authors have declared that no conflict of interest exists.

ABSTRACT

Glioblastoma ranks among the most aggressive and lethal of all human cancers. Self-renewing, highly tumorigenic glioblastoma stem cells (GSCs) contribute to therapeutic resistance and maintain cellular heterogeneity. Here, we interrogated superenhancer landscapes of primary glioblastoma specimens and patient-derived GSCs, revealing a kelch domain-containing gene (KLHDC8A) with a previously unknown function as an epigenetically-driven oncogene. Targeting KLHDC8A decreased GSC proliferation and self-renewal, induced apoptosis, and impaired in vivo tumor growth. Transcription factor control circuitry analyses revealed that the master transcriptional regulator SOX2 stimulated KLHDC8A expression. Mechanistically, KLHDC8A bound Chaperonin-Containing TCP1 (CCT) to promote assembly of primary cilia to activate Hedgehog signaling. KLHDC8A expression correlated with Aurora B/C Kinase inhibitor activity, which induced primary cilia and Hedgehog signaling. Combinatorial targeting of Aurora B/C Kinase and Hedgehog displayed augmented benefit against GSC proliferation. Collectively, superenhancer-based discovery revealed KLHDC8A as a novel molecular target of cancer stem cells that promotes ciliogenesis to activate the Hedgehog pathway, offering insights into therapeutic vulnerabilities for glioblastoma treatment.

INTRODUCTION

Glioblastoma is the most prevalent primary intrinsic brain tumor in adults, with a median survival of 12-15 months (1, 9). Standard-of-care treatment includes maximal surgical resection followed by chemoradiation with the oral methylator, temozolomide (TMZ), and adjuvant temozolomide, which marginally improve patient survival (2). While glioblastoma has undergone extensive molecular characterization and classification into subtypes based on transcriptional profiles (15, 29, 35), translation of this knowledge to clinical practice is limited. Self-renewing, highly tumorigenic, and stem-like population of cancer cells, called glioblastoma stem cells (GSCs), contribute to therapeutic resistance and poor prognosis (125, 126). While the cell-of-origin and universal identification markers specific for GSCs remain controversial, GSCs have been reliably demonstrated in glioblastoma to promote tumor angiogenesis, brain invasion, and immune evasion (127-129), highlighting the potential benefit in targeting GSCs.

Glioblastomas and other cancers have traditionally been viewed as a set of diseases that are driven by the accumulation of genetic aberrations. However, treatments focused on genetic drivers, at least in glioblastoma, have been ineffective or only partially effective, suggesting that other effective routes for targeting glioblastoma should be considered. More recently, an increasing body of evidence has emerged that epigenetic abnormalities, in concert with genetic alterations, drive cancer initiation and progression (130). Altered expression of epigenetic and chromatin regulators are linked to malignant phenotypes of glioblastoma (131). Superenhancers are clusters of putative enhancers in close proximity, with strong enrichment for the binding of master transcriptional factors and mediator coactivators, which drive high expression of genes that define cell state and control cell identity (132). We previously demonstrated that targeting ependymoma superenhancer-associated genes impaired the proliferation of patient-derived

neurospheres in vitro and in vivo (21), suggesting that interrogation of superenhancers and their associated genes can provide insights into drug discovery and the mechanisms of disease pathogenesis.

Extracellular signaling is a crucial determinant of cancer cell proliferation, migration, and invasion. Signals derived from the tumor microenvironment are critical for cancer stem cell maintenance (133). Core stem cell pathways, such as WNT, NOTCH, and Sonic hedgehog, promote stemness and inhibit apoptosis of cancer stem cells (134). The Hedgehog pathway, which is mediated by primary cilia in a context-dependent manner, is commonly dysregulated in medulloblastoma and gliomas (135). The inhibitors of Hedgehog pathway have demonstrated clinical efficacy in the treatment of basal cell carcinoma and are under active investigation for other cancer types (136-138). However, resistance to Hedgehog inhibitors has been reported (139, 140). In addition to genetic mutations in Patched 1 (PTCH1), Smoothened (SMO), or other Hedgehog signaling components, which drive the constitutive activation of Hedgehog pathway (114, 141, 142), epigenetic dysregulation also leads to aberrant Hedgehog activation, and inhibition of epigenetic regulatory protein BRD4 downregulates Hedgehog pathway genes and inhibits the growth of Hedgehog-driven tumors resistant to Smoothened antagonists (143). Considering the functional importance of superenhancers and core stem cell pathways, we hypothesized that interrogation of glioblastoma-specific superenhancers and their associated genes by utilizing superenhancer profiling would uncover GSC biology and reveal critical dependencies in GSC.

RESULTS

Identification of epigenetically upregulated genes in GSCs

To identify GSC-specific epigenetic vulnerabilities, we performed unbiased in silico screening to identify superenhancer-associated genes specifically present in glioblastoma surgical specimens and patient-derived GSCs (Figure 3.1A). We profiled 11 glioblastoma surgical resection specimens for superenhancer loci through histone 3 lysine 27 acetylation chromatin immunoprecipitation followed by sequencing (H3K27ac ChIP-seq) datasets (48, 144). To identify glioblastoma superenhancer-associated genes, we prioritized superenhancers present in all 11 glioblastoma tissues, yielding 2,620 genes regulated by glioblastoma superenhancers. Superenhancer-associated genes across 11 glioblastoma tissues included EGFR, POUF3, SOX2, and AVIL, which were each previously shown to contribute to glioblastoma tumorigenesis (Figure 3.S1A). Next, we interrogated GSC H3K27ac ChIP-seq datasets (145) and identified the superenhancer loci and genes shared by >70% of GSCs, which we hypothesized may represent key factors controlling GSC identity or tumorigenesis. We focused on the superenhancer-associated genes that were shared by glioblastoma tissues and GSCs to identify stem-specific features with in vivo relevance. 252 superenhancer-associated genes (Figure 3.1B) were enriched for pathways involved in neural development, cell motility, cell cycle, and structure morphogenesis (Figure 3.1C and Figure 3.S1B). The selected GSC superenhancers were enriched for transcriptional motifs, including NR4A2, SMAD3, and ETV4, which have been previously reported to promote glioblastoma malignancy (146-148) (Figure 3.1D). The majority of superenhancers were located in the promoters and distal intergenic and intron regions (Figure 3.S1C). Higher expression of superenhancer-associated genes informed poor prognosis of

glioblastoma patients in The Cancer Genome Atlas (TCGA) and Chinese Glioma Genome Atlas (CGGA) datasets (Figure 3.S1D).

To prioritize the 252 superenhancer-associated genes for further investigation, we took a three-stage approach: 1) genes with elevated expression in glioblastoma tissues from TCGA datasets compared to normal brain specimens from GTex datasets (Figure 3.1E); 2) genes for which high expression was associated with poor patient prognosis (Figure 3.1F); and 3) mRNA expression of 13 genes meeting these criteria was compared across 3 GSC models and matched serum-differentiated glioma cells (DGCs). Among all the candidate genes, KLHDC8A was the only gene displaying elevated expression levels in GSCs compared to DGCs (Figure 3.1G). Collectively, this superenhancer-identification approach strongly indicated KLHDC8A as a lead candidate for further investigation.

KLHDC8A promotes GSC growth and maintenance

To interrogate the functional importance of KLHDC8A in GSCs, KLHDC8A was targeted by shRNA-mediated knockdown in patient-derived GSCs and matched DGCs using two non-overlapping shRNAs targeting KLHDC8A compared with a non-targeting control shRNA sequence that did not match any sequence in the mammalian genome. Inhibition of KLHDC8A expression impaired proliferation in GSCs, whereas targeting KLHDC8A marginally reduced the proliferation of DGCs (Figure 3.2, A-D). Extreme limiting dilution assay (ELDA) is a surrogate of self-renewal capacity, which is one of the defining characteristics of a stem cell. Upon downregulation of KLHDC8A, stem-cell frequency and self-renewal capacity were diminished in two patient-derived GSCs (Figure 3.2, E and F). GSCs transduced with KLHDC8A shRNAs

showed increased apoptotic cell death, as measured by Annexin V apoptotic assay and cleavage of poly(ADP-ribose)polymerase-1 (PARP1) (Figure 3.2, G-I). To determine the specific role of KLHDC8A in glioblastoma, we interrogated the functional importance of KLHDC8A in several non-neoplastic neural cells, including neural stem or progenitor cells (NSCs or NPCs) and nonmalignant neural cells (NMs) derived from epilepsy surgical resection specimens. Depletion of KLHDC8A impaired the proliferation of NSCs but had minimal effect on the proliferation of nonmalignant brain cultures, indicating a potential role of KLHDC8A in regulating stemness of GSCs and NSCs Figure 3.2, A and B). As expected, KLHDC8A knockdown decreased the expression of GSC markers, OLIG2 and SOX2, in GSCs (Figure 3.2J). To understand the role of KLHDC8A across cell types and tissues, we interrogated The Cancer Dependency Map (Depmap) portal (www.depmap.org), which contains whole-genome CRISPR-knockout screen data across 558 cell lines. KLHDC8A was not a pan-essential gene in a panel of cancer types (Figure 3.S2C), which underscores the potential value of targeting KLHDC8A in glioblastoma. In sum, KLHDC8A plays a critical role in GSC proliferation, maintenance, and survival.

Transcriptional regulation of KLHDC8A in GSCs

To define the epigenetic regulation of KLHDC8A, we interrogated the chromatin landscape of KLHDC8A in a cohort of patient-derived GSCs, three matched DGCs, and three nonmalignant (NM) neural cell lines, which revealed strong enrichment of active chromatin regions in close proximity to KLHDC8A gene promoter region in GSCs (Figure 3.S2D). In accordance with strong H3K27ac signals within the superenhancer region, GSCs displayed elevated mRNA and protein expression of KLHDC8A compared to DGCs (Figure 3.3, A and B). Differentiation of GSCs was validated by downregulation of stemness transcription factors, SOX2

and OLIG2, and upregulation of the differentiation marker, GFAP (Figure 3.S3, A-C). Next, we leveraged available GSC H3K27ac, SOX2, and OLIG2 ChIP-seq data (149) and identified two master stem cell regulators, SOX2 and OLIG2, as potential drivers of KLHDC8A expression. OLIG2 and SOX2 displayed increased binding within 500 bp of the KLHDC8A superenhancer in GSCs (Figure 3.3C), suggesting that binding of these transcription factors at this superenhancer locus may drive the expression of KLHDC8A. Furthermore, KLHDC8A expression positively correlated with the expression of SOX2 and OLIG2 in glioblastoma patients from TCGA and CGGA databases (Figure 3.3D and Figure 3.S3D). Knockdown of SOX2 with two non-overlapping shRNAs decreased mRNA expression of KLHDC8A (Figure 3.3E and Figure 3.S3, E and F). In single-cell RNA-seq data from 28 glioblastoma patients, KLHDC8A was preferentially expressed in neuronal and neoplastic populations, and KLHDC8A expression overlapped with SOX2+ glioblastoma cells (Figure 3.S3, G and H). The expression of superenhancer-associated genes is mediated by the binding of transcriptional coactivators, prominently BRD4 (Bromodomain Containing 4). Inhibition of BRD4 leads to selective loss of the expression of superenhancer-driven genes (150). To validate that the expression of KLHDC8A was driven by a superenhancer, we treated GSCs with JQ1, which preferentially inhibits BRD4, in two GSC lines and observed downregulation of KLHDC8A mRNA expression in a concentration-dependent manner (Figure 3.3F). To interrogate the functional role of the predicted superenhancer locus in regulating KLHDC8A expression, we utilized a CRISPR-dCas9-KRAB system, a targetable repressive epigenetic factor that induces histone methylation and deacetylation (151), to selectively inhibit the predicted superenhancer locus. Inhibition of the predicted superenhancer region reduced KLHDC8A mRNA expression and GSC proliferation (Figure 3.3, G-I), supporting

the essentiality of the non-coding superenhancer element and further orthogonal validation of the shRNA knockdown approach.

FIGURES

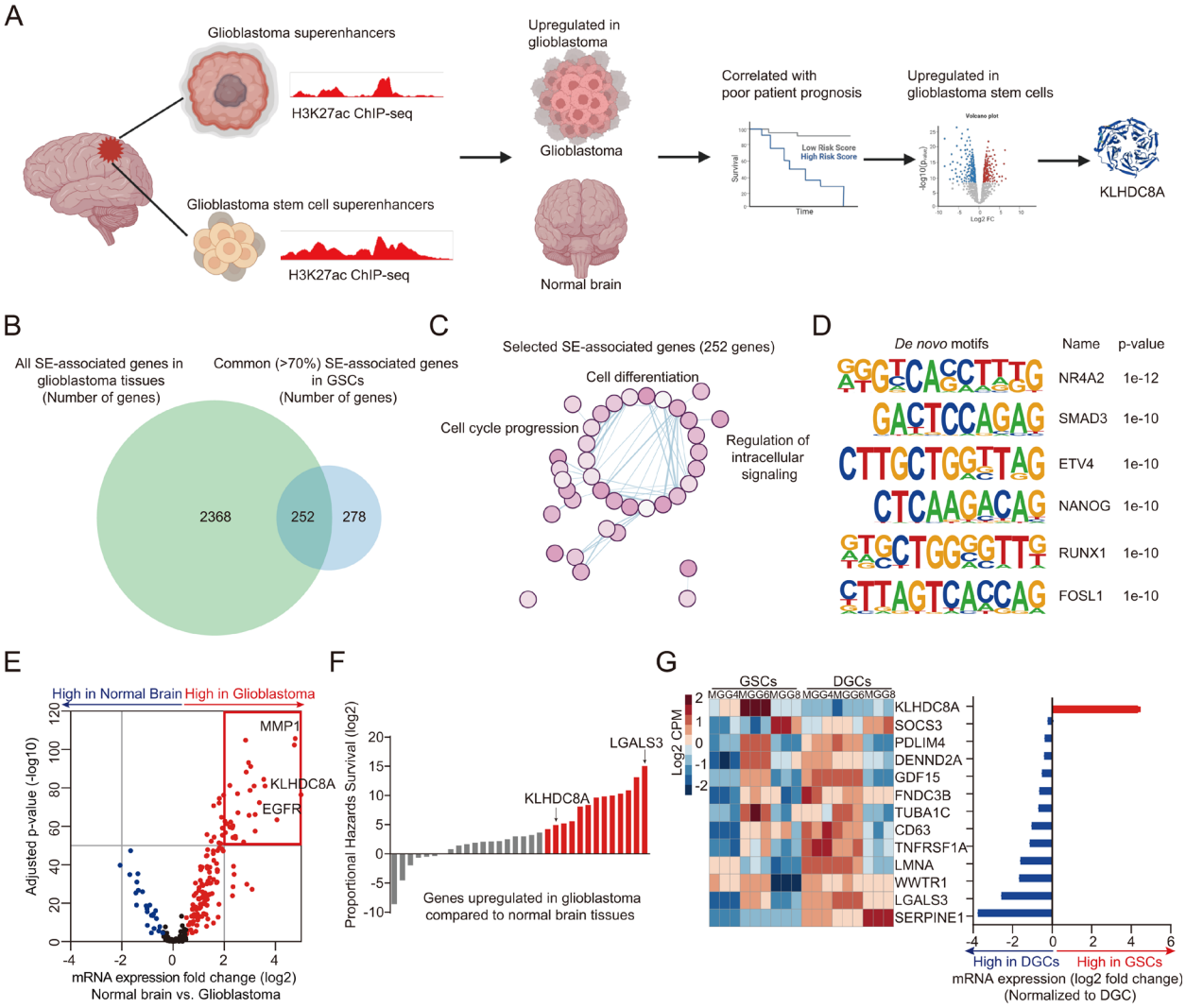

Figure 3.1. Superenhancer screen identified a potential GSC vulnerability.
(**A**) Diagram depicting the superenhancer screen and target prioritization approach. (**B**) Venn diagram demonstrating the intersection between all superenhancer-associated genes in 11 glioblastoma tissues and common (>70%) superenhancer-associated genes in 37 GSCs. (**C**) Gene set enrichment analysis of the correlation of Hallmark, Curated, and GO pathway genesets with the H3K27ac signal intensity of GSC superenhancer-associated genes. (**D**) De novo HOMER motif analysis of 252 selected GSC superenhancers, as described in **B**. (**E**) Volcano plot showing the mRNA expression of 252 superenhancer-associated genes in TCGA HG-U133A dataset. Red dots indicate upregulated genes, while blue dots show downregulated genes in glioblastoma tissues compared to normal brain tissues. (**F**) Bar plot showing the Proportional Hazards Survival of 32 upregulated superenhancer-associated genes, as described in **E**. Red bars indicate the genes correlated with high Proportional Hazards Survival at a log2 value > 4. (**G**) Heatmap and bar plot showing the mRNA expression of 13 selected superenhancer-associated genes, as described in **F**, in three paired GSC and DGC models analyzed by R package Limma.

Figure 3.2. KLHDC8A is necessary for GSC maintenance.
(**A** and **B**) Cell viability was measured by CellTiter-Glo assay in paired GSC23, GSC3028, and differentiated counterparts (DGC23 and DGC3028) following KLHDC8A knockdown. *n*=4. Quantitative data from 4 technical replicates are shown as mean ± SD (error bars). Statistical significance was determined using two-way ANOVA followed by Dunnett's multiple comparisons. ** $P < 0.01$, ****$P<0.0001$. (**C** and **D**) The knockdown of KLHDC8A was validated by qPCR in GSCs (C) and DGCs (D). Quantitative data from 4 biological replicates are presented as mean ± SD. Statistical significance was determined using one-way ANOVA followed by Tukey's multiple comparisons **** $P < 0.0001$. (**E**) *In vitro* extreme limiting dilution assay in GSC23 and GSC3028 after depletion of KLHDC8A. 24 wells were quantified for each condition. Statistical significance was determined using $\chi 2$ test. **** $P < 0.0001$. (**F**) The knockdown of KLHDC8A was validated by qPCR in GSC3028 and GSC23. Quantitative data from 4 biological replicates are presented as mean ± SD. Statistical significance was determined using one-way ANOVA followed by Tukey's multiple comparisons. **** $P < 0.0001$. (**G**) Immunoblot showing protein levels of PARP and cleaved PARP in GSC3028 and GSC23 following KLHDC8A knockdown. β-Actin is used as the loading control. (**H**) Annexin V-positive cells of GSC23 and GSC3028 was performed following knockdown of KLHDC8A. (**I**) Quantification of Annexin V-positive GSC3028 and GSC23. Quantitative data from 3 technical replicates are shown as mean ± SD (error bars). Statistical significance was determined using one-way ANOVA followed by Tukey's multiple comparisons. **** $P < 0.0001$. (**J**) Protein levels of OLIG2 and SOX2 following KLHDC8A knockdown were measured by immunoblot. β-Actin is used as the loading control.

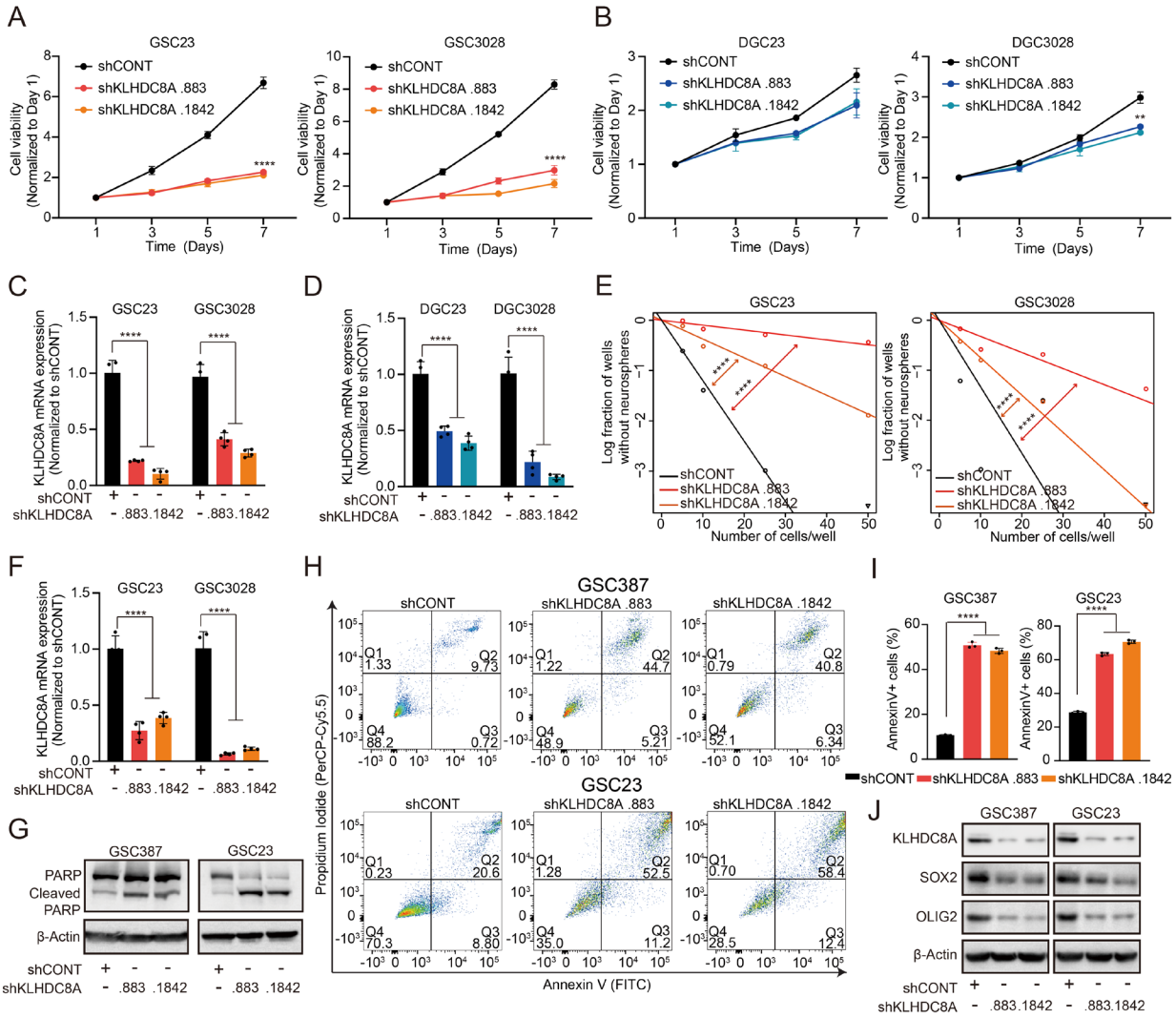
A
GSC23
GSC3028
shCONT
shKLHDC8A .883
shKLHDC8A .1842
Cell viability (Normalized to Day 1)
Time (Days)
B
DGC23
DGC3028
C
D
KLHDC8A mRNA expression (Normalized to shCONT)
E
Log fraction of wells without neurospheres
Number of cells/well
F
G
PARP
Cleaved PARP
β-Actin
H
GSC387
GSC23
Propidium Iodide (PerCP-Cy5.5)
Annexin V (FITC)
I
AnnexinV+ cells (%)
J
KLHDC8A
SOX2
OLIG2

Figure 3.3. KLHDC8A expression is driven by SOX2 and a GSC superenhancer in GSCs. (**A**) KLHDC8A mRNA expression was measured in three matched pairs of GSCs and DGCs by qPCR analysis. Quantitative data from 3 biological replicates are presented as mean ± SD. Statistical significance was determined using Student's t-test followed by the Holm–Sidak multiple test correction. * $P < 0.05$, ***, $P < 0.001$. (**B**) Protein levels of KLHDC8A were measured by immunoblot following KLHDC8A knockdown. SOX2 was used as the stemness marker. β-Actin was used as the loading control. (**C**) H3K27ac enrichment at the KLHDC8A superenhancer region in matched GSCs and DGCs. Enrichment of SOX2 and OLIG2 was identified at the superenhancer region of MGG8. (**D**) Correlation of mRNA expression between KLHDC8A, OLIG2, and SOX2 in the TCGA glioblastoma dataset. Numbers indicated the correlation coefficient. *** $P < 0.001$. (**E**) mRNA expression of SOX2 and KLHDC8A upon knockdown of SOX2. Quantitative data from 3 biological replicates are presented as mean ± SD. Statistical significance was determined using two-way ANOVA followed by Dunnett's multiple test correction. ** $P < 0.01$, *** $P < 0.001$, **** $P < 0.0001$. (**F**) KLHDC8A mRNA expression after treating GSCs with two concentrations of JQ1 (1.5 and 3 μM) for 24 hours. Quantitative data from 3 biological replicates are presented as mean ± SD. Statistical significance was determined using two-way ANOVA followed by Dunnett's multiple test correction. ** $P < 0.01$, **** $P < 0.0001$. (**G**) Schematic representation of using the dCas9-KRAB system with 5 non-overlapping sgRNAs targeting a critical KLHDC8A superenhancer locus. (**H**) KLHDC8A mRNA expression in GSC23 and GSC3028 was measured by qPCR. Quantitative data from 4 biological replicates are presented as mean ± SD. Statistical significance was determined using two-way ANOVA followed by Dunnett's multiple comparison. **** $P < 0.0001$. (**I**) Cell viability of GSCs measured by CellTiter-Glo assay in GSC23 and GSC3028 overexpressing dCas9-KRAB and 5 sgRNAs over a 6-day time course. $n=4$. Quantitative data from 4 technical replicates are presented as mean ± SD (error bars). Statistical significance was determined using two-way ANOVA followed by Dunnett multiple test correction. **** $P < 0.0001$.

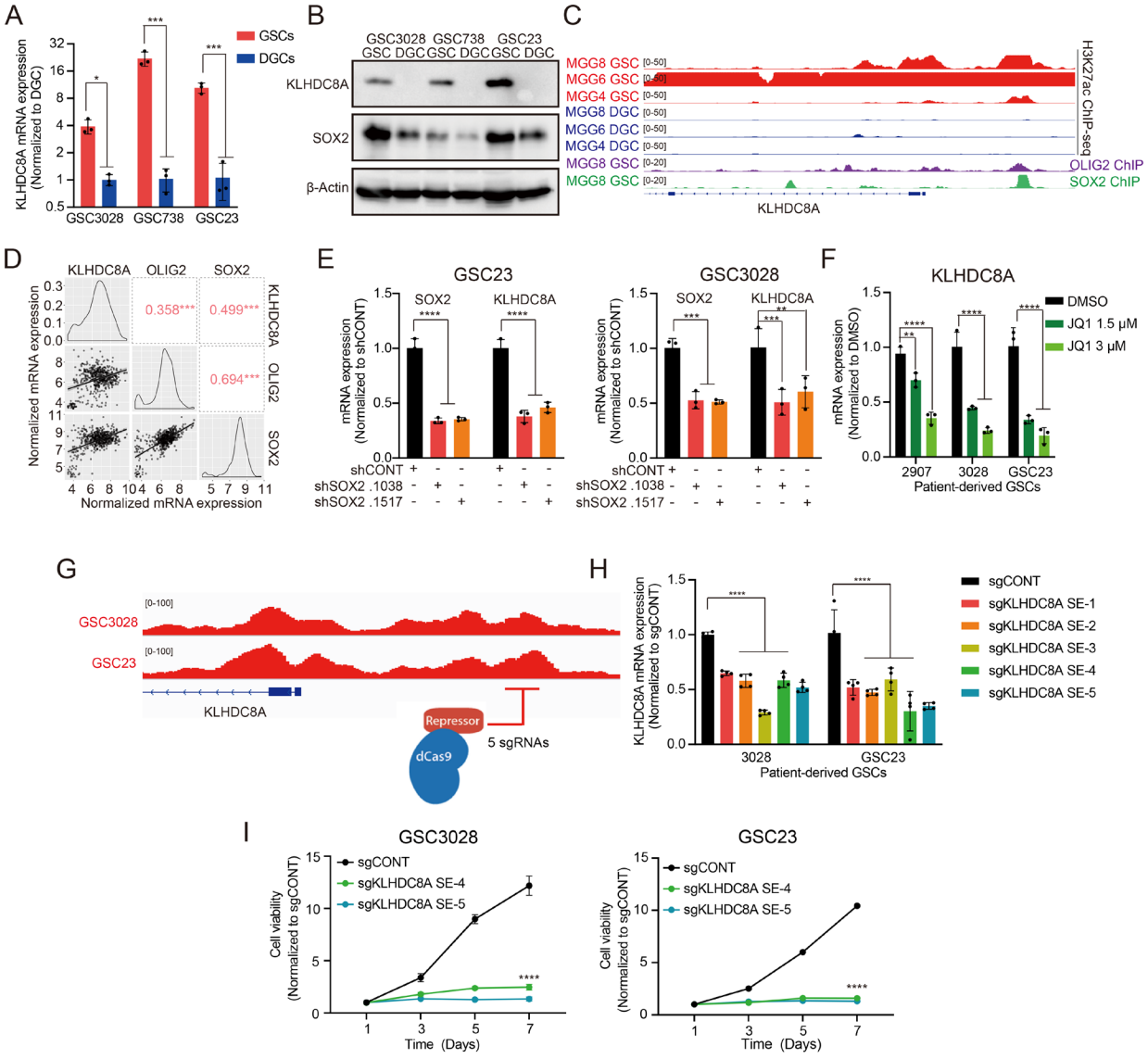
A
KLHDC8A mRNA expression (Normalized to DGC)
GSCs
DGCs
GSC3028
GSC738
GSC23
B
GSC3028 GSC738 GSC23
GSC DGC GSC DGC GSC DGC
KLHDC8A
SOX2
β-Actin
C
MGG8 GSC
MGG6 GSC
MGG4 GSC
MGG8 DGC
MGG6 DGC
MGG4 DGC
H3K27ac ChIP-seq
OLIG2 ChIP
SOX2 ChIP
KLHDC8A
D
KLHDC8A
OLIG2
SOX2
0.358***
0.499***
0.694***
Normalized mRNA expression
E
GSC23
GSC3028
SOX2
KLHDC8A
mRNA expression (Normalized to shCONT)
shCONT
shSOX2 .1038
shSOX2 .1517
F
KLHDC8A
DMSO
JQ1 1.5 μM
JQ1 3 μM
mRNA expression (Normalized to DMSO)
2907
3028
GSC23
Patient-derived GSCs
G
GSC3028
GSC23
KLHDC8A
Repressor
dCas9
5 sgRNAs
H
KLHDC8A mRNA expression (Normalized to sgCONT)
sgCONT
sgKLHDC8A SE-1
sgKLHDC8A SE-2
sgKLHDC8A SE-3
sgKLHDC8A SE-4
sgKLHDC8A SE-5
3028
GSC23
Patient-derived GSCs
I
GSC3028
GSC23
Cell viability (Normalized to sgCONT)
sgCONT
sgKLHDC8A SE-4
sgKLHDC8A SE-5
Time (Days)

SUPPLEMENTAL FIGURES

Figure 3.S1. In silico superenhancer screen identifies GSC superenhancer-associated targets, related to Figure 3.1.

(**A**) Hockey stick plot showing superenhancer-associated genes from 11 glioblastoma tissues (GBM2907, 3018, 3028, 3038, 3069, 2493, 2585, B39, P69, R28, and S08). Superenhancers were identified by ROSE algorithm and were based on H3K27ac ChIP-seq data and the corresponding input ChIP-seq data. (**B**) Bar plot showing top 14 gene sets associated with the expression of 252 selected GSC superenhancer-associated genes. (**C**) Genome-wide annotations of selected GSC superenhancers, as described in **B**. (**D**) Kaplan-Meier curves displaying survival of patients in the TCGA glioblastoma dataset and the CGGA glioblastoma dataset stratified based on the signature score of selected GSC superenhancer-associated genes. Statistical significance was determined using log-rank test. $P = 0.0101$ for TCGA GBM dataset and $P = 0.044$ for CGGA GBM dataset.

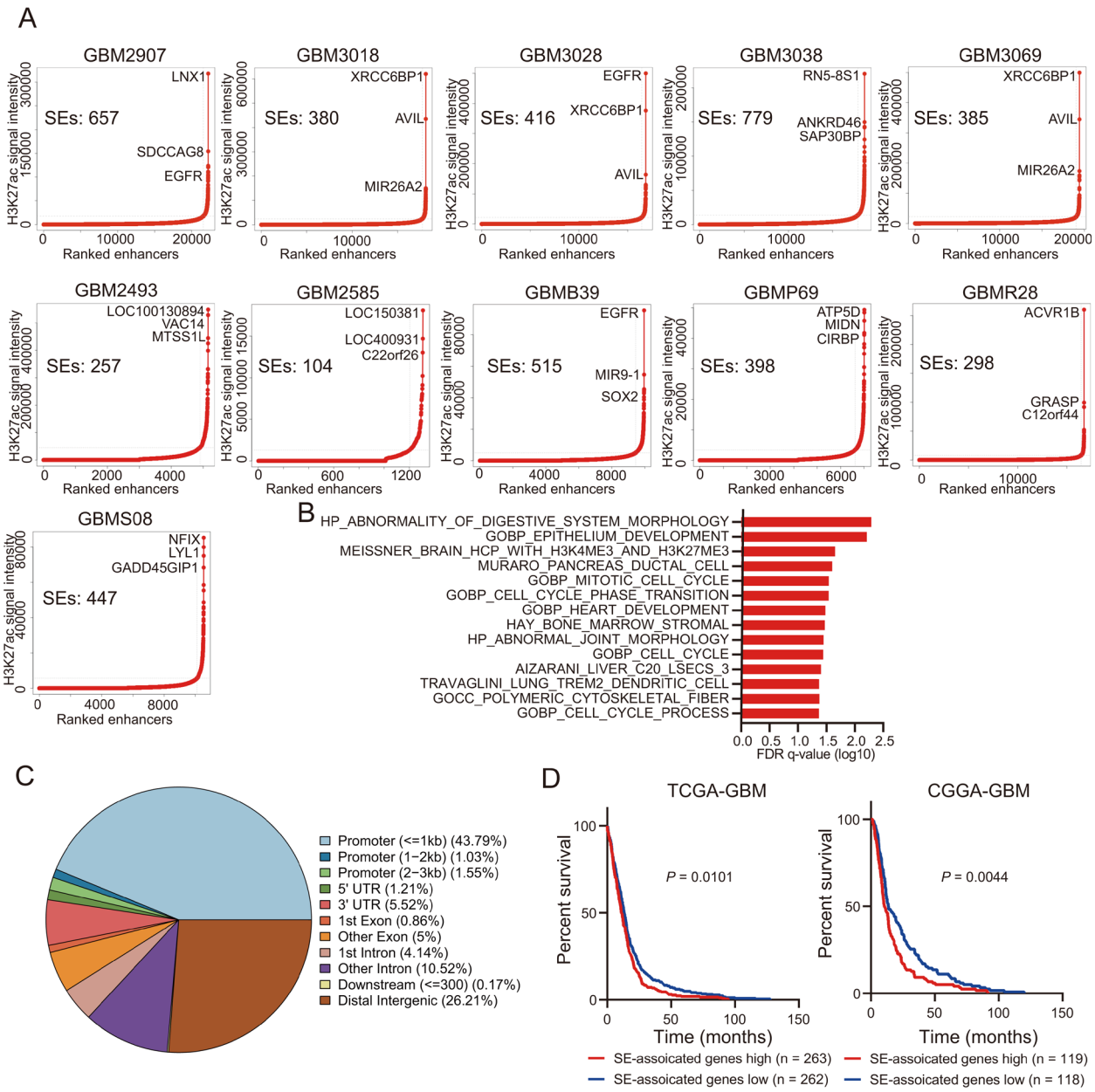
A
GBM2907
SEs: 657
LNX1
SDCCAG8
EGFR
GBM3018
SEs: 380
XRCC6BP1
AVIL
MIR26A2
GBM3028
SEs: 416
EGFR
XRCC6BP1
AVIL
GBM3038
SEs: 779
RN5-8S1
ANKRD46
SAP30BP
GBM3069
SEs: 385
XRCC6BP1
AVIL
MIR26A2
GBM2493
SEs: 257
LOC100130894
VAC14
MTSS1L
GBM2585
SEs: 104
LOC150381
LOC400931
C22orf26
GBMB39
SEs: 515
EGFR
MIR9-1
SOX2
GBMP69
SEs: 398
ATP5D
MIDN
CIRBP
GBMR28
SEs: 298
ACVR1B
GRASP
C12orf44
GBMS08
SEs: 447
NFIX
LYL1
GADD45GIP1
H3K27ac signal intensity
Ranked enhancers
B
HP_ABNORMALITY_OF_DIGESTIVE_SYSTEM_MORPHOLOGY
GOBP_EPITHELIUM_DEVELOPMENT
MEISSNER_BRAIN_HCP_WITH_H3K4ME3_AND_H3K27ME3
MURARO_PANCREAS_DUCTAL_CELL
GOBP_MITOTIC_CELL_CYCLE
GOBP_CELL_CYCLE_PHASE_TRANSITION
GOBP_HEART_DEVELOPMENT
HAY_BONE_MARROW_STROMAL
HP_ABNORMAL_JOINT_MORPHOLOGY
GOBP_CELL_CYCLE
AIZARANI_LIVER_C20_LSECS_3
TRAVAGLINI_LUNG_TREM2_DENDRITIC_CELL
GOCC_POLYMERIC_CYTOSKELETAL_FIBER
GOBP_CELL_CYCLE_PROCESS
FDR q-value (log10)
C
Promoter (<=1kb) (43.79%)
Promoter (1−2kb) (1.03%)
Promoter (2−3kb) (1.55%)
5' UTR (1.21%)
3' UTR (5.52%)
1st Exon (0.86%)
Other Exon (5%)
1st Intron (4.14%)
Other Intron (10.52%)
Downstream (<=300) (0.17%)
Distal Intergenic (26.21%)
D
TCGA-GBM
P = 0.0101
CGGA-GBM
P = 0.0044
Percent survival
Time (months)
SE-assoicated genes high (n = 263)
SE-assoicated genes low (n = 262)
SE-assoicated genes high (n = 119)
SE-assoicated genes low (n = 118)

Figure 3.S2. KLHDC8A is necessary for stem cell populations and is a strongly selective gene across cancer types, related to Figure 3.2.
(**A**) Cell viability measured by CellTiter-Glo assay in 3 neural stem/progenitor cells (ENSA, hNP1, and NSC11) upon knockdown with a control shRNA or two non-overlapping shRNA targeting KLHDC8A (shKLHDC8A.883 or shKLHDC8A.1842). Quantitative data from 4 technical replicates are presented as mean ± SD. Statistical significance was determined using two-way ANOVA followed by Dunnett's multiple hypothesis test correction. **** $P < 0.0001$. (**B**) Cell viability of three nonmalignant brain cells (NM176, NM177, and NM290) upon knockdown with two non-overlapping shRNA targeting KLHDC8A. Quantitative data from 4 technical replicates are presented as mean ± SD. (**C**) KLHDC8A is not a pan-essential gene across 558 cancer cell lines. Genes with 0 dependency score are non-essential, whereas genes with dependency score 1 or -1 are considered pan-essential genes. Dependency score was derived from the Cancer Dependency Map (www.depmap.org). (**D**) H3K27ac signal at the KLHDC8A locus across an overlay of 33 GSCs, 3 DGCs, and 3 NM cells.

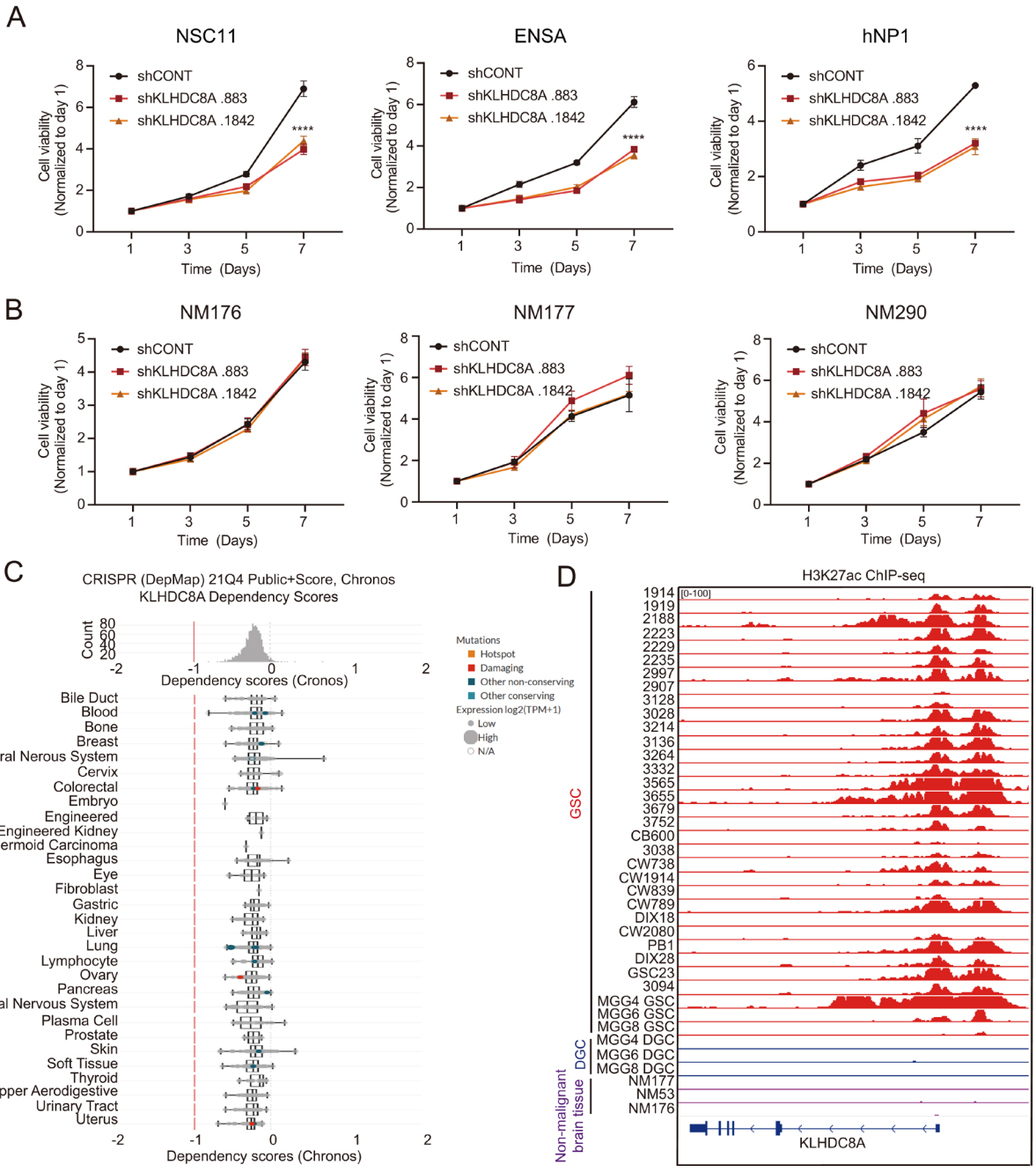
A
NSC11
ENSA
hNP1
shCONT
shKLHDC8A .883
shKLHDC8A .1842
Cell viability (Normalized to day 1)
Time (Days)
****
B
NM176
NM177
NM290
C
CRISPR (DepMap) 21Q4 Public+Score, Chronos
KLHDC8A Dependency Scores
Count
Dependency scores (Cronos)
Mutations
Hotspot
Damaging
Other non-conserving
Other conserving
Expression log2(TPM+1)
Low
High
N/A
Bile Duct
Blood
Bone
Breast
Central Nerous System
Cervix
Colorectal
Embryo
Engineered
Engineered Kidney
Epidermoid Carcinoma
Esophagus
Eye
Fibroblast
Gastric
Kidney
Liver
Lung
Lymphocyte
Ovary
Pancreas
Pheripheral Nervous System
Plasma Cell
Prostate
Skin
Soft Tissue
Thyroid
Upper Aerodigestive
Urinary Tract
Uterus
D
H3K27ac ChIP-seq
[0-100]
1914
1919
2188
2223
2229
2235
2997
2907
3128
3028
3214
3136
3264
3332
3565
3655
3679
3752
CB600
3038
CW738
CW1914
CW839
CW789
DIX18
CW2080
PB1
DIX28
GSC23
3094
MGG4 GSC
MGG6 GSC
MGG8 GSC
MGG4 DGC
MGG6 DGC
MGG8 DGC
NM177
NM53
NM176
GSC
DGC
Non-malignant brain tissue
KLHDC8A

Figure 3.S3. KLHDC8A is preferentially expressed in GSCs and is driven by stem state transcription factor SOX, related to Figure 3.3.
(**A**) mRNA expression of OLIG2 measured by qPCR in three matched GSCs (3028, 738, and GSC23) and DGCs. Quantitative data from 3 biological replicates are presented as mean ± SD. Statistical significance was determined using Student's t-test. ** $P < 0.01$, **** $P < 0.0001$. (**B**) mRNA expression of SOX2 measured by qPCR in three matched GSCs and DGCs. Quantitative data from 3 biological replicates are presented as mean ± SD. Statistical significance was determined using Student's t-test. ** $P < 0.01$, **** $P < 0.0001$. (**C**) mRNA expression of GFAP measured by qPCR in three matched GSCs and DGCs. Quantitative data from 3 biological replicates are presented as mean ± SD. Statistical significance was determined using Student's t-test. ** $P < 0.01$, *** $P < 0.001$. (**D**) Correlation of mRNA expression between KLHDC8A, OLIG2, and SOX2 in the CGGA dataset. Numbers indicate the correlation coefficient. ** $P < 0.01$, *** $P < 0.001$. (**E** and **F**) mRNA expression of OLIG2 and KLHDC8A upon knockdown of OLIG2. Statistical significance was determined using two-way ANOVA followed by the Sidak multiple test correction. **** $P < 0.0001$. (**G**) t-SNE plot showing KLHDC8A expression across 28 glioblastoma tissues. (**H**) Similar single-cell RNA-seq analysis was performed for SOX2 mRNA expression.

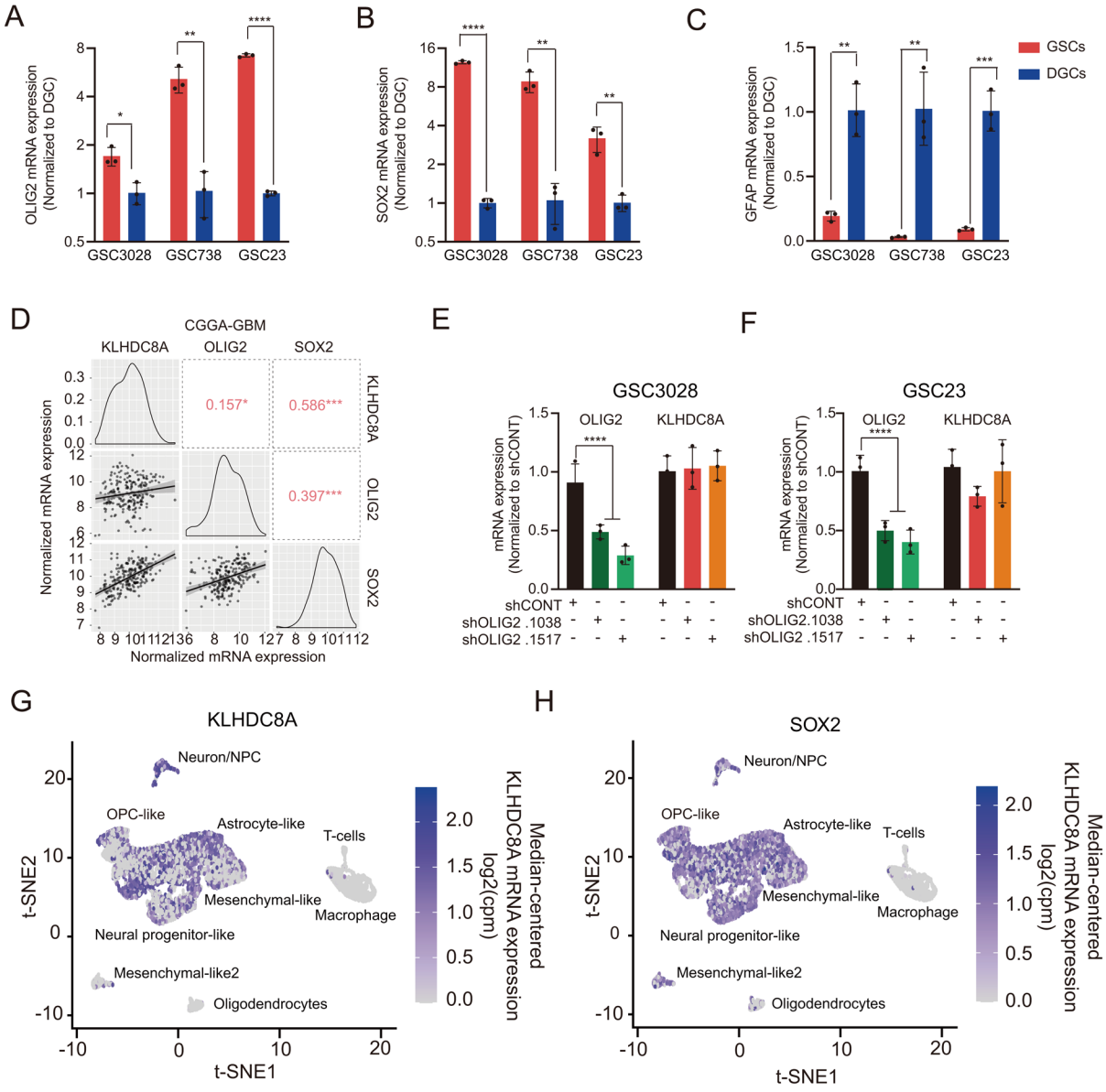
A
OLIG2 mRNA expression (Normalized to DGC)
GSC3028
GSC738
GSC23
B
SOX2 mRNA expression (Normalized to DGC)
C
GFAP mRNA expression (Normalized to DGC)
GSCs
DGCs
D
CGGA-GBM
KLHDC8A
OLIG2
SOX2
0.157*
0.586***
0.397***
Normalized mRNA expression
E
GSC3028
mRNA expression (Normalized to shCONT)
shCONT
shOLIG2 .1038
shOLIG2 .1517
F
GSC23
shOLIG2.1038
G
KLHDC8A
Neuron/NPC
OPC-like
Astrocyte-like
T-cells
Mesenchymal-like
Macrophage
Neural progenitor-like
Mesenchymal-like2
Oligodendrocytes
t-SNE1
t-SNE2
Median-centered KLHDC8A mRNA expression log2(cpm)
H
SOX2

ACKNOWLEDGMENTS

Chapter 3 contains data of the material that has been submitted for publication as it may appear in the Journal of Clinical Investigation, 2022, Derrick Lee, Ryan C. Gimple, Xujia Wu, Briana C. Prager, Zhixin Qiu, Qiulian Wu, Vikas Daggubati, Aruljothi Mariappan, Jay Gopalakrishnan, Matthew R. Sarkisian, David R. Raleigh, Jeremy N. Rich. The dissertation author was the primary researcher and author of this paper. This work was supported by National Institutes of Health: Derrick Lee, CA243296; Briana C. Prager, CA217066; Ryan C. Gimple, CA217065; David R. Raleigh, HD106238, CA251221, CA262311; Jeremy N. Rich, P30 CA047904, CA238662, CA197718, NS103434.

Chapter 4

KLHDC8A promotes ciliogenesis to support Hedgehog signaling

CHAPTER 4

KLHDC8A supports GSC growth through regulation of extracellular matrix and signaling

Little is known about the physiologic and pathologic functions of KLHDC8A in any tissue type or disease process. To elucidate the molecular mechanisms by which KLHDC8A promotes GSC growth, we performed RNA sequencing (RNA-seq) following KLHDC8A knockdown in two patient-derived GSCs, revealing widespread gene expression changes compared to a non-targeting control (Figure 4.1A) and altered expression of gene sets associated with extracellular matrix, cell adhesion, and extracellular stimulus response (Figure 4.1, B and C). In parallel, we leveraged clinical datasets to interrogate gene sets positively or negatively correlated with KLHDC8A expression. Similar to the results of RNA-seq analysis, gene set enrichment analysis (GSEA) revealed that KLHDC8A expression positively correlated with gene sets associated with extracellular matrix, extracellular signaling, and cell morphogenesis. KLHDC8A-associated genes were negatively enriched for processes of chemokine response, immune response, and cancer clusters (Figure 4.1D). Furthermore, KLHDC8A-correlated genes strongly correlated with angiogenesis, epithelial-to-mesenchymal transition, hypoxia, and Hedgehog signaling, which are modulated by the extracellular environment and signals and are molecular processes associated with the progression of glioblastoma (Figure 4.1F). Collectively, these results implicate the potential roles of KLHDC8A in mediating the extracellular signaling pathways.

KLHDC8A supports GSC growth via upregulating Hedgehog signaling

Following KLHDC8A knockdown and the subsequent RNA-seq analysis, Sonic hedgehog (Shh) was the top downregulated gene upon KLHDC8A perturbation (Figure 4.S1A). Single-sample gene set enrichment analysis (ssGSEA) of glioblastoma patients from the TCGA-GBM

dataset revealed strong correlation between KLHDC8A expression, Hedgehog signaling, and primary cilia, an organelle that is required for vertebrate Hedgehog signal transduction in development and cancer (Figure 4.S1, B-D) (152). The Hedgehog pathway drives maintenance and migration of cancer stem cells (135), including in GSCs (153), so we interrogated the role of KLHDC8A in Hedgehog signaling transduction in GSCs. To validate the functional importance of Hedgehog signaling pathway in our patient-derived GSCs, we analyzed the mRNA and protein levels of Hedgehog pathway genes SHH and Gli1 in GSCs and DGCs. mRNA and protein levels of Shh and Gli1 were elevated in GSCs compared to DGCs, suggesting that Hedgehog signaling may promote GSC growth (Figure 4.2, A-C). To assess the effect of KLHDC8A knockdown on Hedgehog signaling, KLHDC8A was targeted with one of two non-overlapping shRNAs, which revealed downregulation of Shh and the downstream effector, Gli1, at both mRNA and protein levels (Figure 4.2, D-F). Targeting KLHDC8A also reduced mRNA expression of several Gli1 target genes, including MYC, JUN, CXCR4, FOXM1, and cell cycle genes (CCND1, CCND2, and CCNE1) (Figure 4.2, G and H). In complementary studies, GSCs and DGCs were treated with the SMO inhibitor, Sonidegib. GSCs were more vulnerable to SMO inhibition than DGCs (Figure 4.2I). These data suggest that KLHDC8A promotes GSC maintenance through upregulating Hedgehog signaling.

KLHDC8A promotes primary cilia formation in GSCs

Primary cilia are microtubule-based structures that function as cellular antennas, sensing and transducing mechanical, optical, or chemical signals in a cell type- and cell-cycle phase-specific manner. Inhibition of primary cilia formation leads to loss of SHH-dependent ventral neural cell types (154). Primary cilia have been linked to glioma differentiation (96), so we

investigated primary cilia in GSCs. Three patient-derived GSCs were stained with primary cilia markers, acetylated-α-tubulin (Ac-tubulin), IFT88, ARL13B, and polyglutamylated-tubulin, which label the axoneme of a cilium. Approximately 25% of GSCs displayed primary cilia detected by positive staining of Ac-tubulin, IFT88, ARL13B, and polyglutamylated-tubulin (Figure 4.3, A and B). GSCs displayed a higher frequency of ciliated cells compared to matched DGCs (Figure 4.3, C and D). To interrogate if KLHDC8A participates in primary cilia formation, we depleted KLHDC8A in two patient-derived GSCs. KLHDC8A depletion reduced the percentage of ciliated cells (Figure 4.4, A-D and Figure 4.S2), so we interrogated the Biological General Repository for Interaction Datasets (BioGRID), which contains 2 million biological interactions for more than 80 species. KLHDC8A interacted with the subunits of Chaperonin-containing TCP1 complex (CCT) (Figure 4.S3A), which mediates actin and tubulin biogenesis and regulates post-translational modification of α-tubulin (155). To confirm this predicted interaction, FLAG-tagged KLHDC8A was expressed in GSCs, as limited reagents for KLHDC8A exist. KLHDC8A co-immunoprecipitated with TCP1 and acetylated-tubulin (Ac-tubulin) (Figure 4.4E). Decreased tubulin acetylation was observed upon KLHDC8A knockdown (Figure 4.4F). Reciprocally, overexpression of FLAG-KLHDC8A promoted tubulin acetylation in GSCs (Figure 4.4G). Treating GSCs with TCP1 inhibitor, HSF1A, decreased Ac-tubulin protein levels (Figure 4.4H), suggesting that KLHDC8A promotes cilia formation via upregulating ac-tubulin.

To confirm the role of KLHDC8A in promoting ciliogenesis, we interrogated the correlation between KLHDC8A expression and two ciliary proteins, IFT88 and ARL13B, in the CGGA dataset. IFT88 is an intraflagellar transport protein and ARL13B is a regulatory GTPase; both are required for ciliogenesis and activation of canonical Hedgehog signaling pathway in basal cell carcinoma (78) and medulloblastoma (156). KLHDC8A mRNA expression correlated with

the IFT88 and ARL13B expression in glioblastoma tissues (Figure 4.S3B). ARL13B was upregulated in glioblastoma tissues compared to normal brain tissues (Figure 4.S2C), and high expression of ARL13B was associated with poor patient prognosis in TCGA GBM Aglient-4502A and TCGA GBM-LGG datasets (Figure 4.S3, D and E). Furthermore, shRNA-mediated knockdown of ARL13B phenocopied KLHDC8A knockdown, as shown by downregulation of Shh and Gli1, as well as reduced cell proliferation (Figure 4.4, I-K). Collectively, these results suggested that KLHDC8A supports Hedgehog signaling by promoting ciliogenesis in GSCs.

KLHDC8A levels correlate with Aurora B/C kinase inhibitor activity

KLHDC8A appears difficult to target due to the lack of small-molecule binding pockets. Therefore, we sought therapeutic dependencies correlated with KLHDC8A by leveraging the Cancer Therapeutics Response Portal (CTRP) and Cancer Cell Line Encyclopedia (CCLE) databases, which contain drug screening data of 481 small-molecule probes in 860 cancer cell lines and mRNA expression of 1000 cancer cell lines, respectively. Elevated KLHDC8A expression was associated with sensitivity as measured by area under curve (AUC) with an Aurora B/C kinase inhibitor, a JMJD3 inhibitor, a pan-cancer inhibitor (BRD-4132) with unknown molecular targets, and an insulin-like growth factor 1 receptor (IGF1R) inhibitor (Figure 4.5A). Supporting the validity of this approach, we recently demonstrated that the IGF1R inhibitor, Linsitinib, targeted GSCs and displayed in vivo efficacy against glioblastoma xenografts (23). The Aurora B/C kinase inhibitor GSK1070916 has been tested in multiple human xenograft cancer types, including breast, colon, and lung, for its anti-tumor effects (157) and was in phase 1 clinical trials for solid tumors. As the Aurora B/C kinase inhibitor was the top hit, we speculated that GSCs, which display greater KLHDC8A expression levels, would be more vulnerable to inhibition of Aurora B/C kinases than

DGCs. Indeed, Aurora B/C kinase treatment (GSK-1070916) inhibited GSC proliferation in a concentration-dependent manner, while DGCs were less sensitive at a concentration approximately 10-fold greater than GSCs (Figure 4.5B). Aurora kinase A activation is known to promote primary cilia disassembly during G1 phase (158). However, the roles of Aurora kinase B and C in regulating primary cilia have not been explored. Furthermore, a previous study demonstrated that SHH-dependent medulloblastoma is sensitive to inhibition of a pan-Aurora kinase inhibitor, Danusertib (159), suggesting a potential interaction between primary cilia, Hedgehog pathway, and Aurora kinase B and C. Therefore, we hypothesized that inhibition of Aurora B/C kinases may promote ciliogenesis and Hedgehog signaling and that treatment with a SMO inhibitor, Sonidegib, and Aurora B/C kinase inhibitor, GSK-1070916, may exert combinatorial effects on GSCs. The frequencies of ciliated GSCs significantly increased after 24h of GSK-1070916 treatment (Figure 4.5, C and D). As revealed by immunoblot, Gli1 was upregulated in cells treated with Aurora B/C kinase inhibitor, suggesting compensatory activation of Hedgehog signaling (Figure 4.5E). Dual treatment of both inhibitors synergistically (synergy score > 1) attenuated GSC proliferation (Figure 4.5F). In vivo tumor initiation is the gold standard assay for cancer stem cells. Thus, we interrogated whether disruption of KLHDC8A expression impaired in vivo tumor formation capacity. We intracranially implanted GSCs transduced with control non-targeting shRNA or one of two non-overlapping shRNAs targeting KLHDC8A in immunocompromised mice. Mice bearing GSCs transduced with KLHDC8A shRNAs displayed prolonged survival compared to mice bearing shCONT GSCs (Figure 4.5, G and H). To gain a clearer insight into the clinical relevance of KLHDC8A, we performed in silico analysis of TCGA data, revealing that KLHDC8A was preferentially expressed in glioblastoma tissues compared to normal brain tissues, and its expression, along with that of SMO, Gli1, and ARL13B, correlated

with mesenchymal and classical subtypes, wild-type IDH tumors, high-grade glioma, and older patients (Figure 4.6, A-D). KLHDC8A expression informed poor patient prognosis of patients in multiple brain tumor datasets (CGGA-GBM, TCGA-LGG/GBM, and Rembrandt) (Figure 4.6, E-G). Collectively, these data suggest that KLHDC8A is a regulator of Hedgehog signaling and primary cilia formation and that targeting KLHDC8A through combinatorial SMO and Aurora B/C kinase inhibition is a promising therapeutic strategy for glioblastoma, serving as a potential therapeutic opportunity for targeting previously undruggable target in glioblastoma.

DISCUSSION

Aberrant epigenetic dysregulation is an essential hallmark of many cancers (160). Superenhancers are enriched at genes that promote tumorigenesis in various cancer types, including medulloblastoma (161), colorectal cancer (162), leukemia (163), B-cell lymphoma (164), and lung cancer (165). Pharmacological inhibitors or genetic ablation targeting key components of superenhancers and target genes impair the proliferation and in vivo tumor initiation capacity of cancer cells (21). Therefore, interrogation of superenhancers and their associated genes improve our understanding of GSC biology and allow for the identification of potential oncogenic drivers that promote tumorigenesis and progression.

Leveraging superenhancer profiling in glioblastoma tissues and GSCs, we identified an epigenetically upregulated gene, KLHDC8A, with expression driven by a superenhancer element located upstream of the gene with contributions from a stemness transcription factor SOX2. KLHDC8A belongs to a large family of kelch proteins, which generally contain 5-7 kelch tandem repeats and form a β-propeller tertiary structure known to mediate protein-protein interactions. Members of kelch proteins function through interaction with distinct binding partners and involve

in a wide range of cellular processes, including signal transduction (68), DNA repair (69), and protein degradation (70). The molecular functions of KLHDC8A had not been explored. In a previous study, KLHDC8A was highly expressed in glioblastoma cell lines that escaped from the treatment of EGFR inhibitor, and KLHDC8A compensated for the loss of a constitutively active variant of EGFR (EGFR VIII) (72). KLHDC8A is induced by lactate in glioblastoma cell lines (73). However, the mechanism by which KLHDC8A functions has been unknown. Our study uncovers a novel function of KLHDC8A in promoting Hedgehog pathway through mediating ciliogenesis in GSCs.

Primary cilia are signaling hubs that host and mediate other signaling pathways besides Hedgehog signaling, including WNT, NOTCH, platelet-derived growth factor (PDGF), and various G-protein coupled receptors. However, the presence of primary cilia in glioblastoma tissues and patient-derived cell lines remains an area of investigation. Defects in primary cilia formation have been noted in glioblastoma biopsies and established glioblastoma cell lines (166). It was recently shown that cilia induction promotes differentiation of a subset of cultured GSCs upon inhibition of Nek2 (96). However, substantial fractions of cells in glioblastoma biopsies and patient-derived human and mouse primary glioblastoma cells are ciliated with ultrastructural normal cilia (93). The distal tips of primary cilia on patient-derived glioblastoma cell lines secrete mitogenic vesicles and promote the proliferation of other ciliated glioblastoma cells (167). We find that approximately 20~25% of our patient-derived GSCs display primary cilia, which are in line with multiple studies that 10-30% of glioblastoma tissues and cells are ciliated. It remains unclear whether only a subpopulation of GSCs is capable of forming cilia or whether the rapid turnover of cells narrows the window of time in which cilia are present. However, ARL13B

knockdown phenocopied the effect of KLHDC8A knockdown on Hedgehog signaling and cell proliferation, suggesting that primary cilia serve an oncogenic role in GSCs.

Mechanistically, we uncovered a novel function of the KLHDC8A in regulating tubulin biogenesis. KLHDC8A interacts with Ac-tubulin and the molecular chaperone CCT, which mediates tubulin biogenesis. Downregulation of KLHDC8A reduced Ac-tubulin expression, while KLHDC8A overexpression promoted tubulin acetylation in GSCs. Given that the β-propeller architecture mediates protein-protein interaction, we reasoned that KLHDC8A may function as an adaptor that facilitates CCT-α-tubulin interaction and the subsequent tubulin folding and acetylation. In addition to regulating tubulin biogenesis, CCT is essential for Bardet-Biedl syndrome protein complex (BBSome) assembly, which exerts a pivotal role in primary cilia homeostasis by promoting cargo entry into cilia (168). Upregulated CCT is associated with enhanced proliferation and growth of breast cancer (169). Furthermore, elevated tubulin acetylation is linked to enhanced invasive migration and therapeutic resistance to chemotherapy agents (170, 171). Genetic ablation of α-tubulin acetyltransferase, αTAT1, suppresses colon cancer proliferation and invasion (172). Thus, the identification of novel KLHDC8A-CCT interaction may provide a further node of therapeutic benefit.

To identify a translational approach for targeting KLHDC8A, we identified Aurora B/C kinases as the potential therapeutic targets in GSCs. GSCs display greater sensitivity to the inhibition of Aurora B/C kinase inhibitor compared to differentiated cells. Gli1 was upregulated upon treatment with Aurora B/C kinase inhibitor, and combined treatment of SMO inhibitor and Aurora B/C kinase inhibitor synergized to kill GSCs, indicating crosstalk between Aurora B/C kinase and Hedgehog pathway. Aurora kinase inhibitors are under development for the treatment of numerous cancers. Our results suggest that these inhibitors either select for cells with primary

cilia and active Hedgehog signaling or induce these states, supporting a likely molecular mechanism of therapeutic resistance. As Aurora kinase B is a mitotic kinase that regulates chromosome segregation and cell cycle progression during mitosis, dual treatment with a SMO inhibitor and Aurora B/C kinase inhibitor might target both ciliated and mitotic tumor cells. In conclusion, these findings demonstrate that KLHDC8A supports Hedgehog signaling via upregulating ciliogenesis. Dual treatment of Hedgehog pathway and Aurora B/C kinase inhibitors may offer a novel therapeutic paradigm for treating glioblastoma.

FIGURES

Figure 4.1. KLHDC8A promotes the expression of ECM and extracellular signaling genes. (**A**) Differentially expressed genes in GSC23 and GSC3028 transduced with shRNAs targeting KLHDC8A or a control shRNA are displayed by volcano plot. Blue dots indicate genes downregulated in KLHDC8A knockdown cells at an adjusted $P < 0.01$ and $\log_2$ fold change < −0.5. Red indicates genes upregulated following KLHDC8A knockdown at an adjusted $P < 0.01$ and $\log_2$ fold change > 0.5. (**B**) Gene set enrichment analysis of GO pathways enriched or depleted upon KLHDC8A depletion in GSC23 and GSC3028 are displayed. Blue dots indicate enrichment in gene sets downregulated following KLHDC8A knockdown at an FDR < 0.15. (**C**) Top 8 downregulated gene sets following KLHDC8A knockdown in GSC23 and GSC3028 are plotted with normalized enrichment score. (**D**) Bubble plots showing gene sets correlated with KLHDC8A expression in the TCGA glioblastoma dataset. Downregulated gene sets were shown in blue, whereas upregulated gene sets were shown in red. (**E**) Gene set enrichment analysis of Hallmark gene sets correlated with KLHDC8A expression in the TCGA glioblastoma HG-U133A dataset are shown.

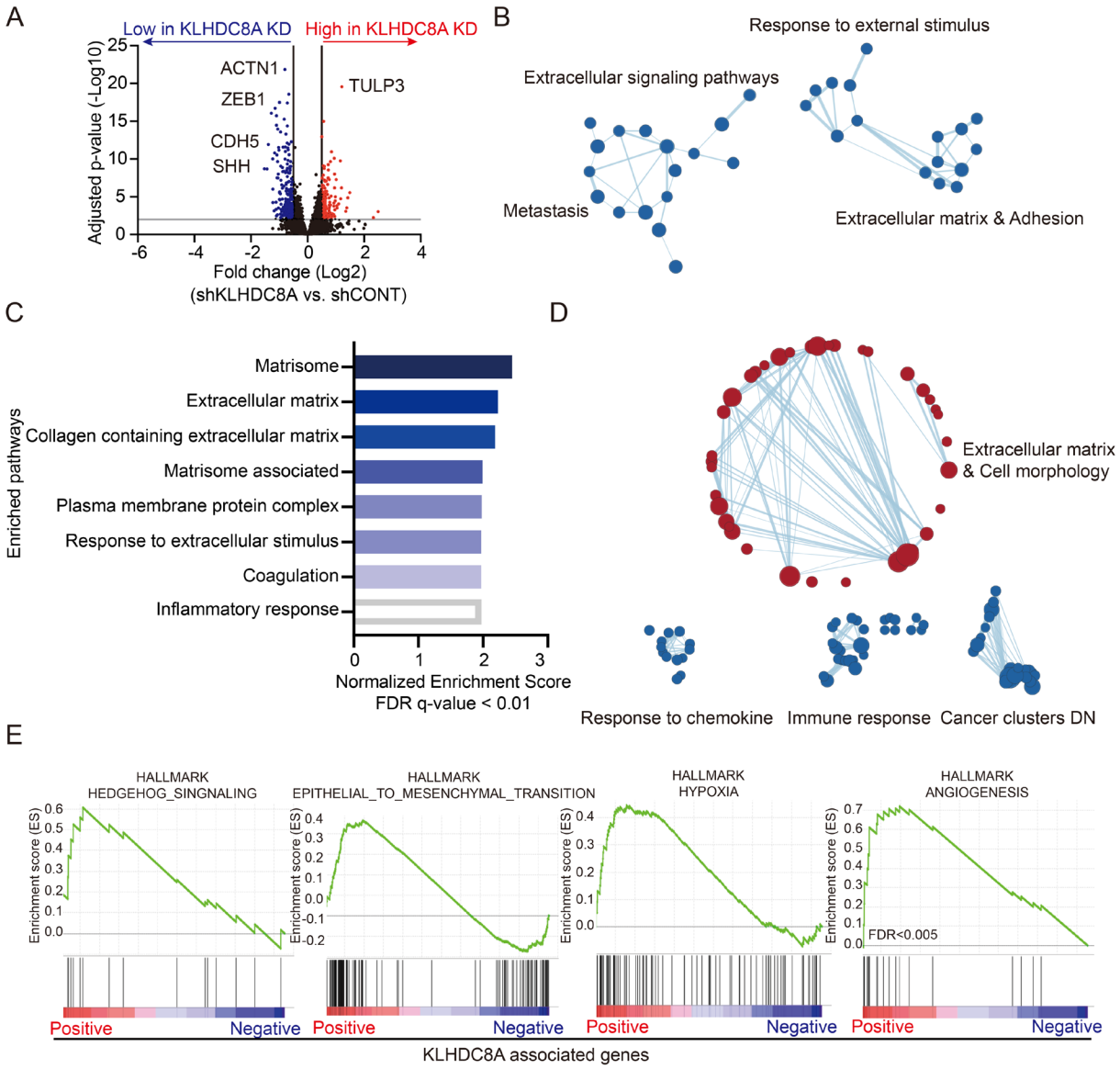
A
Low in KLHDC8A KD
High in KLHDC8A KD
ACTN1
ZEB1
CDH5
SHH
TULP3
Adjusted p-value (-Log10)
Fold change (Log2)
(shKLHDC8A vs. shCONT)
B
Response to external stimulus
Extracellular signaling pathways
Metastasis
Extracellular matrix & Adhesion
C
Enriched pathways
Matrisome
Extracellular matrix
Collagen containing extracellular matrix
Matrisome associated
Plasma membrane protein complex
Response to extracellular stimulus
Coagulation
Inflammatory response
Normalized Enrichment Score
FDR q-value < 0.01
D
Extracellular matrix
& Cell morphology
Response to chemokine
Immune response
Cancer clusters DN
E
HALLMARK
HEDGEHOG_SINGNALING
HALLMARK
EPITHELIAL_TO_MESENCHYMAL_TRANSITION
HALLMARK
HYPOXIA
HALLMARK
ANGIOGENESIS
Enrichment score (ES)
FDR<0.005
Positive
Negative
KLHDC8A associated genes

Figure 4.2. KLHDC8A promotes Hedgehog signaling pathways in GSCs.
(**A** and **B**) mRNA expression of Hedgehog pathway genes (SHH and GLI1) in two GSCs and matched DGCs. n=3. Quantitative data from 3 biological replicates are presented as mean ± SD. Statistical significance was determined using Student's t-test followed by the Holm–Sidak multiple test correction. *** $P < 0.001$, **** $P < 0.0001$. (**C**) Immunoblot showing the protein expression of Shh and Gli1 in three matched pairs of GSCs and DGCs is shown. SOX2 was used to determine the stemness of GSCs. GFAP was used to determine the differentiation of GSCs. β-Actin was used as the loading control. (**D** and **E**) qPCR analysis of KLHDC8A, SHH, and GLI1 mRNA expression in GSC387 and GSC23 following knockdown of KLHDC8A. Quantitative data from 4 biological replicates are presented as mean ± SD. Statistical significance was determined using two-way ANOVA with the Sidak multiple test correction. **** $P < 0.0001$. (**F**) Immunoblot showing the protein expression of GLI1 and SHH upon KLHDC8A knockdown. (**G** and **H**) mRNA expression of GLI1 target genes in GSC387 (**G**) and GSC23 (**H**). Quantitative data from 4 biological replicates are presented as mean ± SD. Statistical significance was determined using Student's t-test followed by Dunnett's multiple test correction. ** $P < 0.01$, *** $P < 0.001$, **** $P < 0.0001$. (**I**) Concentration-response curves of two matched pairs of GSCs and DGCs to SMO inhibitor Sonidegib over a 6-day time course.

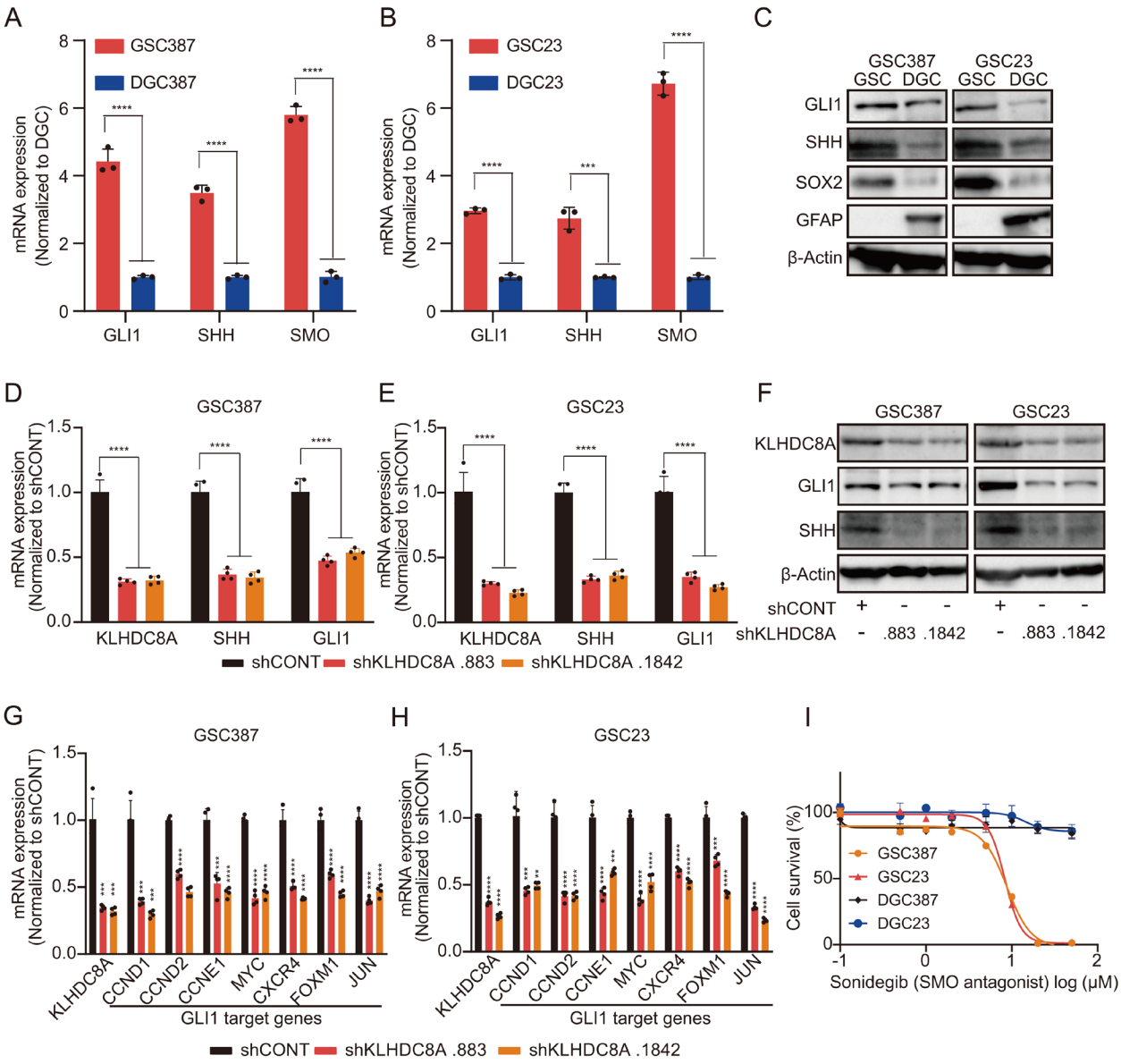
A
GSC387
DGC387
mRNA expression (Normalized to DGC)
GLI1
SHH
SMO
B
GSC23
DGC23
mRNA expression (Normalized to DGC)
GLI1
SHH
SMO
C
GSC387 GSC DGC
GSC23 GSC DGC
GLI1
SHH
SOX2
GFAP
β-Actin
D
GSC387
mRNA expression (Normalized to shCONT)
KLHDC8A
SHH
GLI1
E
GSC23
mRNA expression (Normalized to shCONT)
KLHDC8A
SHH
GLI1
F
GSC387
GSC23
KLHDC8A
GLI1
SHH
β-Actin
shCONT + - - + - -
shKLHDC8A - .883 .1842 - .883 .1842
shCONT
shKLHDC8A .883
shKLHDC8A .1842
G
GSC387
mRNA expression (Normalized to shCONT)
KLHDC8A
CCND1
CCND2
CCNE1
MYC
CXCR4
FOXM1
JUN
GLI1 target genes
H
GSC23
mRNA expression (Normalized to shCONT)
KLHDC8A
CCND1
CCND2
CCNE1
MYC
CXCR4
FOXM1
JUN
GLI1 target genes
shCONT
shKLHDC8A .883
shKLHDC8A .1842
I
Cell survival (%)
GSC387
GSC23
DGC387
DGC23
Sonidegib (SMO antagonist) log (μM)

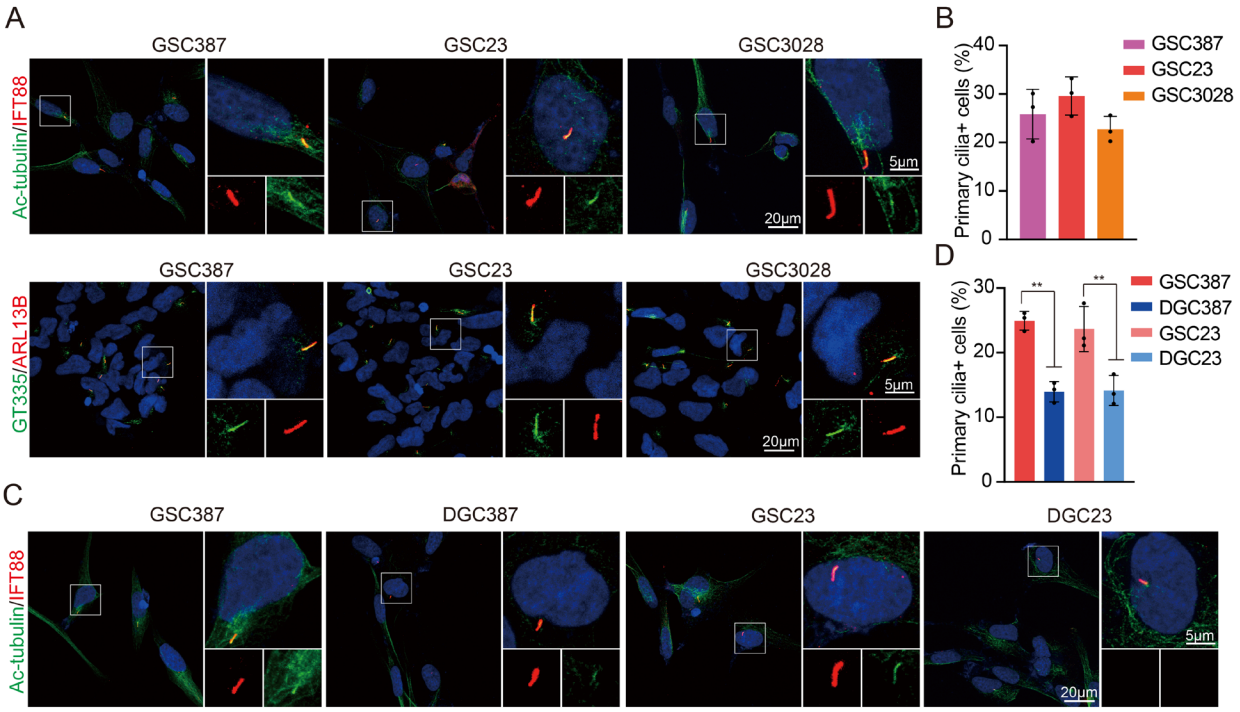

Figure 4.3. GSCs preferentially display primary cilia.
(A) Immunofluorescence imaging of Ac-tubulin, IFT88, polyglutamylated-tubulin, and ARL13B in 3 patient-derived GSCs (GSC387, GSC23, GSC3028). Ac-tubulin or polyglutamylated-tubulin is shown in green, IFT88 or ARL13B in red, and DAPI in blue. Scale bars represent 5 or 20 μm. (**B**) Quantification of primary cilia-positive cells in GSC387, GSC23, and GSC3028. Data are shown as mean ± SD. At least 100 cells in each GSC line from 3 biological replicates were tested. (**C**) Immunostaining of Ac-tubulin and IFT88 in two matched GSCs and DGCs (GSC387 and GSC23). Ac-tubulin is shown in green, IFT88 in red, and DAPI in blue. Scale bars represent 5 or 20 μm. (**D**) Quantification of primary cilia-positive cells in two matched GSCs and DGCs. At least 100 cells in each GSC line from 3 biological replicates were tested. Quantitative data are presented as mean ± SD. Statistical significance was determined using one-way ANOVA followed by Tukey's multiple comparisons. ** $P < 0.01$.

Figure 4.4. KLHDC8A is indispensable for primary cilia formation in GSCs.
(**A** and **B**) Immunofluorescence imaging of primary cilia in GSC387 (**A**) and GSC23 (**B**) transduced with shCONT or two non-overlapping shRNAs targeting KLHDC8A. Polyglutamylated-tubulin was labeled as green, ARL13B as red, and DAPI as blue. Scale bars represent 5 or 20 μm. (**C** and **D**) Quantification of primary cilia positive GSC387 (**C**) and GSC23 (**D**). At least 100 cells in each GSC line from biological replicates were tested. Quantitative data are presented as mean ± SD. Statistical significance was determined using one-way ANOVA followed by Tukey's correction for multiple comparisons. **** $P < 0.0001$. (**E**) Exogenous expression of FLAG-KLHDC8A in GSC23 followed by coimmunoprecipitation with an anti-FLAG antibody or an IgG isotype control antibody. The membrane was probed with anti-Flag, anti-TCP1, anti-Ac-tubulin, and anti-α-Tubulin antibodies. Inputs are indicated. (**F**) Immunoblot of the protein expression of Ac-tubulin following KLHDC8A knockdown is shown. (**G**) Immunoblot of the protein expression of Ac-tubulin following FLAG-KLHDC8A overexpression is shown. (**H**) Immunoblot showing the protein expression of Ac-tubulin, TCP1, and α-Tubulin following treatment of TCP1 inhibitor HSF1A. (**I**) Immunoblot showing the protein expression of ARL13B, Gli1, and Shh following ARL13B knockdown. (**J** and **K**) Cell viability of GSC387 (**J**) and GSC3028 (**K**) upon depletion of ARL13B. Quantitative data from 4 technical replicates are presented as mean ± SD. Statistical significance was determined using two-way ANOVA followed by Tukey's multiple comparison. **** $P < 0.0001$.

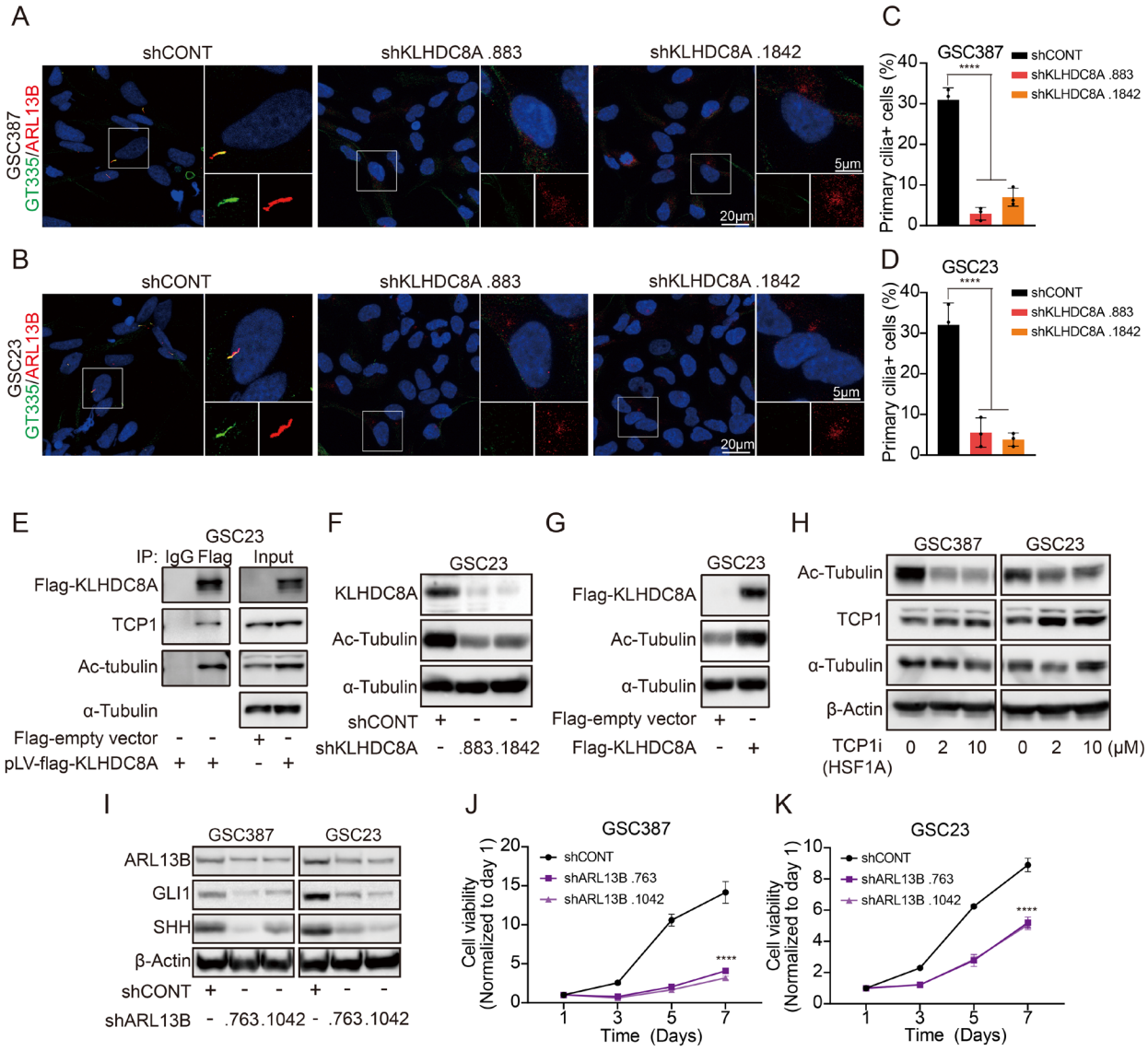
A
shCONT
shKLHDC8A .883
shKLHDC8A .1842
GSC387
GT335/ARL13B
5μm
20μm
B
GSC23
C
GSC387
shCONT
shKLHDC8A .883
shKLHDC8A .1842
Primary cilia+ cells (%)
****
D
GSC23
E
GSC23
IP: IgG Flag Input
Flag-KLHDC8A
TCP1
Ac-tubulin
α-Tubulin
Flag-empty vector
pLV-flag-KLHDC8A
F
GSC23
KLHDC8A
Ac-Tubulin
α-Tubulin
shCONT
shKLHDC8A .883 .1842
G
GSC23
Flag-KLHDC8A
Ac-Tubulin
α-Tubulin
Flag-empty vector
Flag-KLHDC8A
H
GSC387
GSC23
Ac-Tubulin
TCP1
α-Tubulin
β-Actin
TCP1i (HSF1A)
0 2 10 0 2 10 (μM)
I
GSC387
GSC23
ARL13B
GLI1
SHH
β-Actin
shCONT
shARL13B .763 .1042
J
GSC387
shCONT
shARL13B .763
shARL13B .1042
Cell viability (Normalized to day 1)
Time (Days)
K
GSC23

Figure 4.5. *In vivo* dependency and novel therapeutic strategies for targeting KLHDC8A in glioblastoma.
(**A**) Plot showing ranked therapeutic compounds based on correlation of KLHDC8A mRNA expression with drug sensitivity (area under curve, AUC) in brain cancer cell lines in CTRP dataset. (**B**) Dose-response curves of two paired GSCs and DGCs to Aurora B/C kinase inhibitor, GSK1070916. (**C**) Immunofluorescence imaging of primary cilia in GSC3028 and GSC23 following treatment of GSK1070916. Polyglutamylated-tubulin was labeled as green, ARL13B as red, and DAPI as blue. Scale bars represent 5 or 20 μm. (**D**) Quantification of primary cilia-positive GSC3028 and GSC23 cells. At least 100 cells in each GSC line from biological replicates were tested. Quantitative data are presented as mean ± SD. Statistical significance was determined using one-way ANOVA followed by Tukey's correction for multiple comparisons. * $P < 0.05$, ** $P < 0.01$, *** $P < 0.001$. (**E**) Immunoblot showing the protein expression of phospho-Aurora kinase B, Aurora kinase B, and GLI1 following treatment of GSK1070916. (**F**) Synergy plots of Sonidegib and GSK1070916 in GSC387 and GSC23 analyzed by R package Synergyfinder. (**G**) Kaplan-Meier curve showing survival of NSG immunocompromised mice after intracranially injected with GSC23 or GSC3028 upon depletion of KLHDC8A. n=5 per group. Statistical significance was determined using Mantel-Cox log-rank test. ** $P < 0.01$. (**H**) The knockdown of KLHDC8A was validated by qPCR in GSC3028 and GSC23. Quantitative data from 4 biological replicates are presented as mean ± SD (error bars). Statistical significance was determined using one-way ANOVA followed by Tukey's multiple comparisons. *** $P < 0.001$.

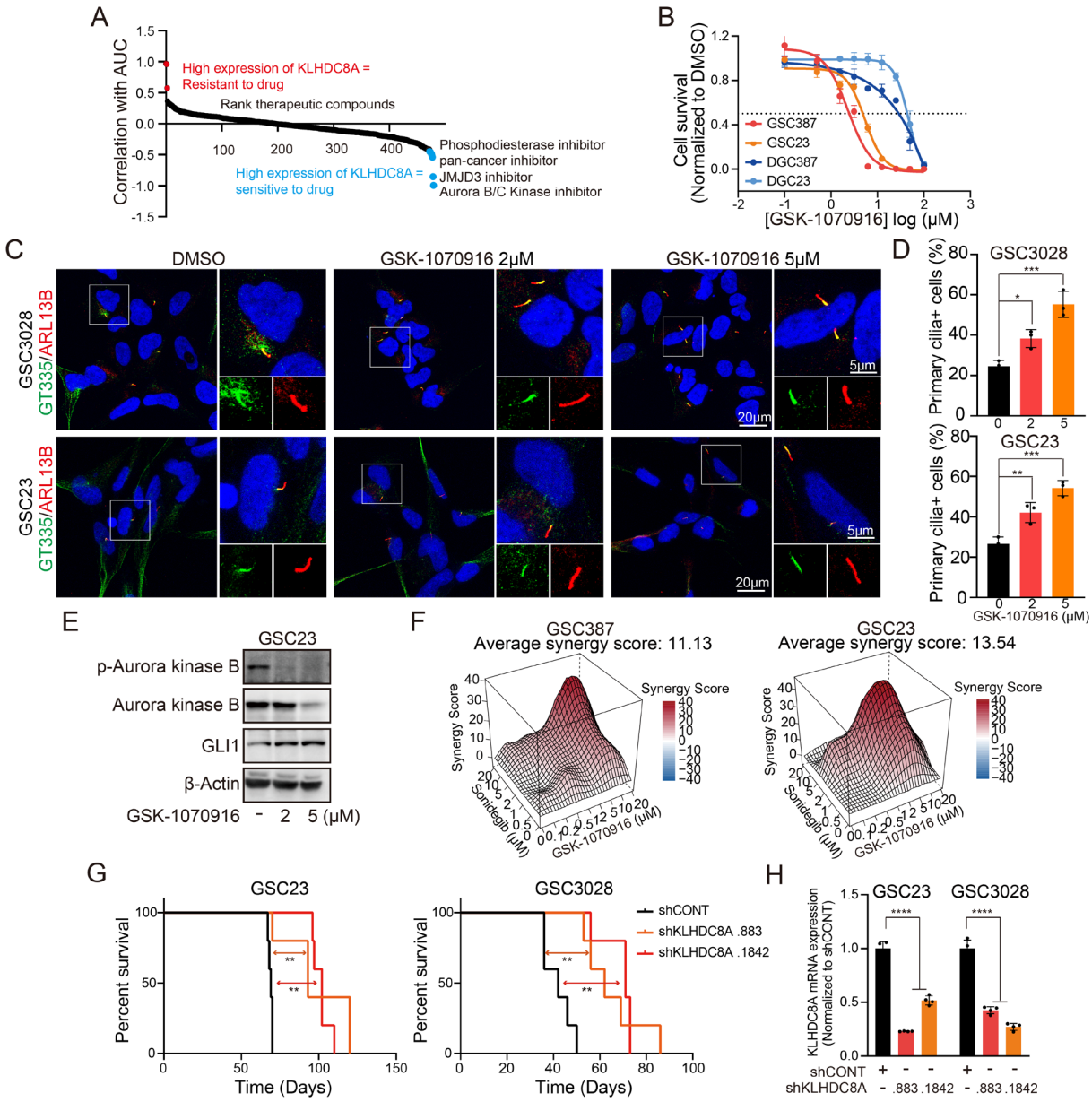
A
Correlation with AUC
High expression of KLHDC8A = Resistant to drug
Rank therapeutic compounds
High expression of KLHDC8A = sensitive to drug
Phosphodiesterase inhibitor
pan-cancer inhibitor
JMJD3 inhibitor
Aurora B/C Kinase inhibitor
B
Cell survival (Normalized to DMSO)
GSC387
GSC23
DGC387
DGC23
[GSK-1070916] log (μM)
C
DMSO
GSK-1070916 2μM
GSK-1070916 5μM
GSC3028 GT335/ARL13B
GSC23 GT335/ARL13B
5μm
20μm
D
GSC3028
GSC23
Primary cilia+ cells (%)
GSK-1070916 (μM)
E
GSC23
p-Aurora kinase B
Aurora kinase B
GLI1
β-Actin
GSK-1070916 - 2 5 (μM)
F
GSC387
Average synergy score: 11.13
GSC23
Average synergy score: 13.54
Synergy Score
Sonidegib (μM)
GSK-1070916 (μM)
G
GSC23
GSC3028
Percent survival
Time (Days)
shCONT
shKLHDC8A .883
shKLHDC8A .1842
H
GSC23
GSC3028
KLHDC8A mRNA expression (Normalized to shCONT)
shCONT
shKLHDC8A

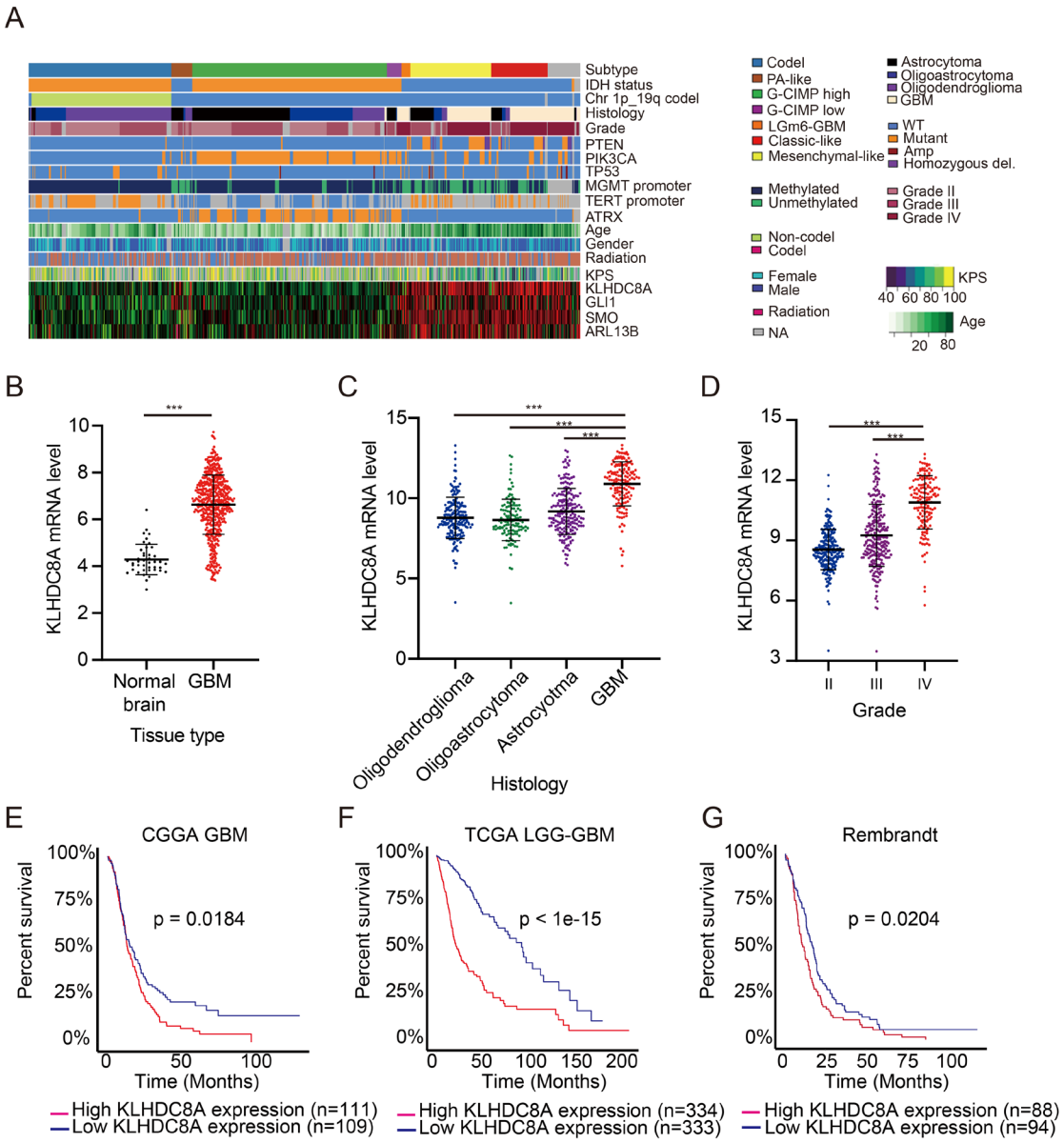

Figure 4.6. Clinical relevance of KLHDC8A.

(**A**) Heatmap showing RNA-seq, whole-exome-seq, and clinical phenotype data along with KLHDC8A, GLI1, SMO, and ARL13B expression in each glioblastoma patient. (**B**) mRNA expression (TPM) of KLHDC8A in glioblastoma ($n = 163$) and normal brain ($n = 21$) in the TCGA GBM dataset. (**C** and **D**) KLHDC8A mRNA levels in different gliomas (**C**) or different grades (**D**) in TCGA glioma datasets. Data are presented as mean ± SD. Statistical significance was determined using one-way ANOVA followed by Tukey's multiple comparisons. *** $P < 0.001$. (**E-G**) Kaplan-Meier curves displaying survival of patients in CCGA GBM (**E**), TCGA LGG-GBM (**F**), and Rembrandt (**G**) datasets stratified based on median mRNA expression of KLHDC8A. Data are presented as mean ± SD. Statistical significance was determined using log-rank test. $P = 0.0184$ for CGGA GBM; P <1e-15 for LGG-GBM; $P = 0.0204$ for Rembrandt.

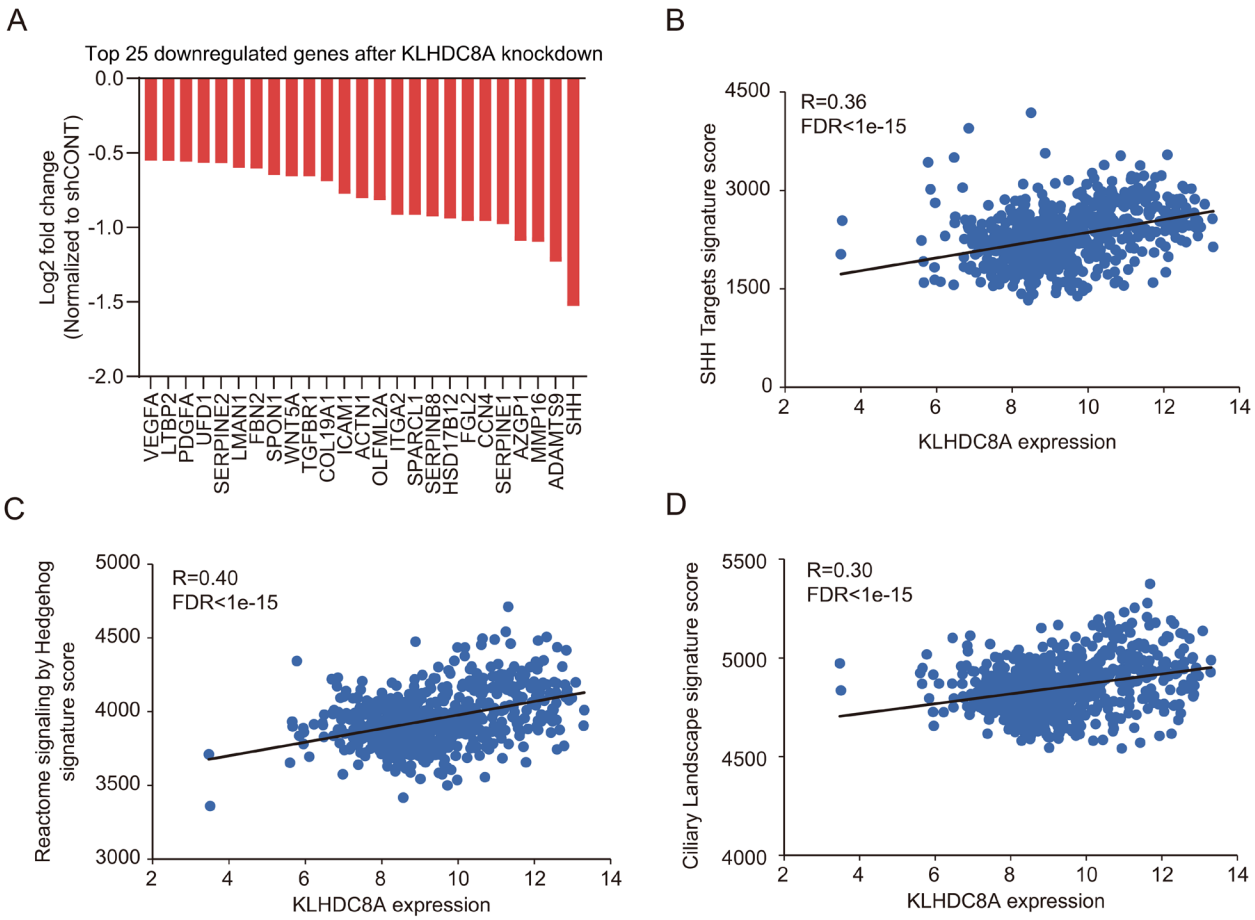

Figure 4.S1. KLHDC8A mRNA expression is positively correlated with Shh and ciliary gene signatures, related to Figures 4.1 and 4.2.

(**A**) Bar plot showing top 25 downregulated genes from RNA-seq analysis after KLHDC8A knockdown. (**B**) Correlation between KLHDC8A expression and the expression of genes from Shh targets signature. (**C**) Correlation between KLHDC8A expression and the expression of genes from Reactome signaling by Hedgehog signature. (**D**) Correlation between KLHDC8A expression and the expression of genes from Ciliary Landscape signature.

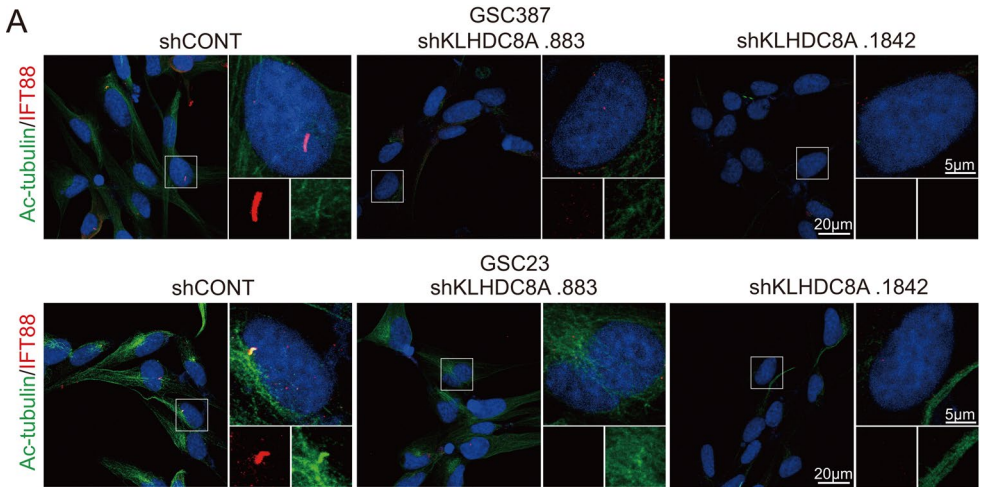

Figure 4.S2. Knockdown of KLHDC8A led to loss of primary cilia, related to Figure 4.3. Immunofluorescence imaging of primary cilia in GSC387 and GSC23 transduced with shCONT or two non-overlapping shRNAs targeting KLHDC8A. Ac-tubulin was labeled as green, IFT88 as red, and DAPI as blue. Scales bars represent 5 or 20 μm.

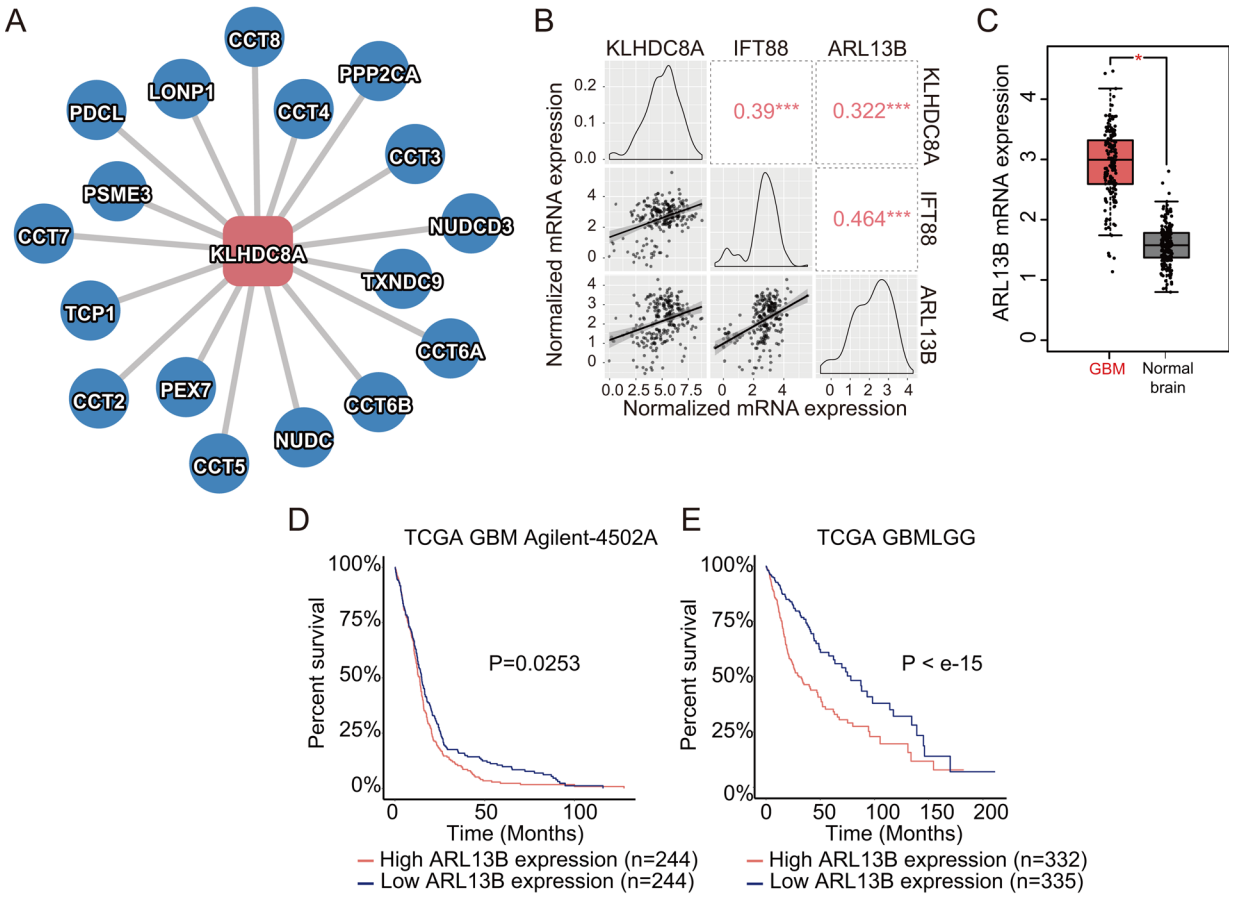

Figure 4.S3. ARL13B is upregulated in glioblastoma tissues and informs poor patient prognosis, related to Figure 4.4.

(**A**) Interaction network analysis of KLHDC8A and KLHDC8A binding proteins. The node in red (rectangular) represents KLHDC8A and the nodes in blue (circle) represent KLHDC8A binding partners. (**B**) Correlation of mRNA expression between KLHDC8A, IFT88, and ARL13B in the CGGA glioblastoma dataset. Numbers indicate the R-value of Spearman correlation. *** $P < 0.001$. (**C**) mRNA expression (TPM) of KLHDC8A in normal brain (GTEx dataset, $n = 207$) and glioblastoma (TCGA dataset, $n = 163$). Statistical significance was determined using four-way ANOVA to control for variables. (**D**) Kaplan-Meier survival curve of glioblastoma patients in the TCGA Agilent-4502A dataset stratified based on median mRNA expression of ARL13B. Statistical significance was determined using log-rank analysis. $P = 0.0253$. (**E**) Kaplan-Meier survival curve of glioma patients in the TCGA GBMLGG dataset stratified based on median mRNA expression of ARL13B. Statistical significance was determined using log-rank analysis. $P < 1e\text{-}15$.

MATERIALS AND METHODS

Derivation and culture of GSCs, nonmalignant brain cultures, and NSCs

Patient-derived GSCs, GSC387, and GSC3028 were generated in our laboratory, as previously described (125). GSC23 was obtained via a material transfer agreement from The University of Texas MD Anderson Cancer Center (Houston, TX). Nonmalignant brain cultures (NM176, NM177, and NM290) were derived in our lab from epilepsy surgical resection specimens. ENSAs are human embryonic stem-derived neural progenitor cells (Millipore). NSCs are human-induced pluripotent-derived neural progenitor cells (ALSTEM). hNP1s are human iPSC-derived neural progenitors derived from the hESC WA09 line. All NSCs and GSCs were cultured in Neurobasal™ media (Invitrogen) supplemented with B27 without vitamin (Invitrogen), sodium pyruvate, Glutamax, epidermal growth factor, and basic fibroblast growth factor (20 ng/ml each; R&D Systems). Differentiated glioblastoma cells derived from GSCs were generated and maintained in DMEM supplemented with 10% FBS. Short tandem repeats analyses were carried out every year to authenticate the identity of each tumor model. GSCs were passaged for less than 20 times *in vitro* from xenografts.

Immunofluorescence staining

Cells were grown on coverslips coated with Matrigel® hESC-Qualified Matrix (Cat#354277; Corning). After treatment, cells were fixed with 4% paraformaldehyde in PBS at room temperature for 10 minutes, followed by permeabilization with PBS containing 0.5% TritonX-100 at room temperature for 15 minutes, and blocking with PBS containing 5% goat serum and 0.1% TritonX-100 at room temperature for at least 1 hour. Cells were incubated with desired primary antibodies overnight at 4°C. All antibodies used in this study are listed in Table 1.

Cells were washed with PBS and incubated with fluorescent-dye conjugated secondary antibodies (1:500; Sigma) at room temperature for 1 hour. Cells were washed with PBS and incubated with PBS supplemented with DAPI at room temperature for 5 minutes. After the final wash with PBS, slides were mounted with ProLong™ Diamond Antifade Mountant (Cat# P36965; ThermoFisher) and imaged with the Leica SP8 CLARITY confocal microscope. Images were captured using 20X air or 100X oil objectives. The interval between the Z stacks was kept 0.5 μm apart. Images were processed using Leica Application Suite X software and Adobe Illustrator CS6.

Western blotting

Cells were lysed in Radio-Immunoprecipitation assay (RIPA) buffer supplemented with protease inhibitors and phosphatase inhibitors on ice for 30 minutes. Lysates were centrifuged at 4°C for 15 minutes at 14,000 x g, and the supernatants were collected. The concentration of lysates was determined by utilizing the Bicinchoninic acid (BCA) assay according to the manufacturer's protocol. Equal amounts of protein samples were mixed with 6x SDS Laemmi loading buffer and were boiled for 10 minutes. The protein samples were used directly for SDS-PAGE electrophoresis or stored at -80°C. The polyvinylidene difluoride (PVDF) membranes with proteins were blocked with 5% non-fat milk in TBST at room temperature for 1 hour, followed by incubation with primary antibodies overnight at 4°C. All the antibodies used in this study are listed in Table 1. The membranes were incubated with desired secondary antibodies and were developed by SuperSignal West Pico Plus Chemiluminescent Substrate (Cat# 34580; Thermo Fisher Scientific) and were imaged using BioRad image lab software.

Plasmids and lentiviral transduction

Lentiviral vectors expressing two non-overlapping shRNAs targeting KLHDC8A, SOX2, ARL13B, or a control shRNA that does not target any known mammalian genes were obtained from Sigma-Aldrich. All shRNAs used in this study were listed in Table 2. For lentivirus production, 293FT cells were co-transfected with lentiviral plasmids bearing shRNA sequences, viral packaging vectors pCMV-dR8.2, and VSVG using LipoD293™ In Vitro DNA Transfection Reagent (SignaGen Cat# SL100668) in DMEM supplemented with 10% FBS according to the manufacturer's protocol. Culture medium was replaced to complete DMEM medium 72 hours after transfection. Medium containing virus particles was collected, and the supernatant was filtered with a 0.45-μm filter. Lenti-X Concentrator (TaKaRa Cat# 631232) was used to concentrate the virus according to the manufacturer's protocol. The virus particles were resuspended in complete Neurobasal medium and were used immediately or stored at −80°C.

Quantitative RT-PCR

Total cellular RNA was isolated using Trizol reagent (Cat# 15596072; Invitrogen) and Direct-zol RNA Miniprep Kits (Cat# R2052; Zymo Research) according to the manufacturer's instructions. The RNA was eluted and dissolved in RNase-free water and was subsequently reversed transcribed by using a cDNA Reverse Transcription kit (Cat# 4368814; Life Technologies). All cDNAs were reverse transcribed from 1 μg total RNA. Quantitative RT-PCR was performed using the Applied Biosystems 7900HT cycler with the Radiant Green Hi-ROX qPCR kit (Cat# QS2050; Alkali Scientific).

Apoptosis assay

Apoptosis was assessed using the FITC Annexin V Apoptosis Detection Kit I (Cat# 556547; BD Bioscience) according to the manufacturer's protocol. Briefly, cells were harvested and washed twice with ice-cold PBS. Appropriated numbers of cells were incubated in 100 µl Annexin-binding buffer containing FITC annexin V and Propidium iodide (PI) at room temperature in the dark for 15 minutes. 400 µl Annexin-binding buffer was subsequently added to each sample. The samples were processed for flow cytometry analysis using a BD LSR Fortessa Flow Cytometer.

Proliferation and neurosphere formation assays

2,000 cells were plated in each well of a 96-well plate with four to five replicates. CellTiter-Glo (Promega) assay was used to measure the cell viability on days 1, 3, 5, and 7 according to the manufacturer's protocol. All data from different time points were normalized to the data of day 0. Error bars were presented as mean +/- standard deviation. Neurosphere formation capacity was assessed by in vitro limiting dilution assay. Briefly, different numbers of cells (50, 20, 10, and 1) were plated into 96-well plates with 24 replicates. After seven days of culture, the number of neurospheres in each well was counted. The frequencies of stem cells were calculated by using software available at http://bioinf.wehi.edu.au/software/elda.

H3K27ac ChIP-seq analysis

H3K27ac ChIP-seq data for glioblastoma tissues and GSCs were accessed and downloaded through GSE101148, GSE72468, and GSE119834. Single-end fastq files of H3K27ac and Input ChIP-seq reads were first trimmed to get rid of adaptor sequences using "Trim Galore!". "Bowtie2" was used to align ChIP-seq reads to the hg19 reference genome. The output SAM files were converted to BAM files and sorted by genomic coordinates using "SAMtools" and "Sambamba".

H3K27ac peaks were called using "MACS2" using ChIP input files as controls with a q-value cutoff of 0.001. To visualize the enrichment patterns at particular locations in the genome and evaluate regions of differential enrichment, Bigwig files were generated from BAM files using "DeepTools" 3.5.0 BamCoverage. Superenhancers in glioblastoma tissues and GSCs were identified by using the Rank-Ordering of Super-Enhancers (ROSE) algorithm on the hg19 human genome. ROSE was performed with a stitching distance of 12,500 bp and a transcriptional start site exclusion distance of 2,500 bp. Superenhancers were ranked by counting the H3K27ac signal in the ChIP file compared to the matched input file. De novo motifs were called from GSC enhancer regions within glioblastoma tissue superenhancers using the Hypergeometric Optimization of Motif EnRichment (HOMER) "findmotifsgenome.pl" script. Top scoring enriched motifs and transcription factors were presented.

In vitro drug treatments and synergy calculations

Cells were plated at 5000 cells per well in 96-well plates with at least five replicates and were incubated with DMSO or desired drugs at multiple concentrations for 72 hours. Cell viability was assessed by performing CellTiter-Glo (Promega) assay according to the manufacturer's protocol. For synergy calculations, synergy indices of Aurora kinase B inhibitor and Sonidegib were analyzed by R package Synergyfinder.

Coimmunoprecipitation assay

GSCs expressing FLAG-KLHDC8A were collected and washed with ice-cold PBS. Cell pellets were resuspended in Pierce™ IP Lysis Buffer (Thermo Scientific™ Cat# 87787) supplemented with protease and phosphatase inhibitors and were placed on ice for 30 minutes.

Cell lysates were centrifuged at 14,000 x g for 15 minutes at 4°C, and the supernatant was harvested. The concentration of lysates was determined by utilizing the Bicinchoninic acid (BCA) assay according to the manufacturer's protocol. 1mg of cell lysate was mixed with Anti-FLAG® M2 Magnetic Beads (MilliporeSigma Cat# M8823) and rotated at 4°C overnight. The beads were washed with Pierce™ IP Lysis Buffer three times and were boiled in 2X SDS Laemmli loading buffer at 95°C for 5 minutes. The supernatant was collected and used for Western blot analysis.

RNA-seq analysis

RNA-seq data for GSC versus DGC comparisons were accessed from Gene expression Omnibus (GEO GSE547391). Three pairs of matched GSCs and DGCs (MGG4, MGG6, and MGG8) were used for this study. Counts-per-million and differential expression were calculated using Limma in R. Differentially expressed genes were filtered with an mRNA expression fold change cutoff of $\log_2 > 2$ or < -2 and with an adjusted P-value of less than 0.001.

For RNA-seq analysis upon KLHDC8A knockdown, total cellular RNAs from GSCs transduced with shCONT or shKLHDC8A were isolated by Trizol reagent (Cat# 15596072; Invitrogen) and Direct-zol RNA Miniprep Kits (Cat# R2052; Zymo Research) according to the manufacturer's instructions. The purified RNA was eluted and dissolved in RNase-free water and was subsequently subjected to RNA sequencing. The fastq files of the RNA-seq data were subjected to quality control using "FastQC", and the adaptor sequences were removed by performing "TrimGalore". The trimmed reads were mapped to hg19 human genome and were counted by using “Salmon”. Salmon output files were further processed by running Tximport, and differential expression analysis was carried out using DESeq2 in R. The volcano plot displaying

differentially expressed genes was generated using GraphPad Prism. A pre-ranked gene list was generated by selecting differentially expressed genes with an adjusted p-value less than 0.05. Gene set enrichment analysis (GSEA) was performed by uploading the pre-ranked gene list into GSEA software. Bubble plots were generated using Cytoscape. All original RNA-seq data generated in this study were deposited in the NCBI's Gene Expression Omnibus (GEO) database (GEO GSE207760).

In vivo tumorigenesis

10,000 GSCs transduced with shCONT or shKLHDC8A were intracranially injected into the right cerebral cortex of NSG (NOD.Cg-*Prkdc*^{scid} *Il2rg*^{tm1Wjl}/SzJ; The Jackson Laboratory) mice at a depth of 3.5 mm. All mouse experiments were performed under a University of California, San Diego, Institutional Animal Care and Use Committee–approved protocol. At least 4 to 6 weeks old, healthy, wild-type male or female NSG mice were randomly selected. All mice were monitored every day until neurological signs, at which point they were sacrificed.

Statistics

For qPCR analysis, statistical significance between 2 groups was determined by Student's t-test. Two-way ANOVA followed by Dunnett multiple comparison were performed for statistical analysis when appropriate. For mice survival analysis, the statistical significance between different treatment groups was determined by using log-rank tests. For cell proliferation assays, two-way ANOVA with Dunnett multiple hypothesis test correction were applied for statistical analysis. For extreme limiting dilution assay, the $\chi 2$ test was used for pairwise differences in evaluating stem cell frequencies. All statistical analyses are provided in the figure legends.

Study approval

All murine experiments were performed under an animal protocol (s17096) approved by the Institutional Animal Care and Use Committee of the University of California, San Diego. This work does not contain human subjects research.

Table 4.1. Antibodies used in this study

All the antibodies used in this study are listed

Antigen	Host	Vendor	Catalog#	Dilution (WB)	Dilution (IF)
KLHDC8A	Rabbit	Novus	NBP1-31181	1:1000	
PARP	Rabbit	Cell signaling	9532	1:1000	
OLIG2	Mouse	Millipore	MABN50	1:1000	
SOX2	Rabbit	AB5604	AB5603	1:1000	
IFT88	Rabbit	Proteintech	13967-1-AP	1:1000	1:200
ARL13B	Rabbit	Proteintech	17711-1-AP	1:1000	1:200
Gli1	Rabbit	Cell signaling	2534T	1:1000	
SHH	Rabbit	Proteintech	20697-1-AP	1:1000	
Acetylated- α -tubulin(Lys40	Mouse	Proteintech	66200-1-lg	1:1000	1:200
α -tubulin	Mouse	Cell signaling	3873S	1:5000	
TCP1	Rabbit	Abcam	Ab225702	1:1000	
β-actin	Rabbit	Proteintech	HRP-60008	1:40000	
GT335	Mouse	Adipogen	AG-20B-0020-C100		1:200
Phospho-Aurora A (Thr288)/Aurora B (Thr232)/Aurora C (Thr198) (D13A11) XP®	Rabbit	Cell signaling	2914	1:500	
Aurora B/AIM1 Antibody	Rabbit	Cell signaling	3094T	1:1000	
GFAP	Rabbit	Proteintech	16825-1-AP	1:1000	

Table 4.2. DNA oligos used in this study

All the DNA oligos used in this study are listed

Primer oligos for quantifying gene expression		
Target	**Strand**	**Sequence (5'->3')**
KLHDC8A	Forward	ATGGAGGTGCCTAACGTCAAG
	Reverse	CCGTTGTCGTCACATCCCC
SOX2	Forward	GCCGAGTGGAAACTTTTGTCG
	Reverse	GGCAGCGTGTACTTATCCTTCT
OLIG2	Forward	CCAGAGCCCGATGACCTTTTT
	Reverse	CACTGCCTCCTAGCTTGTCC
GFAP	Forward	CTGCGGCTCGATCAACTCA
	Reverse	TCCAGCGACTCAATCTTCCTC
SHH	Forward	CTCGCTGCTGGTATGCTCG
	Reverse	ATCGCTCGGAGTTTCTGGAGA
GLI1	Forward	AGCGTGAGCCTGAATCTGTG
	Reverse	CAGCATGTACTGGGCTTTGAA
CCND1	Forward	GCTGCGAAGTGGAAACCATC
	Reverse	CCTCCTTCTGCACACATTTGAA
CCND2	Forward	ACCTTCCGCAGTGCTCCTA
	Reverse	CCCAGCCAAGAAACGGTCC
CCNE1	Forward	AAGGAGCGGGACACCATGA
	Reverse	ACGGTCACGTTTGCCTTCC
c-MYC	Forward	GGCTCCTGGCAAAAGGTCA
	Reverse	CTGCGTAGTTGTGCTGATGT
CXCR4	Forward	ACTACACCGAGGAAATGGGCT
	Reverse	CCCACAATGCCAGTTAAGAAGA
FOXM1	Forward	CGTCGGCCACTGATTCTCAAA
	Reverse	GGCAGGGGATCTCTTAGGTTC
c-JUN	Forward	TCCAAGTGCCGAAAAAGGAAG
	Reverse	CGAGTTCTGAGCTTTCAAGGT
GAPDH	Forward	GGAGCGAGATCCCTCCAAAAT
	Reverse	GGCTGTTGTCATACTTCTCATGG
DNA oligos for shRNA		
Target	**TRC number**	
KLHDC8A	TRCN0000138219	
	TRCN0000138761	
ARL13B	TRCN0000381968	
	TRCN0000381442	
SOX2	TRCN0000355694	
	TRCN0000355638	
DNA oligos for CRISPR Cas9-KRAB gRNA		

Table 4.2. DNA oligos used in this study (Continued)

Target	Strand	Sequence (5'->3')
Non-targeting	Forward	CACCGCTCTGCTGCGGAAGGATTCG
	Reverse	AAACCGAATCCTTCCGCAGCAGAGC
KLHDC8A SE gRNA1	Forward	CACCGCGCGGGGTGGCGATCAATGGAGG
	Reverse	AAACCCTCCATTGATCGCCACCCCGCGC
KLHDC8A SE gRNA2	Forward	CACCGGAACGCGGGGTGGCGATCAATGG
	Reverse	AAACCCATTGATCGCCACCCCGCGTTCC
KLHDC8A SE gRNA3	Forward	CACCGGGCGATCAATGGAGGATTACCGG
	Reverse	AAACCCGGTAATCCTCCATTGATCGCCC
KLHDC8A SE gRNA4	Forward	CACCGTTGTTCCAGCCGAAATTAGCAGG
	Reverse	AAACCCTGCTAATTTCGGCTGGAACAAC
KLHDC8A SE gRNA5	Forward	CACCGATTACCGGAAGATGTGCAAATGG
	Reverse	AAACCCATTTGCACATCTTCCGGTAATC

DISCLOSURE OF POTENTIAL CONFLICTS OF INTEREST

The authors declare no competing interests.

AUTHOR CONTRIBUTION

D.L. conceptualized and designed the study, acquired and analyzed the results, and wrote the manuscript. R.C.G. analyzed RNA-Seq data and revised the manuscript. B.C.P. analyzed and interpreted the bioinformatics data. Z.Q. analyzed the bioinformatic data and provided experimental assistance of animal experiments. Q.W. provided experimental assistance of intracranial injections. J.G. and V.D. revised the manuscript and provided technical support. D.R.R. and J.N.R. designed the study, wrote and revised the manuscript, and provided study supervision, administrative, and material support.

ACKNOWLEDGMENTS

Chapter 4 contains data of the material that has been submitted for publication as it may appear in the Journal of Clinical Investigation, 2022, Derrick Lee, Ryan C. Gimple, Xujia Wu, Briana C. Prager, Zhixin Qiu, Qiulian Wu, Vikas Daggubati, Aruljothi Mariappan, Jay Gopalakrishnan, Matthew R. Sarkisian, David R. Raleigh, Jeremy N. Rich. The dissertation author was the primary researcher and author of this paper. This work was supported by National Institutes of Health: Derrick Lee, CA243296; Briana C. Prager, CA217066; Ryan C. Gimple, CA217065; David R. Raleigh, HD106238, CA251221, CA262311; Jeremy N. Rich, P30 CA047904, CA238662, CA197718, NS103434.

CHAPTER 5

CONCLUSION

Glioblastoma is a devastating disease with a median survival of less than 15 months and with limited therapeutic modalities. Despite intensive efforts in defining its molecular characteristics, including its genetics and epigenetics, current knowledge has not been translated into clinical practice due to high intra- and intertumoral heterogeneity within the tumors and extensive cellular plasticity and enhanced invasiveness of glioblastoma stem cells. Furthermore, the interactions between GSCs and differentiated progeny and between cancer cells and their microenvironment, which includes the surrounding immune cells and vasculature, contribute to the resistance and resilience of GSCs. Therefore, understanding the molecular processes that support GSC growth will allow us to identify the core GSC regulators and potential therapeutic vulnerabilities.

To interrogate the therapeutic vulnerabilities among GSCs, we leveraged superenhancer screening approaches and identified KLHDC8A, a protein with previously unknown function. KLHDC8A is upregulated in GSCs at both mRNA and protein levels, and targeting KLHDC8A reduced cell proliferation, induced apoptosis, and inhibited the *in vivo* tumor formation capacity of multiple GSC lines, suggesting that KLHDC8A may be a universal molecular target for GSCs, and that inhibiting KLHDC8A and its downstream molecular pathways may offer therapeutic benefits for targeting the heterogeneity of GSCs. Further investigation revealed that KLHDC8A promotes ciliogenesis to support Hedgehog signaling. Hedgehog signaling has been identified as a key signaling pathway that is critical in embryonic development, stem cell population maintenance in adult tissues, and tumorigenesis of cancer cells. Several Hedgehog pathway inhibitors have been developed to combat multiple cancers and their clinical efficacy is observed

in multiple cancer types, but therapeutic resistance to these inhibitors has been reported, suggesting that novel therapeutic strategies for targeting this pathway, including combinatorial treatments with chemotherapy agents or inhibitors targeting other signaling pathways, should be considered. Given that KLHDC8A is undruggable based on its molecular structure, we leveraged the CTRP dataset, which stores drug sensitivity and mRNA expression data of cancer cells and identified Aurora B/C kinase inhibitor as a potential molecular target for GSCs. Unexpectedly, we found that treating GSCs with Aurora B/C kinase inhibitor promoted ciliogenesis and Hedgehog signaling, which has never been reported before. Dual targeting of Hedgehog signaling and Aurora B/C kinases synergistically inhibited GSC growth, offering a novel paradigm for treating glioblastoma.

FUTURE DIRECTIONS

Aim 1. Determine the functional importance and frequency of primary cilia-positive cells in GSCs and glioblastoma tissues.

In this report, we found that approximately 25-30% of GSCs display primary cilia and that targeting critical primary cilia regulator ARL13B led to suppression of cell proliferation and downregulation of Hedgehog signaling, suggesting that primary cilia play an essential role in promoting GSC maintenance in a context-dependent manner. However, whether primary cilia are preferentially found in stem-like populations, and the frequency of primary cilia-positive cells in glioblastoma tissues and other GSCs, remain areas of investigation. It is also intriguing to ask whether the presence of primary cilia is associated with a quiescent or proliferating cell state. Furthermore, the staining of primary cilia in GSCs was done in 2D culture, with GSCs attached to Matrigel-coated cell culture plates. However, GSCs exhibit anchorage-independent growth capability and grow as spheres in serum-free media. It will also be interesting to see if GSCs still

display primary cilia and if the frequency of ciliated GSCs is higher or lower in 3D culture systems, such as organoids and mouse xenografts.

Experimental approaches

Determine the prevalence of primary cilia in other GSC lines and glioblastoma tissues.

To understand the percentage of ciliated cells in glioblastoma tissues and other GSC lines, I will stain GSCs and glioblastoma tissues with two different combinations of antibodies, such as anti-polyglutaminated tubulin and IFT88, ARL13B, and gamma-tubulin, to evaluate the structure of primary cilia and perform immunofluorescence using confocal microscopy. The percentage of ciliated cells will be counted and calculated with at least 300 cells per group. Furthermore, to interrogate if primary cilia formation is associated with stemness and proliferation, I will stain primary cilia in GSCs and glioblastoma tissues using anti-ploy glutamylated tubulin and stemness marker SOX2 or proliferation marker Ki67.

Interrogate the presence and the frequency of ciliated GSCs in 3D culture systems

To assess the primary cilia in 3D culture systems, we will use a 3D bioprinting technique developed by our lab and others to generate 3D bioprinted organoids. These bioprinted organoids derived by GSCs alone or with other cell types, such as astrocytes and macrophages, can recapitulate glioblastoma transcriptional profiles, model complex cellular interactions and migrations, and serve as a platform for high-throughput drug screening. Briefly, GSCs with or without other cell types are dissociated into single cells. Cell suspensions are mixed with photosensitive prepolymer solution containing 8% (w/v) GelMA, 0.5% (w/v) GMHA, and 0.6% (w/v) lithium phenyl(2,4,6-trimethylbenzoyl)phosphinate in a 1:1 ratio. The two-step bioprinting

process is carried out first by loading the cell-material mixture onto the printing stage and then by shining the laser onto the mixture. To assess the primary cilia in 3D bioprited samples, I will use serial section electron tomography (SSET) to evaluate the structure of primary cilia and the percentages of primary cilia-positive GSCs within the organoids. Additionally, laser scanning confocal fluorescence microscopy will be utilized to interrogate the percentage of GSCs within organoids displaying primary cilia. In addition to 3D bioprinted organoids, we will generate an orthotopic xenograft mouse model by performing an intracranial injection of 10,000 GSCs into the mouse brain. The tumors will be harvested and subjected to immunofluorescence staining using anti-polyglutamylated tubulin and anti-ARL13 antibodies.

Aim 2. Determine the molecular mechanisms by which Aurora B/C kinases regulate ciliogenesis.

In our previous work, we found that inhibition of Aurora B/C kinases led to a significant increase in the frequency of ciliated cells. The role of Aurora kinase A in ciliogenesis has been demonstrated by other groups, finding that Aurora kinase A activation induces primary cilia disassembly via interacting and activating HDAC6, a deacetylase which catalyzes the deacetylation of tubulins and triggers the reabsorption of primary cilia to ensure proper cell cycle progression. However, the role of Aurora B/C kinases in ciliogenesis is still unclear. Aurora kinase A and B have very distinct functions, with Aurora kinase A regulating centrosome dynamic and spindle assembly, and Aurora kinase B involved in proper chromosome segregation and cell cycle progression in mitosis. However, recent studies have demonstrated that Aurora kinase A and B share similar functions in regulating spindle formation and chromosome segregation. Inactivation of both Aurora kinase A and B completely abrogated chromosome segregation, suggesting an

overlapping function of Aurora kinase A and B in mitosis. Based on this finding, it is possible that Aurora kinase B also regulates primary cilia, similar to Aurora kinase A. To identify the potential molecular mechanism of how Aurora kinase B regulates ciliogenesis, we interrogated the BIOGRID dataset, which has the protein-protein interaction data of more than 20,000 proteins, and found that Aurora kinase B interacts with NEK2 and family members of the ciliary disassembly complex (CDC) (Figure 5.1A). Additionally, Aurora kinase B expression is positively correlated to the expression of NEK2 and CDC20 (Figure 5.1B), suggesting that the Aurora kinase B may interact and promote the activation of NEK2 and CDC, which then trigger primary cilia disassembly, before entering mitosis.

Experimental approaches

As a proof-of-principle rescue experiment, I will first interrogate if there is an interaction between Aurora kinase B, NEK2, and CDC20 in GSCs. I will perform a co-immunoprecipitation (Co-IP) assay using anti-Aurora kinase B antibody and then blot the membrane with anti-NEK2 and anti-CDC20 antibodies. Additionally, I will also probe the membrane with anti-p-Aurora kinase B to see if the activation of Aurora kinase B is required for interacting with NEK2 and CDC20. Additionally, I will perform reciprocal pulldown using anti-NEK2 or anti-CDC20 antibody and the subsequent immunoblot experiment. To assess if the increased frequency of ciliated cells after Aurora B/C kinase inhibition is mediated by NEK2, we will treat GSCs first with NEK2 inhibitor JH295 and then add Aurora B/C kinases inhibitor GSK1070916. The presence and structure of primary cilia will be validated by confocal microscopy. These experiments will allow us to understand the molecular mechanisms of how Aurora B/C kinases regulate primary cilia formation.

Aim 3. Evaluate the combinatorial efficacy of epigenetic inhibitors, Hedgehog inhibitors, and Aurora B/C kinase inhibitors

Our study demonstrated that superenhancer-activation of KLHDC8A promotes ciliogenesis to support Hedgehog signaling, and that targeting Aurora B/C kinases in GSCs is a novel KLHDC8A-based therapeutic dependency. Dual inhibition of Aurora B/C kinases and Hedgehog signaling synergistically inhibited GSC growth *in vitro.* However, this novel combination treatment has not yet been tested in preclinical models. Moreover, treating GSCs with the epigenetic inhibitor GSK620, which preferentially inhibits the expression of superenhancer-associated genes, led to downregulation of KLHDC8A expression and reduced cell proliferation. Given the role of KLHDC8A in promoting ciliogenesis, we hypothesize that targeting superenhancers with small molecule inhibitors in combination with Aurora B/C kinase inhibitor or Hedgehog inhibitor may serve as a novel therapeutic strategy for killing GSCs.

Experimental Approaches

Determine the efficacy of dual targeting Aurora B/C kinase and Hedgehog signaling in *vivo*

To assess the efficacy of this combination treatment, we will perform an intracranial injection of 1,000 GSCs into the right cerebral cortex of NSG mice (NOD.Cg-Prkdcscid Il2rgtm1Wjl/SzJ). After 7 days of recovery, mice are given either 50 mg/kg of the Aurora kinase B inhibitor Barasertib, 50 mg/kg of the Hedgehog inhibitor Sonidegib, or a pre-mixed combination of 50 mg/kg of both inhibitors daily with intraperitoneal injection. Mice are monitored for tumor volume and overall survival until neurological signs are observed. The mouse brains will be harvested, and hematoxylin and eosin (H&E) staining will be performed for histological analysis.

Evaluate the combinatorial effect of epigenetic inhibitors with Aurora B/C kinase inhibitors or Hedgehog inhibitors *in vitro* and *in vivo*

Bromo- and extra-terminal domain (BET) family members promote tumorigenesis by altering chromatin modification in various cancers. Recent efforts devoted to the development of BET inhibitors have achieved clinical success (173). However, BET proteins are critical for the expression of genes that control a wide range of important cellular processes, and high concentrations of BET inhibitors may lead to systemic toxicities. Therefore, alternative approaches, such as low concentration of BET inhibitors in combination with other pathway inhibitors, will be essential for overcoming these toxicities.

To evaluate the combination treatment of epigenetic inhibitors with Aurora kinase B or Hedgehog inhibitors, we will first perform an intracranial injection of 5,000 GSCs into NSG mice, as described above. After 7 days of injection, mice will be treated daily with Aurora kinase B inhibitor Barasertib (50mg/kg) or Hedgehog inhibitor Sonidegib (50mg/kg), alone or in combination with the pan-bromodomain 2 inhibitor GSK620 (50 mg/kg), a potent and orally active inhibitior with good pharmacokinetics and low side effects. The overall survival of mice will be monitored every day until neurological signs are observed.

FIGURES

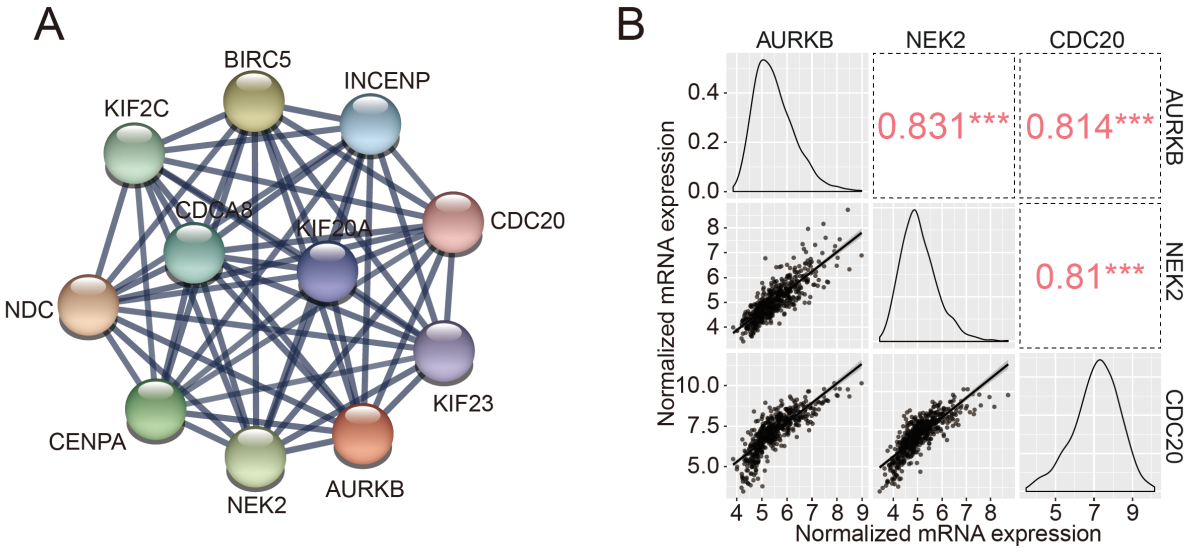

Figure 5.1. Aurora kinase B is associated with primary cilia-disassociation related genes. (**A**) Interaction network analysis of Aurora kinase B and Aurora kinase B binding proteins. The node in red (circle) represents Aurora kinase B and the other nodes represent Aurora kinase B binding partners. (**B**) Correlation of mRNA expression between Aurora kinase B, NEK2, and CDC20 in the TCGA glioblastoma dataset. Numbers indicate the R-value of Spearman correlation. *** $P < 0.001$.

DISCUSSION

Glioblastoma is a deadly disease with limited therapeutic modalities. Our investigation of the superenhancer landscape in GSCs and glioblastoma tissues has uncovered GSC-specific vulnerabilities. Superenhancers drive the expression of genes that define the cell state and regulate cell-type-dependent transcriptional networks. Targeting superenhancer and superenhancer-associated genes using Bromodomain inhibitors led to downregulation of superenhancer-associated genes and stemness markers, including OLIG2 and SOX2, suggesting that targeting superenhancers may provide a novel therapeutic strategy for glioblastoma. Furthermore, dual targeting Aurora B/C kinases and hedgehog signaling exerted a synergistic effect on killing GSCs, suggesting that this treatment may eliminate the GSCs in glioblastoma tissues, inhibit tumor regeneration, and completely eradicate tumors with the combination of standard therapy. However, there are still limitations in the GSC models and intracranial xenograft models. GSCs have high intra- and inter- heterogeneity and display plasticity when they interact with other cell types and receive environmental cues. To recapitulate rapid disease progression and complex tumor ecosystems, we need better patient-derived GSC and glioblastoma tissue models that preserve heterogeneity. Technological advances in organoids, such as 3D biopriting models, have allowed us to model and recapitulate cellular interactions, such as with macrophages and pericytes. Furthermore, maintaining patient-derived glioblastoma tissues in mice can preserve the heterogeneity of GSCs, DGCs, immune cells, and endothelial cell lineages. Nevertheless, this study has advanced our understanding of GSC biology and its therapeutic dependencies, which contributes to the development of therapeutics and improves the lives of glioblastoma patients in the future.

ACKNOWLEDGMENTS

Chapter 5 contains unpublished materials that may or may not appear in future publications. The dissertation author solely completed all the work presented in chapter 5. This work was supported by National Institutes of Health: Derrick Lee, CA243296; Briana C. Prager, CA217066; Ryan C. Gimple, CA217065; David R. Raleigh, HD106238, CA251221, CA262311; Jeremy N. Rich, P30 CA047904, CA238662, CA197718, NS103434.

REFERENCES

1. Ostrom, Q.T., N. Patil, G. Cioffi, K. Waite, C. Kruchko, and J.S. Barnholtz-Sloan Corrigendum to: CBTRUS Statistical Report: Primary Brain and Other Central Nervous System Tumors Diagnosed in the United States in 2013-2017. *Neuro Oncol*. 2020.

2. Stupp, R., M.E. Hegi, W.P. Mason, M.J. van den Bent, M.J. Taphoorn, R.C. Janzer, S.K. Ludwin, A. Allgeier, B. Fisher, K. Belanger, P. Hau, A.A. Brandes, J. Gijtenbeek, C. Marosi, C.J. Vecht, K. Mokhtari, P. Wesseling, S. Villa, E. Eisenhauer, T. Gorlia, M. Weller, D. Lacombe, J.G. Cairncross, and R.O. Mirimanoff Effects of radiotherapy with concomitant and adjuvant temozolomide versus radiotherapy alone on survival in glioblastoma in a randomised phase III study: 5-year analysis of the EORTC-NCIC trial. *Lancet Oncol*. 2009. **10**(5): p. 459-66.

3. Stupp, R., S. Taillibert, A. Kanner, W. Read, D. Steinberg, B. Lhermitte, S. Toms, A. Idbaih, M.S. Ahluwalia, K. Fink, F. Di Meco, F. Lieberman, J.J. Zhu, G. Stragliotto, D. Tran, S. Brem, A. Hottinger, E.D. Kirson, G. Lavy-Shahaf, U. Weinberg, C.Y. Kim, S.H. Paek, G. Nicholas, J. Bruna, H. Hirte, M. Weller, Y. Palti, M.E. Hegi, and Z. Ram Effect of Tumor-Treating Fields Plus Maintenance Temozolomide vs Maintenance Temozolomide Alone on Survival in Patients With Glioblastoma: A Randomized Clinical Trial. *Jama*. 2017. **318**(23): p. 2306-2316.

4. Wick, W., T. Gorlia, M. Bendszus, M. Taphoorn, F. Sahm, I. Harting, A.A. Brandes, W. Taal, J. Domont, A. Idbaih, M. Campone, P.M. Clement, R. Stupp, M. Fabbro, E. Le Rhun, F. Dubois, M. Weller, A. von Deimling, V. Golfinopoulos, J.C. Bromberg, M. Platten, M. Klein, and M.J. van den Bent Lomustine and Bevacizumab in Progressive Glioblastoma. *N Engl J Med*. 2017. **377**(20): p. 1954-1963.

5. Gilbert, M.R., J.J. Dignam, T.S. Armstrong, J.S. Wefel, D.T. Blumenthal, M.A. Vogelbaum, H. Colman, A. Chakravarti, S. Pugh, M. Won, R. Jeraj, P.D. Brown, K.A. Jaeckle, D. Schiff, V.W. Stieber, D.G. Brachman, M. Werner-Wasik, I.W. Tremont-Lukats, E.P. Sulman, K.D. Aldape, W.J. Curran, Jr., and M.P. Mehta A randomized trial of bevacizumab for newly diagnosed glioblastoma. *N Engl J Med*. 2014. **370**(8): p. 699-708.

6. Chinot, O.L., W. Wick, W. Mason, R. Henriksson, F. Saran, R. Nishikawa, A.F. Carpentier, K. Hoang-Xuan, P. Kavan, D. Cernea, A.A. Brandes, M. Hilton, L. Abrey, and T. Cloughesy Bevacizumab plus radiotherapy-temozolomide for newly diagnosed glioblastoma. *N Engl J Med*. 2014. **370**(8): p. 709-22.

7. Killela, P.J., Z.J. Reitman, Y. Jiao, C. Bettegowda, N. Agrawal, L.A. Diaz, A.H. Friedman, H. Friedman, G.L. Gallia, B.C. Giovanella, A.P. Grollman, T.-C. He, Y. He, R.H. Hruban, G.I. Jallo, N. Mandahl, A.K. Meeker, F. Mertens, G.J. Netto, B.A. Rasheed, G.J. Riggins, T.A. Rosenquist, M. Schiffman, I.-M. Shih, D. Theodorescu, M.S. Torbenson, V.E. Velculescu, T.-L. Wang, N. Wentzensen, L.D. Wood, M. Zhang, R.E. McLendon, D.D. Bigner, K.W. Kinzler, B. Vogelstein, N. Papadopoulos, and H. Yan TERT

promoter mutations occur frequently in gliomas and a subset of tumors derived from cells with low rates of self-renewal. 2013. **110**(15): p. 6021-6026.

8. Brennan, C.W., R.G. Verhaak, A. McKenna, B. Campos, H. Noushmehr, S.R. Salama, S. Zheng, D. Chakravarty, J.Z. Sanborn, S.H. Berman, R. Beroukhim, B. Bernard, C.J. Wu, G. Genovese, I. Shmulevich, J. Barnholtz-Sloan, L. Zou, R. Vegesna, S.A. Shukla, G. Ciriello, W.K. Yung, W. Zhang, C. Sougnez, T. Mikkelsen, K. Aldape, D.D. Bigner, E.G. Van Meir, M. Prados, A. Sloan, K.L. Black, J. Eschbacher, G. Finocchiaro, W. Friedman, D.W. Andrews, A. Guha, M. Iacocca, B.P. O'Neill, G. Foltz, J. Myers, D.J. Weisenberger, R. Penny, R. Kucherlapati, C.M. Perou, D.N. Hayes, R. Gibbs, M. Marra, G.B. Mills, E. Lander, P. Spellman, R. Wilson, C. Sander, J. Weinstein, M. Meyerson, S. Gabriel, P.W. Laird, D. Haussler, G. Getz, and L. Chin The somatic genomic landscape of glioblastoma. *Cell*. 2013. **155**(2): p. 462-77.

9. Comprehensive genomic characterization defines human glioblastoma genes and core pathways. *Nature*. 2008. **455**(7216): p. 1061-8.

10. Cortés-Ciriano, I., J.J.-K. Lee, R. Xi, D. Jain, Y.L. Jung, L. Yang, D. Gordenin, L.J. Klimczak, C.-Z. Zhang, D.S. Pellman, K.C. Akdemir, E.G. Alvarez, A. Baez-Ortega, R. Beroukhim, P.C. Boutros, D.D.L. Bowtell, B. Brors, K.H. Burns, P.J. Campbell, K. Chan, K. Chen, I. Cortés-Ciriano, A. Dueso-Barroso, A.J. Dunford, P.A. Edwards, X. Estivill, D. Etemadmoghadam, L. Feuerbach, J.L. Fink, M. Frenkel-Morgenstern, D.W. Garsed, M. Gerstein, D.A. Gordenin, D. Haan, J.E. Haber, J.M. Hess, B. Hutter, M. Imielinski, D.T.W. Jones, Y.S. Ju, M.D. Kazanov, L.J. Klimczak, Y. Koh, J.O. Korbel, K. Kumar, E.A. Lee, J.J.-K. Lee, Y. Li, A.G. Lynch, G. Macintyre, F. Markowetz, I. Martincorena, A. Martinez-Fundichely, S. Miyano, H. Nakagawa, F.C.P. Navarro, S. Ossowski, P.J. Park, J.V. Pearson, M. Puiggròs, K. Rippe, N.D. Roberts, S.A. Roberts, B. Rodriguez-Martin, S.E. Schumacher, R. Scully, M. Shackleton, N. Sidiropoulos, L. Sieverling, C. Stewart, D. Torrents, J.M.C. Tubio, I. Villasante, N. Waddell, J.A. Wala, J. Weischenfeldt, L. Yang, X. Yao, S.-S. Yoon, J. Zamora, C.-Z. Zhang, P.J. Park, P.S.V.W. Group, and P. Consortium Comprehensive analysis of chromothripsis in 2,658 human cancers using whole-genome sequencing. *Nature Genetics*. 2020. **52**(3): p. 331-341.

11. deCarvalho, A.C., H. Kim, L.M. Poisson, M.E. Winn, C. Mueller, D. Cherba, J. Koeman, S. Seth, A. Protopopov, M. Felicella, S. Zheng, A. Multani, Y. Jiang, J. Zhang, D.H. Nam, E.F. Petricoin, L. Chin, T. Mikkelsen, and R.G.W. Verhaak Discordant inheritance of chromosomal and extrachromosomal DNA elements contributes to dynamic disease evolution in glioblastoma. *Nat Genet*. 2018. **50**(5): p. 708-717.

12. Turner, K.M., V. Deshpande, D. Beyter, T. Koga, J. Rusert, C. Lee, B. Li, K. Arden, B. Ren, D.A. Nathanson, H.I. Kornblum, M.D. Taylor, S. Kaushal, W.K. Cavenee, R. Wechsler-Reya, F.B. Furnari, S.R. Vandenberg, P.N. Rao, G.M. Wahl, V. Bafna, and P.S. Mischel Extrachromosomal oncogene amplification drives tumour evolution and genetic heterogeneity. *Nature*. 2017. **543**(7643): p. 122-125.

13. Ceccarelli, M., F.P. Barthel, T.M. Malta, T.S. Sabedot, S.R. Salama, B.A. Murray, O. Morozova, Y. Newton, A. Radenbaugh, S.M. Pagnotta, S. Anjum, J. Wang, G. Manyam, P. Zoppoli, S. Ling, A.A. Rao, M. Grifford, A.D. Cherniack, H. Zhang, L. Poisson, C.G. Carlotti, Jr., D.P. Tirapelli, A. Rao, T. Mikkelsen, C.C. Lau, W.K. Yung, R. Rabadan, J. Huse, D.J. Brat, N.L. Lehman, J.S. Barnholtz-Sloan, S. Zheng, K. Hess, G. Rao, M. Meyerson, R. Beroukhim, L. Cooper, R. Akbani, M. Wrensch, D. Haussler, K.D. Aldape, P.W. Laird, D.H. Gutmann, H. Noushmehr, A. Iavarone, and R.G. Verhaak Molecular Profiling Reveals Biologically Discrete Subsets and Pathways of Progression in Diffuse Glioma. *Cell*. 2016. **164**(3): p. 550-63.

14. Liu, A., C. Hou, H. Chen, X. Zong, and P. Zong Genetics and Epigenetics of Glioblastoma: Applications and Overall Incidence of IDH1 Mutation. *Front Oncol*. 2016. **6**: p. 16.

15. Noushmehr, H., D.J. Weisenberger, K. Diefes, H.S. Phillips, K. Pujara, B.P. Berman, F. Pan, C.E. Pelloski, E.P. Sulman, K.P. Bhat, R.G. Verhaak, K.A. Hoadley, D.N. Hayes, C.M. Perou, H.K. Schmidt, L. Ding, R.K. Wilson, D. Van Den Berg, H. Shen, H. Bengtsson, P. Neuvial, L.M. Cope, J. Buckley, J.G. Herman, S.B. Baylin, P.W. Laird, and K. Aldape Identification of a CpG island methylator phenotype that defines a distinct subgroup of glioma. *Cancer Cell*. 2010. **17**(5): p. 510-22.

16. Vanyushin, B.F., A.N. Belozersky, N.A. Kokurina, and D.X. Kadirova 5-methylcytosine and 6-methylamino-purine in bacterial DNA. *Nature*. 1968. **218**(5146): p. 1066-7.

17. Fu, Y., G.Z. Luo, K. Chen, X. Deng, M. Yu, D. Han, Z. Hao, J. Liu, X. Lu, L.C. Dore, X. Weng, Q. Ji, L. Mets, and C. He N6-methyldeoxyadenosine marks active transcription start sites in Chlamydomonas. *Cell*. 2015. **161**(4): p. 879-892.

18. Zhang, G., H. Huang, D. Liu, Y. Cheng, X. Liu, W. Zhang, R. Yin, D. Zhang, P. Zhang, J. Liu, C. Li, B. Liu, Y. Luo, Y. Zhu, N. Zhang, S. He, C. He, H. Wang, and D. Chen N6-methyladenine DNA modification in Drosophila. *Cell*. 2015. **161**(4): p. 893-906.

19. Wu, T.P., T. Wang, M.G. Seetin, Y. Lai, S. Zhu, K. Lin, Y. Liu, S.D. Byrum, S.G. Mackintosh, M. Zhong, A. Tackett, G. Wang, L.S. Hon, G. Fang, J.A. Swenberg, and A.Z. Xiao DNA methylation on N(6)-adenine in mammalian embryonic stem cells. *Nature*. 2016. **532**(7599): p. 329-33.

20. Xie, Q., T.P. Wu, R.C. Gimple, Z. Li, B.C. Prager, Q. Wu, Y. Yu, P. Wang, Y. Wang, D.U. Gorkin, C. Zhang, A.V. Dowiak, K. Lin, C. Zeng, Y. Sui, L.J.Y. Kim, T.E. Miller, L. Jiang, C.H. Lee, Z. Huang, X. Fang, K. Zhai, S.C. Mack, M. Sander, S. Bao, A.E. Kerstetter-Fogle, A.E. Sloan, A.Z. Xiao, and J.N. Rich N(6)-methyladenine DNA Modification in Glioblastoma. *Cell*. 2018. **175**(5): p. 1228-1243.e20.

21. Mack, S.C., K.W. Pajtler, L. Chavez, K. Okonechnikov, K.C. Bertrand, X. Wang, S. Erkek, A. Federation, A. Song, C. Lee, X. Wang, L. McDonald, J.J. Morrow, A. Saiakhova, P. Sin-Chan, Q. Wu, K.A. Michaelraj, T.E. Miller, C.G. Hubert, M. Ryzhova, L. Garzia, L. Donovan, S. Dombrowski, D.C. Factor, B. Luu, C.L.L. Valentim, R.C. Gimple, A. Morton,

L. Kim, B.C. Prager, J.J.Y. Lee, X. Wu, J. Zuccaro, Y. Thompson, B.L. Holgado, J. Reimand, S.Q. Ke, A. Tropper, S. Lai, S. Vijayarajah, S. Doan, V. Mahadev, A.F. Miñan, S.N. Gröbner, M. Lienhard, M. Zapatka, Z. Huang, K.D. Aldape, A.M. Carcaboso, P.J. Houghton, S.T. Keir, T. Milde, H. Witt, Y. Li, C.J. Li, X.W. Bian, D.T.W. Jones, I. Scott, S.K. Singh, A. Huang, P.B. Dirks, E. Bouffet, J.E. Bradner, V. Ramaswamy, N. Jabado, J.T. Rutka, P.A. Northcott, M. Lupien, P. Lichter, A. Korshunov, P.C. Scacheri, S.M. Pfister, M. Kool, M.D. Taylor, and J.N. Rich Therapeutic targeting of ependymoma as informed by oncogenic enhancer profiling. *Nature*. 2018. **553**(7686): p. 101-105.

22. Prager, B.C., H.N. Vasudevan, D. Dixit, J.A. Bernatchez, Q. Wu, L.C. Wallace, S. Bhargava, D. Lee, B.H. King, A.R. Morton, R.C. Gimple, M. Pekmezci, Z. Zhu, J.L. Siqueira-Neto, X. Wang, Q. Xie, C. Chen, G.H. Barnett, M.A. Vogelbaum, S.C. Mack, L. Chavez, A. Perry, D.R. Raleigh, and J.N. Rich The Meningioma Enhancer Landscape Delineates Novel Subgroups and Drives Druggable Dependencies. *Cancer Discov*. 2020. **10**(11): p. 1722-1741.

23. Dixit, D., B.C. Prager, R.C. Gimple, T.E. Miller, Q. Wu, S. Yomtoubian, R.L. Kidwell, D. Lv, L. Zhao, Z. Qiu, G. Zhang, D. Lee, D.E. Park, R.J. Wechsler-Reya, X. Wang, S. Bao, and J.N. Rich Glioblastoma stem cells reprogram chromatin in vivo to generate selective therapeutic dependencies on DPY30 and phosphodiesterases. *Sci Transl Med*. 2022. **14**(626): p. eabf3917.

24. Dixit, D., B.C. Prager, R.C. Gimple, H.X. Poh, Y. Wang, Q. Wu, Z. Qiu, R.L. Kidwell, L.J.Y. Kim, Q. Xie, K. Vitting-Seerup, S. Bhargava, Z. Dong, L. Jiang, Z. Zhu, P. Hamerlik, S.R. Jaffrey, J.C. Zhao, X. Wang, and J.N. Rich The RNA m6A Reader YTHDF2 Maintains Oncogene Expression and Is a Targetable Dependency in Glioblastoma Stem Cells. *Cancer Discovery*. 2021. **11**(2): p. 480-499.

25. Cui, Q., H. Shi, P. Ye, L. Li, Q. Qu, G. Sun, G. Sun, Z. Lu, Y. Huang, C.G. Yang, A.D. Riggs, C. He, and Y. Shi m(6)A RNA Methylation Regulates the Self-Renewal and Tumorigenesis of Glioblastoma Stem Cells. *Cell Rep*. 2017. **18**(11): p. 2622-2634.

26. Qiu, Z., L. Zhao, J.Z. Shen, Z. Liang, Q. Wu, K. Yang, L. Min, R.C. Gimple, Q. Yang, S. Bhargava, C. Jin, C. Kim, D. Hinz, D. Dixit, J.A. Bernatchez, B.C. Prager, G. Zhang, Z. Dong, D. Lv, X. Wang, L.J.Y. Kim, Z. Zhu, K.A. Jones, Y. Zheng, X. Wang, J.L. Siqueira-Neto, L. Chavez, X.D. Fu, C. Spruck, and J.N. Rich Transcription Elongation Machinery Is a Druggable Dependency and Potentiates Immunotherapy in Glioblastoma Stem Cells. *Cancer Discov*. 2022. **12**(2): p. 502-521.

27. Verhaak, R.G., K.A. Hoadley, E. Purdom, V. Wang, Y. Qi, M.D. Wilkerson, C.R. Miller, L. Ding, T. Golub, J.P. Mesirov, G. Alexe, M. Lawrence, M. O'Kelly, P. Tamayo, B.A. Weir, S. Gabriel, W. Winckler, S. Gupta, L. Jakkula, H.S. Feiler, J.G. Hodgson, C.D. James, J.N. Sarkaria, C. Brennan, A. Kahn, P.T. Spellman, R.K. Wilson, T.P. Speed, J.W. Gray, M. Meyerson, G. Getz, C.M. Perou, and D.N. Hayes Integrated genomic analysis identifies clinically relevant subtypes of glioblastoma characterized by abnormalities in PDGFRA, IDH1, EGFR, and NF1. *Cancer Cell*. 2010. **17**(1): p. 98-110.

28. Puchalski, R.B., N. Shah, J. Miller, R. Dalley, S.R. Nomura, J.-G. Yoon, K.A. Smith, M. Lankerovich, D. Bertagnolli, K. Bickley, A.F. Boe, K. Brouner, S. Butler, S. Caldejon, M. Chapin, S. Datta, N. Dee, T. Desta, T. Dolbeare, N. Dotson, A. Ebbert, D. Feng, X. Feng, M. Fisher, G. Gee, J. Goldy, L. Gourley, B.W. Gregor, G. Gu, N. Hejazinia, J. Hohmann, P. Hothi, R. Howard, K. Joines, A. Kriedberg, L. Kuan, C. Lau, F. Lee, H. Lee, T. Lemon, F. Long, N. Mastan, E. Mott, C. Murthy, K. Ngo, E. Olson, M. Reding, Z. Riley, D. Rosen, D. Sandman, N. Shapovalova, C.R. Slaughterbeck, A. Sodt, G. Stockdale, A. Szafer, W. Wakeman, P.E. Wohnoutka, S.J. White, D. Marsh, R.C. Rostomily, L. Ng, C. Dang, A. Jones, B. Keogh, H.R. Gittleman, J.S. Barnholtz-Sloan, P.J. Cimino, M.S. Uppin, C.D. Keene, F.R. Farrokhi, J.D. Lathia, M.E. Berens, A. Iavarone, A. Bernard, E. Lein, J.W. Phillips, S.W. Rostad, C. Cobbs, M.J. Hawrylycz, and G.D. Foltz An anatomic transcriptional atlas of human glioblastoma. 2018. **360**(6389): p. 660-663.

29. Patel, A.P., I. Tirosh, J.J. Trombetta, A.K. Shalek, S.M. Gillespie, H. Wakimoto, D.P. Cahill, B.V. Nahed, W.T. Curry, R.L. Martuza, D.N. Louis, O. Rozenblatt-Rosen, M.L. Suvà, A. Regev, and B.E. Bernstein Single-cell RNA-seq highlights intratumoral heterogeneity in primary glioblastoma. *Science*. 2014. **344**(6190): p. 1396-401.

30. Reinartz, R., S. Wang, S. Kebir, D.J. Silver, A. Wieland, T. Zheng, M. Küpper, L. Rauschenbach, R. Fimmers, T.M. Shepherd, D. Trageser, A. Till, N. Schäfer, M. Glas, A.M. Hillmer, S. Cichon, A.A. Smith, T. Pietsch, Y. Liu, B.A. Reynolds, A. Yachnis, D.W. Pincus, M. Simon, O. Brüstle, D.A. Steindler, and B. Scheffler Functional Subclone Profiling for Prediction of Treatment-Induced Intratumor Population Shifts and Discovery of Rational Drug Combinations in Human Glioblastoma. *Clinical Cancer Research*. 2017. **23**(2): p. 562-574.

31. Szerlip, N.J., A. Pedraza, D. Chakravarty, M. Azim, J. McGuire, Y. Fang, T. Ozawa, E.C. Holland, J.T. Huse, S. Jhanwar, M.A. Leversha, T. Mikkelsen, and C.W. Brennan Intratumoral heterogeneity of receptor tyrosine kinases EGFR and PDGFRA amplification in glioblastoma defines subpopulations with distinct growth factor response. *Proc Natl Acad Sci U S A*. 2012. **109**(8): p. 3041-6.

32. Meyer, M., J. Reimand, X. Lan, R. Head, X. Zhu, M. Kushida, J. Bayani, J.C. Pressey, A.C. Lionel, I.D. Clarke, M. Cusimano, J.A. Squire, S.W. Scherer, M. Bernstein, M.A. Woodin, G.D. Bader, and P.B. Dirks Single cell-derived clonal analysis of human glioblastoma links functional and genomic heterogeneity. *Proc Natl Acad Sci U S A*. 2015. **112**(3): p. 851-6.

33. Ravi, V.M., P. Will, J. Kueckelhaus, N. Sun, K. Joseph, H. Salié, L. Vollmer, U. Kuliesiute, J. von Ehr, J.K. Benotmane, N. Neidert, M. Follo, F. Scherer, J.M. Goeldner, S.P. Behringer, P. Franco, M. Khiat, J. Zhang, U.G. Hofmann, C. Fung, F.L. Ricklefs, K. Lamszus, M. Boerries, M. Ku, J. Beck, R. Sankowski, M. Schwabenland, M. Prinz, U. Schüller, S. Killmer, B. Bengsch, A.K. Walch, D. Delev, O. Schnell, and D.H. Heiland Spatially resolved multi-omics deciphers bidirectional tumor-host interdependence in glioblastoma. *Cancer Cell*. 2022. **40**(6): p. 639-655.e13.

34. Bhat, Krishna P.L., V. Balasubramaniyan, B. Vaillant, R. Ezhilarasan, K. Hummelink, F. Hollingsworth, K. Wani, L. Heathcock, Johanna D. James, Lindsey D. Goodman, S. Conroy, L. Long, N. Lelic, S. Wang, J. Gumin, D. Raj, Y. Kodama, A. Raghunathan, A. Olar, K. Joshi, Christopher E. Pelloski, A. Heimberger, Se H. Kim, Daniel P. Cahill, G. Rao, Wilfred F.A. Den Dunnen, Hendrikus W.G.M. Boddeke, Heidi S. Phillips, I. Nakano, Frederick F. Lang, H. Colman, Erik P. Sulman, and K. Aldape Mesenchymal Differentiation Mediated by NF-κB Promotes Radiation Resistance in Glioblastoma. *Cancer Cell*. 2013. **24**(3): p. 331-346.

35. Neftel, C., J. Laffy, M.G. Filbin, T. Hara, M.E. Shore, G.J. Rahme, A.R. Richman, D. Silverbush, M.L. Shaw, C.M. Hebert, J. Dewitt, S. Gritsch, E.M. Perez, L.N. Gonzalez Castro, X. Lan, N. Druck, C. Rodman, D. Dionne, A. Kaplan, M.S. Bertalan, J. Small, K. Pelton, S. Becker, D. Bonal, Q.D. Nguyen, R.L. Servis, J.M. Fung, R. Mylvaganam, L. Mayr, J. Gojo, C. Haberler, R. Geyeregger, T. Czech, I. Slavc, B.V. Nahed, W.T. Curry, B.S. Carter, H. Wakimoto, P.K. Brastianos, T.T. Batchelor, A. Stemmer-Rachamimov, M. Martinez-Lage, M.P. Frosch, I. Stamenkovic, N. Riggi, E. Rheinbay, M. Monje, O. Rozenblatt-Rosen, D.P. Cahill, A.P. Patel, T. Hunter, I.M. Verma, K.L. Ligon, D.N. Louis, A. Regev, B.E. Bernstein, I. Tirosh, and M.L. Suvà An Integrative Model of Cellular States, Plasticity, and Genetics for Glioblastoma. *Cell*. 2019. **178**(4): p. 835-849.e21.

36. Wang, L., H. Babikir, S. Müller, G. Yagnik, K. Shamardani, F. Catalan, G. Kohanbash, B. Alvarado, E. Di Lullo, A. Kriegstein, S. Shah, H. Wadhwa, S.M. Chang, J.J. Phillips, M.K. Aghi, and A.A. Diaz The Phenotypes of Proliferating Glioblastoma Cells Reside on a Single Axis of Variation. *Cancer Discovery*. 2019. **9**(12): p. 1708-1719.

37. Guilhamon, P., C. Chesnelong, M.M. Kushida, A. Nikolic, D. Singhal, G. MacLeod, S.A. Madani Tonekaboni, F.M.G. Cavalli, C. Arlidge, N. Rajakulendran, N. Rastegar, X. Hao, R. Hassam, L.J. Smith, H. Whetstone, F.J. Coutinho, B. Nadorp, K.I. Ellestad, H.A. Luchman, J.A.-w. Chan, M.S. Shoichet, M.D. Taylor, B. Haibe-Kains, S. Weiss, S. Angers, M. Gallo, P.B. Dirks, and M. Lupien Single-cell chromatin accessibility profiling of glioblastoma identifies an invasive cancer stem cell population associated with lower survival. *eLife*. 2021. **10**: p. e64090.

38. Garofano, L., S. Migliozzi, Y.T. Oh, F. D'Angelo, R.D. Najac, A. Ko, B. Frangaj, F.P. Caruso, K. Yu, J. Yuan, W. Zhao, A. Luisa Di Stefano, F. Bielle, T. Jiang, P. Sims, M.L. Suvà, F. Tang, X.D. Su, M. Ceccarelli, M. Sanson, A. Lasorella, and A. Iavarone Pathway-based classification of glioblastoma uncovers a mitochondrial subtype with therapeutic vulnerabilities. *Nat Cancer*. 2021. **2**(2): p. 141-156.

39. Schmitt, M.J., C. Company, Y. Dramaretska, I. Barozzi, A. Göhrig, S. Kertalli, M. Großmann, H. Naumann, M.P. Sanchez-Bailon, D. Hulsman, R. Glass, M. Squatrito, M. Serresi, and G. Gargiulo Phenotypic Mapping of Pathologic Cross-Talk between Glioblastoma and Innate Immune Cells by Synthetic Genetic Tracing. *Cancer Discovery*. 2021. **11**(3): p. 754-777.

40. Bayin, N.S., J.D. Frenster, R. Sen, S. Si, A.S. Modrek, N. Galifianakis, I. Dolgalev, V. Ortenzi, I. Illa-Bochaca, A. Khahera, J. Serrano, L. Chiriboga, D. Zagzag, J.G. Golfinos, W. Doyle, A. Tsirigos, A. Heguy, M. Chesler, M.H. Barcellos-Hoff, M. Snuderl, and D.G. Placantonakis Notch signaling regulates metabolic heterogeneity in glioblastoma stem cells. *Oncotarget*. 2017. **8**(39): p. 64932-64953.

41. Wang, J., S.L. Xu, J.J. Duan, L. Yi, Y.F. Guo, Y. Shi, L. Li, Z.Y. Yang, X.M. Liao, J. Cai, Y.Q. Zhang, H.L. Xiao, L. Yin, H. Wu, J.N. Zhang, S.Q. Lv, Q.K. Yang, X.J. Yang, T. Jiang, X. Zhang, X.W. Bian, and S.C. Yu Invasion of white matter tracts by glioma stem cells is regulated by a NOTCH1-SOX2 positive-feedback loop. *Nat Neurosci*. 2019. **22**(1): p. 91-105.

42. Liau, B.B., C. Sievers, L.K. Donohue, S.M. Gillespie, W.A. Flavahan, T.E. Miller, A.S. Venteicher, C.H. Hebert, C.D. Carey, S.J. Rodig, S.J. Shareef, F.J. Najm, P. van Galen, H. Wakimoto, D.P. Cahill, J.N. Rich, J.C. Aster, M.L. Suvà, A.P. Patel, and B.E. Bernstein Adaptive Chromatin Remodeling Drives Glioblastoma Stem Cell Plasticity and Drug Tolerance. *Cell Stem Cell*. 2017. **20**(2): p. 233-246.e7.

43. Wang, R., K. Chadalavada, J. Wilshire, U. Kowalik, K.E. Hovinga, A. Geber, B. Fligelman, M. Leversha, C. Brennan, and V. Tabar Glioblastoma stem-like cells give rise to tumour endothelium. *Nature*. 2010. **468**(7325): p. 829-33.

44. Rajakulendran, N., K.J. Rowland, H.J. Selvadurai, M. Ahmadi, N.I. Park, S. Naumenko, S. Dolma, R.J. Ward, M. So, L. Lee, G. MacLeod, C. Pasiliao, C. Brandon, I.D. Clarke, M.D. Cusimano, M. Bernstein, N. Batada, S. Angers, and P.B. Dirks Wnt and Notch signaling govern self-renewal and differentiation in a subset of human glioblastoma stem cells. *Genes Dev*. 2019. **33**(9-10): p. 498-510.

45. Hu, B., Q. Wang, Y.A. Wang, S. Hua, C.G. Sauvé, D. Ong, Z.D. Lan, Q. Chang, Y.W. Ho, M.M. Monasterio, X. Lu, Y. Zhong, J. Zhang, P. Deng, Z. Tan, G. Wang, W.T. Liao, L.J. Corley, H. Yan, J. Zhang, Y. You, N. Liu, L. Cai, G. Finocchiaro, J.J. Phillips, M.S. Berger, D.J. Spring, J. Hu, E.P. Sulman, G.N. Fuller, L. Chin, R.G.W. Verhaak, and R.A. DePinho Epigenetic Activation of WNT5A Drives Glioblastoma Stem Cell Differentiation and Invasive Growth. *Cell*. 2016. **167**(5): p. 1281-1295.e18.

46. Binda, E., A. Visioli, F. Giani, N. Trivieri, O. Palumbo, S. Restelli, F. Dezi, T. Mazza, C. Fusilli, F. Legnani, M. Carella, F. Di Meco, R. Duggal, and A.L. Vescovi Wnt5a Drives an Invasive Phenotype in Human Glioblastoma Stem-like Cells. *Cancer Res*. 2017. **77**(4): p. 996-1007.

47. Nager, M., D. Bhardwaj, C. Cantí, L. Medina, P. Nogués, and J. Herreros β-Catenin Signalling in Glioblastoma Multiforme and Glioma-Initiating Cells. *Chemother Res Pract*. 2012. **2012**: p. 192362.

48. Liu, F., G.C. Hon, G.R. Villa, K.M. Turner, S. Ikegami, H. Yang, Z. Ye, B. Li, S. Kuan, A.Y. Lee, C. Zanca, B. Wei, G. Lucey, D. Jenkins, W. Zhang, C.L. Barr, F.B. Furnari, T.F.

Cloughesy, W.H. Yong, T.C. Gahman, A.K. Shiau, W.K. Cavenee, B. Ren, and P.S. Mischel EGFR Mutation Promotes Glioblastoma through Epigenome and Transcription Factor Network Remodeling. *Mol Cell*. 2015. **60**(2): p. 307-18.

49. Guo, D., R.M. Prins, J. Dang, D. Kuga, A. Iwanami, H. Soto, K.Y. Lin, T.T. Huang, D. Akhavan, M.B. Hock, S. Zhu, A.A. Kofman, S.J. Bensinger, W.H. Yong, H.V. Vinters, S. Horvath, A.D. Watson, J.G. Kuhn, H.I. Robins, M.P. Mehta, P.Y. Wen, L.M. DeAngelis, M.D. Prados, I.K. Mellinghoff, T.F. Cloughesy, and P.S. Mischel EGFR signaling through an Akt-SREBP-1-dependent, rapamycin-resistant pathway sensitizes glioblastomas to antilipogenic therapy. *Sci Signal*. 2009. **2**(101): p. ra82.

50. Lv, D., R.C. Gimple, C. Zhong, Q. Wu, K. Yang, B.C. Prager, B. Godugu, Z. Qiu, L. Zhao, G. Zhang, D. Dixit, D. Lee, J.Z. Shen, X. Li, Q. Xie, X. Wang, S. Agnihotri, and J.N. Rich PDGF signaling inhibits mitophagy in glioblastoma stem cells through N(6)-methyladenosine. *Dev Cell*. 2022. **57**(12): p. 1466-1481.e6.

51. Jin, X., H.M. Jeon, X. Jin, E.J. Kim, J. Yin, H.Y. Jeon, Y.W. Sohn, S.Y. Oh, J.K. Kim, S.H. Kim, J.E. Jung, S. Kwak, K.F. Tang, Y. Xu, J.N. Rich, and H. Kim The ID1-CULLIN3 Axis Regulates Intracellular SHH and WNT Signaling in Glioblastoma Stem Cells. *Cell Rep*. 2016. **16**(6): p. 1629-1641.

52. Anido, J., A. Sáez-Borderías, A. Gonzàlez-Juncà, L. Rodón, G. Folch, M.A. Carmona, R.M. Prieto-Sánchez, I. Barba, E. Martínez-Sáez, L. Prudkin, I. Cuartas, C. Raventós, F. Martínez-Ricarte, M.A. Poca, D. García-Dorado, M.M. Lahn, J.M. Yingling, J. Rodón, J. Sahuquillo, J. Baselga, and J. Seoane TGF-β Receptor Inhibitors Target the CD44(high)/Id1(high) Glioma-Initiating Cell Population in Human Glioblastoma. *Cancer Cell*. 2010. **18**(6): p. 655-68.

53. Osswald, M., E. Jung, F. Sahm, G. Solecki, V. Venkataramani, J. Blaes, S. Weil, H. Horstmann, B. Wiestler, M. Syed, L. Huang, M. Ratliff, K. Karimian Jazi, F.T. Kurz, T. Schmenger, D. Lemke, M. Gömmel, M. Pauli, Y. Liao, P. Häring, S. Pusch, V. Herl, C. Steinhäuser, D. Krunic, M. Jarahian, H. Miletic, A.S. Berghoff, O. Griesbeck, G. Kalamakis, O. Garaschuk, M. Preusser, S. Weiss, H. Liu, S. Heiland, M. Platten, P.E. Huber, T. Kuner, A. von Deimling, W. Wick, and F. Winkler Brain tumour cells interconnect to a functional and resistant network. *Nature*. 2015. **528**(7580): p. 93-98.

54. Wang, X., B.C. Prager, Q. Wu, L.J.Y. Kim, R.C. Gimple, Y. Shi, K. Yang, A.R. Morton, W. Zhou, Z. Zhu, E.A.A. Obara, T.E. Miller, A. Song, S. Lai, C.G. Hubert, X. Jin, Z. Huang, X. Fang, D. Dixit, W. Tao, K. Zhai, C. Chen, Z. Dong, G. Zhang, S.M. Dombrowski, P. Hamerlik, S.C. Mack, S. Bao, and J.N. Rich Reciprocal Signaling between Glioblastoma Stem Cells and Differentiated Tumor Cells Promotes Malignant Progression. *Cell Stem Cell*. 2018. **22**(4): p. 514-528.e5.

55. Venkataramani, V., Y. Yang, M.C. Schubert, E. Reyhan, S.K. Tetzlaff, N. Wißmann, M. Botz, S.J. Soyka, C.A. Beretta, R.L. Pramatarov, L. Fankhauser, L. Garofano, A. Freudenberg, J. Wagner, D.I. Tanev, M. Ratliff, R. Xie, T. Kessler, D.C. Hoffmann, L.

Hai, Y. Dörflinger, S. Hoppe, Y.A. Yabo, A. Golebiewska, S.P. Niclou, F. Sahm, A. Lasorella, M. Slowik, L. Döring, A. Iavarone, W. Wick, T. Kuner, and F. Winkler Glioblastoma hijacks neuronal mechanisms for brain invasion. *Cell*. 2022. **185**(16): p. 2899-2917.e31.

56. Tardito, S., A. Oudin, S.U. Ahmed, F. Fack, O. Keunen, L. Zheng, H. Miletic, P. Sakariassen, A. Weinstock, A. Wagner, S.L. Lindsay, A.K. Hock, S.C. Barnett, E. Ruppin, S.H. Mørkve, M. Lund-Johansen, A.J. Chalmers, R. Bjerkvig, S.P. Niclou, and E. Gottlieb Glutamine synthetase activity fuels nucleotide biosynthesis and supports growth of glutamine-restricted glioblastoma. *Nat Cell Biol*. 2015. **17**(12): p. 1556-68.

57. Villa, G.R., J.J. Hulce, C. Zanca, J. Bi, S. Ikegami, G.L. Cahill, Y. Gu, K.M. Lum, K. Masui, H. Yang, X. Rong, C. Hong, K.M. Turner, F. Liu, G.C. Hon, D. Jenkins, M. Martini, A.M. Armando, O. Quehenberger, T.F. Cloughesy, F.B. Furnari, W.K. Cavenee, P. Tontonoz, T.C. Gahman, A.K. Shiau, B.F. Cravatt, and P.S. Mischel An LXR-Cholesterol Axis Creates a Metabolic Co-Dependency for Brain Cancers. *Cancer Cell*. 2016. **30**(5): p. 683-693.

58. Zhang, H., Y. Zhou, B. Cui, Z. Liu, and H. Shen Novel insights into astrocyte-mediated signaling of proliferation, invasion and tumor immune microenvironment in glioblastoma. *Biomed Pharmacother*. 2020. **126**: p. 110086.

59. Li, Z., S. Bao, Q. Wu, H. Wang, C. Eyler, S. Sathornsumetee, Q. Shi, Y. Cao, J. Lathia, R.E. McLendon, A.B. Hjelmeland, and J.N. Rich Hypoxia-inducible factors regulate tumorigenic capacity of glioma stem cells. *Cancer Cell*. 2009. **15**(6): p. 501-13.

60. Feng, X., H. Zhang, L. Meng, H. Song, Q. Zhou, C. Qu, P. Zhao, Q. Li, C. Zou, X. Liu, and Z. Zhang Hypoxia-induced acetylation of PAK1 enhances autophagy and promotes brain tumorigenesis via phosphorylating ATG5. *Autophagy*. 2021. **17**(3): p. 723-742.

61. Treps, L., R. Perret, S. Edmond, D. Ricard, and J. Gavard Glioblastoma stem-like cells secrete the pro-angiogenic VEGF-A factor in extracellular vesicles. *J Extracell Vesicles*. 2017. **6**(1): p. 1359479.

62. Ricci-Vitiani, L., R. Pallini, M. Biffoni, M. Todaro, G. Invernici, T. Cenci, G. Maira, E.A. Parati, G. Stassi, L.M. Larocca, and R. De Maria Tumour vascularization via endothelial differentiation of glioblastoma stem-like cells. *Nature*. 2010. **468**(7325): p. 824-8.

63. Zhou, W., C. Chen, Y. Shi, Q. Wu, R.C. Gimple, X. Fang, Z. Huang, K. Zhai, S.Q. Ke, Y.F. Ping, H. Feng, J.N. Rich, J.S. Yu, S. Bao, and X.W. Bian Targeting Glioma Stem Cell-Derived Pericytes Disrupts the Blood-Tumor Barrier and Improves Chemotherapeutic Efficacy. *Cell Stem Cell*. 2017. **21**(5): p. 591-603.e4.

64. Lee, J.H., J.E. Lee, J.Y. Kahng, S.H. Kim, J.S. Park, S.J. Yoon, J.-Y. Um, W.K. Kim, J.-K. Lee, J. Park, E.H. Kim, J.-H. Lee, J.-H. Lee, W.-S. Chung, Y.S. Ju, S.-H. Park, J.H.

Chang, S.-G. Kang, and J.H. Lee Human glioblastoma arises from subventricular zone cells with low-level driver mutations. *Nature*. 2018. **560**(7717): p. 243-247.

65. Zhu, Y., F. Guignard, D. Zhao, L. Liu, D.K. Burns, R.P. Mason, A. Messing, and L.F. Parada Early inactivation of p53 tumor suppressor gene cooperating with NF1 loss induces malignant astrocytoma. *Cancer Cell*. 2005. **8**(2): p. 119-30.

66. Holland, E.C., J. Celestino, C. Dai, L. Schaefer, R.E. Sawaya, and G.N. Fuller Combined activation of Ras and Akt in neural progenitors induces glioblastoma formation in mice. *Nat Genet*. 2000. **25**(1): p. 55-7.

67. Bhaduri, A., E. Di Lullo, D. Jung, S. Müller, E.E. Crouch, C.S. Espinosa, T. Ozawa, B. Alvarado, J. Spatazza, C.R. Cadwell, G. Wilkins, D. Velmeshev, S.J. Liu, M. Malatesta, M.G. Andrews, M.A. Mostajo-Radji, E.J. Huang, T.J. Nowakowski, D.A. Lim, A. Diaz, D.R. Raleigh, and A.R. Kriegstein Outer Radial Glia-like Cancer Stem Cells Contribute to Heterogeneity of Glioblastoma. *Cell Stem Cell*. 2020. **26**(1): p. 48-63.e6.

68. Harashima, T., S. Anderson, J.R. Yates, 3rd, and J. Heitman The kelch proteins Gpb1 and Gpb2 inhibit Ras activity via association with the yeast RasGAP neurofibromin homologs Ira1 and Ira2. *Mol Cell*. 2006. **22**(6): p. 819-830.

69. Hu, J., W. Yuan, M. Tang, Y. Wang, X. Fan, X. Mo, Y. Li, Z. Ying, Y. Wan, K. Ocorr, R. Bodmer, Y. Deng, and X. Wu KBTBD7, a novel human BTB-kelch protein, activates transcriptional activities of SRE and AP-1. *BMB Rep*. 2010. **43**(1): p. 17-22.

70. Mulvaney, K.M., J.P. Matson, P.F. Siesser, T.Y. Tamir, D. Goldfarb, T.M. Jacobs, E.W. Cloer, J.S. Harrison, C. Vaziri, J.G. Cook, and M.B. Major Identification and Characterization of MCM3 as a Kelch-like ECH-associated Protein 1 (KEAP1) Substrate. *J Biol Chem*. 2016. **291**(45): p. 23719-23733.

71. Marshall, J., L.A. Blair, and J.D. Singer BTB-Kelch proteins and ubiquitination of kainate receptors. *Adv Exp Med Biol*. 2011. **717**: p. 115-25.

72. Mukasa, A., J. Wykosky, K.L. Ligon, L. Chin, W.K. Cavenee, and F. Furnari Mutant EGFR is required for maintenance of glioma growth in vivo, and its ablation leads to escape from receptor dependence. 2010. **107**(6): p. 2616-2621.

73. Zhu, X., T. Chen, H. Yang, and K. Lv Lactate induced up-regulation of KLHDC8A (Kelch domain-containing 8A) contributes to the proliferation, migration and apoptosis of human glioma cells. *J Cell Mol Med*. 2020. **24**(20): p. 11691-11702.

74. Higgins, M., I. Obaidi, and T. McMorrow Primary cilia and their role in cancer. *Oncol Lett*. 2019. **17**(3): p. 3041-3047.

75. Yanardag, S. and E.N. Pugacheva Primary Cilium Is Involved in Stem Cell Differentiation and Renewal through the Regulation of Multiple Signaling Pathways. 2021. **10**(6): p. 1428.

76. Janke, C. and J.C. Bulinski Post-translational regulation of the microtubule cytoskeleton: mechanisms and functions. *Nat Rev Mol Cell Biol*. 2011. **12**(12): p. 773-86.

77. Fabbri, L., F. Bost, and N.M. Mazure Primary Cilium in Cancer Hallmarks. *Int J Mol Sci*. 2019. **20**(6).

78. Wong, S.Y., A.D. Seol, P.L. So, A.N. Ermilov, C.K. Bichakjian, E.H. Epstein, Jr., A.A. Dlugosz, and J.F. Reiter Primary cilia can both mediate and suppress Hedgehog pathway-dependent tumorigenesis. *Nat Med*. 2009. **15**(9): p. 1055-61.

79. Corbit, K.C., A.E. Shyer, W.E. Dowdle, J. Gaulden, V. Singla, M.H. Chen, P.T. Chuang, and J.F. Reiter Kif3a constrains beta-catenin-dependent Wnt signalling through dual ciliary and non-ciliary mechanisms. *Nat Cell Biol*. 2008. **10**(1): p. 70-6.

80. Seeley, E.S. and M.V. Nachury Constructing and deconstructing roles for the primary cilium in tissue architecture and cancer. *Methods Cell Biol*. 2009. **94**: p. 299-313.

81. Emoto, K., Y. Masugi, K. Yamazaki, K. Effendi, H. Tsujikawa, M. Tanabe, Y. Kitagawa, and M. Sakamoto Presence of primary cilia in cancer cells correlates with prognosis of pancreatic ductal adenocarcinoma. *Hum Pathol*. 2014. **45**(4): p. 817-25.

82. Seeley, E.S., C. Carrière, T. Goetze, D.S. Longnecker, and M. Korc Pancreatic cancer and precursor pancreatic intraepithelial neoplasia lesions are devoid of primary cilia. *Cancer Res*. 2009. **69**(2): p. 422-30.

83. Yuan, K., N. Frolova, Y. Xie, D. Wang, L. Cook, Y.J. Kwon, A.D. Steg, R. Serra, and A.R. Frost Primary cilia are decreased in breast cancer: analysis of a collection of human breast cancer cell lines and tissues. *J Histochem Cytochem*. 2010. **58**(10): p. 857-70.

84. Lee, J., K.C. Park, H.J. Sul, H.J. Hong, K.-H. Kim, J. Kero, and M. Shong Loss of primary cilia promotes mitochondria-dependent apoptosis in thyroid cancer. *Scientific Reports*. 2021. **11**(1): p. 4181.

85. Egeberg, D.L., M. Lethan, R. Manguso, L. Schneider, A. Awan, T.S. Jørgensen, A.G. Byskov, L.B. Pedersen, and S.T. Christensen Primary cilia and aberrant cell signaling in epithelial ovarian cancer. *Cilia*. 2012. **1**(1): p. 15.

86. Dere, R., A.L. Perkins, T. Bawa-Khalfe, D. Jonasch, and C.L. Walker β-Catenin Links von Hippel-Lindau to Aurora Kinase A and Loss of Primary Cilia in Renal Cell Carcinoma. 2015. **26**(3): p. 553-564.

87. Yang, N., E.L. Leung, C. Liu, L. Li, T. Eguether, X.J. Jun Yao, E.C. Jones, D.A. Norris, A. Liu, R.A. Clark, D.R. Roop, G.J. Pazour, K.R. Shroyer, and J. Chen INTU is essential for oncogenic Hh signaling through regulating primary cilia formation in basal cell carcinoma. *Oncogene*. 2017. **36**(35): p. 4997-5005.

88. Kim, J., S. Dabiri, and E.S. Seeley Primary cilium depletion typifies cutaneous melanoma in situ and malignant melanoma. *PLoS One*. 2011. **6**(11): p. e27410.

89. Coelho, P.A., L. Bury, M.N. Shahbazi, K. Liakath-Ali, P.H. Tate, S. Wormald, C.J. Hindley, M. Huch, J. Archer, W.C. Skarnes, M. Zernicka-Goetz, and D.M. Glover Over-expression of Plk4 induces centrosome amplification, loss of primary cilia and associated tissue hyperplasia in the mouse. *Open Biol*. 2015. **5**(12): p. 150209.

90. Zingg, D., J. Debbache, R. Peña-Hernández, A.T. Antunes, S.M. Schaefer, P.F. Cheng, D. Zimmerli, J. Haeusel, R.R. Calçada, E. Tuncer, Y. Zhang, R. Bossart, K.K. Wong, K. Basler, R. Dummer, R. Santoro, M.P. Levesque, and L. Sommer EZH2-Mediated Primary Cilium Deconstruction Drives Metastatic Melanoma Formation. *Cancer Cell*. 2018. **34**(1): p. 69-84.e14.

91. Breunig, J.J., M.R. Sarkisian, J.I. Arellano, Y.M. Morozov, A.E. Ayoub, S. Sojitra, B. Wang, R.A. Flavell, P. Rakic, and T. Town Primary cilia regulate hippocampal neurogenesis by mediating sonic hedgehog signaling. 2008. **105**(35): p. 13127-13132.

92. Han, Y.G., N. Spassky, M. Romaguera-Ros, J.M. Garcia-Verdugo, A. Aguilar, S. Schneider-Maunoury, and A. Alvarez-Buylla Hedgehog signaling and primary cilia are required for the formation of adult neural stem cells. *Nat Neurosci*. 2008. **11**(3): p. 277-84.

93. Sarkisian, M.R., D. Siebzehnrubl, L. Hoang-Minh, L. Deleyrolle, D.J. Silver, F.A. Siebzehnrubl, S.M. Guadiana, G. Srivinasan, S. Semple-Rowland, J.K. Harrison, D.A. Steindler, and B.A. Reynolds Detection of primary cilia in human glioblastoma. *J Neurooncol*. 2014. **117**(1): p. 15-24.

94. Allen, M., M. Bjerke, H. Edlund, S. Nelander, and B. Westermark Origin of the U87MG glioma cell line: Good news and bad news. *Sci Transl Med*. 2016. **8**(354): p. 354re3.

95. Hoang-Minh, L.B., L.P. Deleyrolle, N.S. Nakamura, A.K. Parker, R.T. Martuscello, B.A. Reynolds, and M.R. Sarkisian PCM1 Depletion Inhibits Glioblastoma Cell Ciliogenesis and Increases Cell Death and Sensitivity to Temozolomide. *Transl Oncol*. 2016. **9**(5): p. 392-402.

96. Goranci-Buzhala, G., A. Mariappan, L. Ricci-Vitiani, N. Josipovic, S. Pacioni, M. Gottardo, J. Ptok, H. Schaal, G. Callaini, K. Rajalingam, B. Dynlacht, K. Hadian, A. Papantonis, R. Pallini, and J. Gopalakrishnan Cilium induction triggers differentiation of glioma stem cells. *Cell Reports*. 2021. **36**(10): p. 109656.

97. Han, Y.-G., H.J. Kim, A.A. Dlugosz, D.W. Ellison, R.J. Gilbertson, and A. Alvarez-Buylla Dual and opposing roles of primary cilia in medulloblastoma development. *Nature Medicine*. 2009. **15**(9): p. 1062-1065.

98. Youn, Y.H., S. Hou, C.C. Wu, D. Kawauchi, B.A. Orr, G.W. Robinson, D. Finkelstein, M.M. Taketo, R.J. Gilbertson, M.F. Roussel, and Y.G. Han Primary cilia control translation and the cell cycle in medulloblastoma. *Genes Dev*. 2022. **36**(11-12): p. 737-751.

99. Shi, P., J. Tian, B.S. Ulm, J.C. Mallinger, H. Khoshbouei, L.P. Deleyrolle, and M.R. Sarkisian Tumor Treating Fields Suppression of Ciliogenesis Enhances Temozolomide Toxicity. *Front Oncol*. 2022. **12**: p. 837589.

100. Wei, L., W. Ma, H. Cai, S.P. Peng, H.B. Tian, J.F. Wang, L. Gao, and J.P. He Inhibition of Ciliogenesis Enhances the Cellular Sensitivity to Temozolomide and Ionizing Radiation in Human Glioblastoma Cells. *Biomed Environ Sci*. 2022. **35**(5): p. 419-436.

101. Jenks, A.D., S. Vyse, J.P. Wong, E. Kostaras, D. Keller, T. Burgoyne, A. Shoemark, A. Tsalikis, M. de la Roche, M. Michaelis, J. Cinatl, Jr., P.H. Huang, and B.E. Tanos Primary Cilia Mediate Diverse Kinase Inhibitor Resistance Mechanisms in Cancer. *Cell Rep*. 2018. **23**(10): p. 3042-3055.

102. de Almeida Magalhães, T., G. Alencastro Veiga Cruzeiro, G. Ribeiro de Sousa, B. Englinger, L.F. Peinado Nagano, M. Ancliffe, K. Rodrigues da Silva, L. Jiang, J. Gojo, Y. Cherry Liu, B. Carline, M. Kuchibhotla, F. Pinto Saggioro, S. Kazue Nagahashi Marie, S. Mieko Oba-Shinjo, J. Andres Yunes, R. Gomes de Paula Queiroz, C. Alberto Scrideli, R. Endersby, M.G. Filbin, K. Silva Borges, A. Salic, L. Gonzaga Tone, and E. Terci Valera Activation of Hedgehog signaling by the oncogenic RELA fusion reveals a primary cilia-dependent vulnerability in Supratentorial Ependymoma. *Neuro Oncol*. 2022.

103. Zhao, X., E. Pak, K.J. Ornell, M.F. Pazyra-Murphy, E.L. MacKenzie, E.J. Chadwick, T. Ponomaryov, J.F. Kelleher, and R.A. Segal A Transposon Screen Identifies Loss of Primary Cilia as a Mechanism of Resistance to SMO Inhibitors. *Cancer Discov*. 2017. **7**(12): p. 1436-1449.

104. Varjosalo, M. and J. Taipale Hedgehog: functions and mechanisms. *Genes Dev*. 2008. **22**(18): p. 2454-72.

105. Briscoe, J. and P.P. Thérond The mechanisms of Hedgehog signalling and its roles in development and disease. *Nat Rev Mol Cell Biol*. 2013. **14**(7): p. 416-29.

106. Amakye, D., Z. Jagani, and M. Dorsch Unraveling the therapeutic potential of the Hedgehog pathway in cancer. *Nat Med*. 2013. **19**(11): p. 1410-22.

107. Hui, M., A. Cazet, R. Nair, D.N. Watkins, S.A. O'Toole, and A. Swarbrick The Hedgehog signalling pathway in breast development, carcinogenesis and cancer therapy. *Breast Cancer Res*. 2013. **15**(2): p. 203.

108. Ok, C.Y., R.R. Singh, and F. Vega Aberrant activation of the hedgehog signaling pathway in malignant hematological neoplasms. *Am J Pathol*. 2012. **180**(1): p. 2-11.

109. Teglund, S. and R. Toftgård Hedgehog beyond medulloblastoma and basal cell carcinoma. *Biochim Biophys Acta*. 2010. **1805**(2): p. 181-208.

110. Otsuka, A., J. Dreier, P.F. Cheng, M. Nägeli, H. Lehmann, L. Felderer, I.J. Frew, S. Matsushita, M.P. Levesque, and R. Dummer Hedgehog pathway inhibitors promote adaptive immune responses in basal cell carcinoma. *Clin Cancer Res*. 2015. **21**(6): p. 1289-97.

111. Furmanski, A.L., J.I. Saldana, M. Ono, H. Sahni, N. Paschalidis, F. D'Acquisto, and T. Crompton Tissue-derived hedgehog proteins modulate Th differentiation and disease. *J Immunol*. 2013. **190**(6): p. 2641-9.

112. Rowbotham, N.J., A.L. Furmanski, A.L. Hager-Theodorides, S.E. Ross, E. Drakopoulou, C. Koufaris, S.V. Outram, and T. Crompton Repression of hedgehog signal transduction in T-lineage cells increases TCR-induced activation and proliferation. *Cell Cycle*. 2008. **7**(7): p. 904-8.

113. Raffel, C., R.B. Jenkins, L. Frederick, D. Hebrink, B. Alderete, D.W. Fults, and C.D. James Sporadic medulloblastomas contain PTCH mutations. *Cancer Res*. 1997. **57**(5): p. 842-5.

114. Taylor, M.D., L. Liu, C. Raffel, C.C. Hui, T.G. Mainprize, X. Zhang, R. Agatep, S. Chiappa, L. Gao, A. Lowrance, A. Hao, A.M. Goldstein, T. Stavrou, S.W. Scherer, W.T. Dura, B. Wainwright, J.A. Squire, J.T. Rutka, and D. Hogg Mutations in SUFU predispose to medulloblastoma. *Nat Genet*. 2002. **31**(3): p. 306-10.

115. Zhao, C., A. Chen, C.H. Jamieson, M. Fereshteh, A. Abrahamsson, J. Blum, H.Y. Kwon, J. Kim, J.P. Chute, D. Rizzieri, M. Munchhof, T. VanArsdale, P.A. Beachy, and T. Reya Hedgehog signalling is essential for maintenance of cancer stem cells in myeloid leukaemia. *Nature*. 2009. **458**(7239): p. 776-9.

116. Dierks, C., R. Beigi, G.R. Guo, K. Zirlik, M.R. Stegert, P. Manley, C. Trussell, A. Schmitt-Graeff, K. Landwerlin, H. Veelken, and M. Warmuth Expansion of Bcr-Abl-positive leukemic stem cells is dependent on Hedgehog pathway activation. *Cancer Cell*. 2008. **14**(3): p. 238-49.

117. Queiroz, K.C., R.R. Ruela-de-Sousa, G.M. Fuhler, H.L. Aberson, C.V. Ferreira, M.P. Peppelenbosch, and C.A. Spek Hedgehog signaling maintains chemoresistance in myeloid leukemic cells. *Oncogene*. 2010. **29**(48): p. 6314-22.

118. Skoda, A.M., D. Simovic, V. Karin, V. Kardum, S. Vranic, and L. Serman The role of the Hedgehog signaling pathway in cancer: A comprehensive review. *Bosnian Journal of Basic Medical Sciences*. 2018. **18**(1): p. 8-20.

119. Rimkus, T.K., R.L. Carpenter, S. Qasem, M. Chan, and H.-W. Lo Targeting the Sonic Hedgehog Signaling Pathway: Review of Smoothened and GLI Inhibitors. 2016. **8**(2): p. 22.

120. Sekulic, A., M.R. Migden, A.E. Oro, L. Dirix, K.D. Lewis, J.D. Hainsworth, J.A. Solomon, S. Yoo, S.T. Arron, P.A. Friedlander, E. Marmur, C.M. Rudin, A.L.S. Chang, J.A. Low, H.M. Mackey, R.L. Yauch, R.A. Graham, J.C. Reddy, and A. Hauschild Efficacy and Safety of Vismodegib in Advanced Basal-Cell Carcinoma. 2012. **366**(23): p. 2171-2179.

121. Goel, V., E. Hurh, A. Stein, J. Nedelman, J. Zhou, O. Chiparus, P.H. Huang, S. Gogov, and D. Sellami Population pharmacokinetics of sonidegib (LDE225), an oral inhibitor of hedgehog pathway signaling, in healthy subjects and in patients with advanced solid tumors. *Cancer Chemother Pharmacol*. 2016. **77**(4): p. 745-55.

122. Kim, J., B.T. Aftab, J.Y. Tang, D. Kim, A.H. Lee, M. Rezaee, J. Kim, B. Chen, E.M. King, A. Borodovsky, G.J. Riggins, E.H. Epstein, Jr., P.A. Beachy, and C.M. Rudin Itraconazole and arsenic trioxide inhibit Hedgehog pathway activation and tumor growth associated with acquired resistance to smoothened antagonists. *Cancer Cell*. 2013. **23**(1): p. 23-34.

123. Lauth, M., A. Bergström, T. Shimokawa, and R. Toftgård Inhibition of GLI-mediated transcription and tumor cell growth by small-molecule antagonists. *Proc Natl Acad Sci U S A*. 2007. **104**(20): p. 8455-60.

124. Long, J., B. Li, J. Rodriguez-Blanco, C. Pastori, C.H. Volmar, C. Wahlestedt, A. Capobianco, F. Bai, X.H. Pei, N.G. Ayad, and D.J. Robbins The BET bromodomain inhibitor I-BET151 acts downstream of smoothened protein to abrogate the growth of hedgehog protein-driven cancers. *J Biol Chem*. 2014. **289**(51): p. 35494-502.

125. Bao, S., Q. Wu, R.E. McLendon, Y. Hao, Q. Shi, A.B. Hjelmeland, M.W. Dewhirst, D.D. Bigner, and J.N. Rich Glioma stem cells promote radioresistance by preferential activation of the DNA damage response. *Nature*. 2006. **444**(7120): p. 756-60.

126. Chen, J., Y. Li, T.S. Yu, R.M. McKay, D.K. Burns, S.G. Kernie, and L.F. Parada A restricted cell population propagates glioblastoma growth after chemotherapy. *Nature*. 2012. **488**(7412): p. 522-6.

127. Zhou, W., S.Q. Ke, Z. Huang, W. Flavahan, X. Fang, J. Paul, L. Wu, A.E. Sloan, R.E. McLendon, X. Li, J.N. Rich, and S. Bao Periostin secreted by glioblastoma stem cells recruits M2 tumour-associated macrophages and promotes malignant growth. *Nat Cell Biol*. 2015. **17**(2): p. 170-82.

128. Calabrese, C., H. Poppleton, M. Kocak, T.L. Hogg, C. Fuller, B. Hamner, E.Y. Oh, M.W. Gaber, D. Finklestein, M. Allen, A. Frank, I.T. Bayazitov, S.S. Zakharenko, A. Gajjar, A. Davidoff, and R.J. Gilbertson A perivascular niche for brain tumor stem cells. *Cancer Cell*. 2007. **11**(1): p. 69-82.

129. Pietras, A., A.M. Katz, E.J. Ekström, B. Wee, J.J. Halliday, K.L. Pitter, J.L. Werbeck, N.M. Amankulor, J.T. Huse, and E.C. Holland Osteopontin-CD44 signaling in the glioma perivascular niche enhances cancer stem cell phenotypes and promotes aggressive tumor growth. *Cell Stem Cell*. 2014. **14**(3): p. 357-69.

130. Baylin, S.B. and P.A. Jones Epigenetic Determinants of Cancer. *Cold Spring Harb Perspect Biol*. 2016. **8**(9).

131. Flavahan, W.A., E. Gaskell, and B.E. Bernstein Epigenetic plasticity and the hallmarks of cancer. *Science*. 2017. **357**(6348).

132. Pott, S. and J.D. Lieb What are super-enhancers? *Nature Genetics*. 2015. **47**(1): p. 8-12.

133. Rubenstein, B.M. and L.J. Kaufman The role of extracellular matrix in glioma invasion: a cellular Potts model approach. *Biophys J*. 2008. **95**(12): p. 5661-80.

134. Reya, T., S.J. Morrison, M.F. Clarke, and I.L. Weissman Stem cells, cancer, and cancer stem cells. *Nature*. 2001. **414**(6859): p. 105-111.

135. Hung, H.C., C.C. Liu, J.Y. Chuang, C.L. Su, and P.W. Gean Inhibition of Sonic Hedgehog Signaling Suppresses Glioma Stem-Like Cells Likely Through Inducing Autophagic Cell Death. *Front Oncol*. 2020. **10**: p. 1233.

136. LoRusso, P.M., C.M. Rudin, J.C. Reddy, R. Tibes, G.J. Weiss, M.J. Borad, C.L. Hann, J.R. Brahmer, I. Chang, W.C. Darbonne, R.A. Graham, K.L. Zerivitz, J.A. Low, and D.D. Von Hoff Phase I trial of hedgehog pathway inhibitor vismodegib (GDC-0449) in patients with refractory, locally advanced or metastatic solid tumors. *Clin Cancer Res*. 2011. **17**(8): p. 2502-11.

137. Rudin, C.M., C.L. Hann, J. Laterra, R.L. Yauch, C.A. Callahan, L. Fu, T. Holcomb, J. Stinson, S.E. Gould, B. Coleman, P.M. LoRusso, D.D. Von Hoff, F.J. de Sauvage, and J.A. Low Treatment of medulloblastoma with hedgehog pathway inhibitor GDC-0449. *N Engl J Med*. 2009. **361**(12): p. 1173-8.

138. Von Hoff, D.D., P.M. LoRusso, C.M. Rudin, J.C. Reddy, R.L. Yauch, R. Tibes, G.J. Weiss, M.J. Borad, C.L. Hann, J.R. Brahmer, H.M. Mackey, B.L. Lum, W.C. Darbonne, J.C. Marsters, Jr., F.J. de Sauvage, and J.A. Low Inhibition of the hedgehog pathway in advanced basal-cell carcinoma. *N Engl J Med*. 2009. **361**(12): p. 1164-72.

139. Buonamici, S., J. Williams, M. Morrissey, A. Wang, R. Guo, A. Vattay, K. Hsiao, J. Yuan, J. Green, B. Ospina, Q. Yu, L. Ostrom, P. Fordjour, D.L. Anderson, J.E. Monahan, J.F. Kelleher, S. Peukert, S. Pan, X. Wu, S.M. Maira, C. García-Echeverría, K.J. Briggs, D.N. Watkins, Y.M. Yao, C. Lengauer, M. Warmuth, W.R. Sellers, and M. Dorsch Interfering with resistance to smoothened antagonists by inhibition of the PI3K pathway in medulloblastoma. *Sci Transl Med*. 2010. **2**(51): p. 51ra70.

140. Yauch, R.L., G.J. Dijkgraaf, B. Alicke, T. Januario, C.P. Ahn, T. Holcomb, K. Pujara, J. Stinson, C.A. Callahan, T. Tang, J.F. Bazan, Z. Kan, S. Seshagiri, C.L. Hann, S.E. Gould, J.A. Low, C.M. Rudin, and F.J. de Sauvage Smoothened mutation confers resistance to a Hedgehog pathway inhibitor in medulloblastoma. *Science*. 2009. **326**(5952): p. 572-4.

141. Xie, J., R.L. Johnson, X. Zhang, J.W. Bare, F.M. Waldman, P.H. Cogen, A.G. Menon, R.S. Warren, L.C. Chen, M.P. Scott, and E.H. Epstein, Jr. Mutations of the PATCHED gene in several types of sporadic extracutaneous tumors. *Cancer Res*. 1997. **57**(12): p. 2369-72.

142. Pugh, T.J., S.D. Weeraratne, T.C. Archer, D.A. Pomeranz Krummel, D. Auclair, J. Bochicchio, M.O. Carneiro, S.L. Carter, K. Cibulskis, R.L. Erlich, H. Greulich, M.S. Lawrence, N.J. Lennon, A. McKenna, J. Meldrim, A.H. Ramos, M.G. Ross, C. Russ, E. Shefler, A. Sivachenko, B. Sogoloff, P. Stojanov, P. Tamayo, J.P. Mesirov, V. Amani, N. Teider, S. Sengupta, J.P. Francois, P.A. Northcott, M.D. Taylor, F. Yu, G.R. Crabtree, A.G. Kautzman, S.B. Gabriel, G. Getz, N. Jäger, D.T. Jones, P. Lichter, S.M. Pfister, T.M. Roberts, M. Meyerson, S.L. Pomeroy, and Y.J. Cho Medulloblastoma exome sequencing uncovers subtype-specific somatic mutations. *Nature*. 2012. **488**(7409): p. 106-10.

143. Tang, Y., S. Gholamin, S. Schubert, M.I. Willardson, A. Lee, P. Bandopadhayay, G. Bergthold, S. Masoud, B. Nguyen, N. Vue, B. Balansay, F. Yu, S. Oh, P. Woo, S. Chen, A. Ponnuswami, M. Monje, S.X. Atwood, R.J. Whitson, S. Mitra, S.H. Cheshier, J. Qi, R. Beroukhim, J.Y. Tang, R. Wechsler-Reya, A.E. Oro, B.A. Link, J.E. Bradner, and Y.-J. Cho Epigenetic targeting of Hedgehog pathway transcriptional output through BET bromodomain inhibition. *Nature Medicine*. 2014. **20**(7): p. 732-740.

144. Wang, X., Z. Huang, Q. Wu, B.C. Prager, S.C. Mack, K. Yang, L.J.Y. Kim, R.C. Gimple, Y. Shi, S. Lai, Q. Xie, T.E. Miller, C.G. Hubert, A. Song, Z. Dong, W. Zhou, X. Fang, Z. Zhu, V. Mahadev, S. Bao, and J.N. Rich MYC-Regulated Mevalonate Metabolism Maintains Brain Tumor-Initiating Cells. *Cancer Res*. 2017. **77**(18): p. 4947-4960.

145. Mack, S.C., I. Singh, X. Wang, R. Hirsch, Q. Wu, R. Villagomez, J.A. Bernatchez, Z. Zhu, R.C. Gimple, L.J.Y. Kim, A. Morton, S. Lai, Z. Qiu, B.C. Prager, K.C. Bertrand, C. Mah, W. Zhou, C. Lee, G.H. Barnett, M.A. Vogelbaum, A.E. Sloan, L. Chavez, S. Bao, P.C. Scacheri, J.L. Siqueira-Neto, C.Y. Lin, and J.N. Rich Chromatin landscapes reveal developmentally encoded transcriptional states that define human glioblastoma. *J Exp Med*. 2019. **216**(5): p. 1071-1090.

146. Jiang, L., J. Zhou, D. Zhong, Y. Zhou, W. Zhang, W. Wu, Z. Zhao, W. Wang, W. Xu, L. He, Y. Ma, Y. Hu, W. Zhang, and J. Li Overexpression of SMC4 activates TGFβ/Smad signaling and promotes aggressive phenotype in glioma cells. *Oncogenesis*. 2017. **6**(3): p. e301-e301.

147. Karki, K., X. Li, U.H. Jin, K. Mohankumar, M. Zarei, S.K. Michelhaugh, S. Mittal, R. Tjalkens, and S. Safe Nuclear receptor 4A2 (NR4A2) is a druggable target for glioblastomas. *J Neurooncol*. 2020. **146**(1): p. 25-39.

148. Wang, J., C. Sun, J. Li, H. Jiang, Y. Qiu, and M. Gong Knockdown of ETV4 promotes autophagy-dependent apoptosis in GBM cells by reducing the transcriptional activation of EMP1. *Oncol Lett*. 2022. **23**(2): p. 41.

149. Suvà, M.L., E. Rheinbay, S.M. Gillespie, A.P. Patel, H. Wakimoto, S.D. Rabkin, N. Riggi, A.S. Chi, D.P. Cahill, B.V. Nahed, W.T. Curry, R.L. Martuza, M.N. Rivera, N. Rossetti, S. Kasif, S. Beik, S. Kadri, I. Tirosh, I. Wortman, A.K. Shalek, O. Rozenblatt-Rosen, A. Regev, D.N. Louis, and B.E. Bernstein Reconstructing and reprogramming the tumor-propagating potential of glioblastoma stem-like cells. *Cell*. 2014. **157**(3): p. 580-94.

150. Lovén, J., H.A. Hoke, C.Y. Lin, A. Lau, D.A. Orlando, C.R. Vakoc, J.E. Bradner, T.I. Lee, and R.A. Young Selective inhibition of tumor oncogenes by disruption of super-enhancers. *Cell*. 2013. **153**(2): p. 320-34.

151. Thakore, P.I., A.M. D'Ippolito, L. Song, A. Safi, N.K. Shivakumar, A.M. Kabadi, T.E. Reddy, G.E. Crawford, and C.A. Gersbach Highly specific epigenome editing by CRISPR-Cas9 repressors for silencing of distal regulatory elements. *Nat Methods*. 2015. **12**(12): p. 1143-9.

152. Raleigh, D.R. and J.F. Reiter Misactivation of Hedgehog signaling causes inherited and sporadic cancers. *J Clin Invest*. 2019. **129**(2): p. 465-475.

153. Clement, V., P. Sanchez, N. de Tribolet, I. Radovanovic, and A. Ruiz i Altaba HEDGEHOG-GLI1 signaling regulates human glioma growth, cancer stem cell self-renewal, and tumorigenicity. *Curr Biol*. 2007. **17**(2): p. 165-72.

154. Bangs, F. and K.V. Anderson Primary Cilia and Mammalian Hedgehog Signaling. *Cold Spring Harb Perspect Biol*. 2017. **9**(5).

155. Martin-Cofreces, N.B., F.J. Chichon, E. Calvo, D. Torralba, E. Bustos-Moran, S.G. Dosil, A. Rojas-Gomez, E. Bonzon-Kulichenko, J.A. Lopez, J. Otón, A. Sorrentino, J.C. Zabala, I. Vernos, J. Vazquez, J.M. Valpuesta, and F. Sanchez-Madrid The chaperonin CCT controls T cell receptor-driven 3D configuration of centrioles. *Sci Adv*. 2020. **6**(49).

156. Bay, S.N., A.B. Long, and T. Caspary Disruption of the ciliary GTPase Arl13b suppresses Sonic hedgehog overactivation and inhibits medulloblastoma formation. 2018. **115**(7): p. 1570-1575.

157. Hardwicke, M.A., C.A. Oleykowski, R. Plant, J. Wang, Q. Liao, K. Moss, K. Newlander, J.L. Adams, D. Dhanak, J. Yang, Z. Lai, D. Sutton, and D. Patrick GSK1070916, a potent Aurora B/C kinase inhibitor with broad antitumor activity in tissue culture cells and human tumor xenograft models. *Molecular Cancer Therapeutics*. 2009. **8**(7): p. 1808-1817.

158. Nishimura, Y., D. Yamakawa, T. Shiromizu, and M. Inagaki Aurora A and AKT Kinase Signaling Associated with Primary Cilia. 2021. **10**(12): p. 3602.

159. Markant, S.L., L.A. Esparza, J. Sun, K.L. Barton, L.M. McCoig, G.A. Grant, J.R. Crawford, M.L. Levy, P.A. Northcott, D. Shih, M. Remke, M.D. Taylor, and R.J. Wechsler-Reya Targeting sonic hedgehog-associated medulloblastoma through inhibition of Aurora and Polo-like kinases. *Cancer Res*. 2013. **73**(20): p. 6310-22.

160. Sharma, S., T.K. Kelly, and P.A. Jones Epigenetics in cancer. *Carcinogenesis*. 2010. **31**(1): p. 27-36.

161. Northcott, P.A., C. Lee, T. Zichner, A.M. Stütz, S. Erkek, D. Kawauchi, D.J. Shih, V. Hovestadt, M. Zapatka, D. Sturm, D.T. Jones, M. Kool, M. Remke, F.M. Cavalli, S. Zuyderduyn, G.D. Bader, S. VandenBerg, L.A. Esparza, M. Ryzhova, W. Wang, A. Wittmann, S. Stark, L. Sieber, H. Seker-Cin, L. Linke, F. Kratochwil, N. Jäger, I. Buchhalter, C.D. Imbusch, G. Zipprich, B. Raeder, S. Schmidt, N. Diessl, S. Wolf, S. Wiemann, B. Brors, C. Lawerenz, J. Eils, H.J. Warnatz, T. Risch, M.L. Yaspo, U.D. Weber, C.C. Bartholomae, C. von Kalle, E. Turányi, P. Hauser, E. Sanden, A. Darabi, P. Siesjö, J. Sterba, K. Zitterbart, D. Sumerauer, P. van Sluis, R. Versteeg, R. Volckmann, J. Koster, M.U. Schuhmann, M. Ebinger, H.L. Grimes, G.W. Robinson, A. Gajjar, M. Mynarek, K. von Hoff, S. Rutkowski, T. Pietsch, W. Scheurlen, J. Felsberg, G. Reifenberger, A.E. Kulozik, A. von Deimling, O. Witt, R. Eils, R.J. Gilbertson, A. Korshunov, M.D. Taylor, P. Lichter, J.O. Korbel, R.J. Wechsler-Reya, and S.M. Pfister Enhancer hijacking activates GFI1 family oncogenes in medulloblastoma. *Nature*. 2014. **511**(7510): p. 428-34.

162. Li, Q.L., X. Lin, Y.L. Yu, L. Chen, Q.X. Hu, M. Chen, N. Cao, C. Zhao, C.Y. Wang, C.W. Huang, L.Y. Li, M. Ye, and M. Wu Genome-wide profiling in colorectal cancer identifies PHF19 and TBC1D16 as oncogenic super enhancers. *Nat Commun*. 2021. **12**(1): p. 6407.

163. Mansour, M.R., B.J. Abraham, L. Anders, A. Berezovskaya, A. Gutierrez, A.D. Durbin, J. Etchin, L. Lawton, S.E. Sallan, L.B. Silverman, M.L. Loh, S.P. Hunger, T. Sanda, R.A. Young, and A.T. Look Oncogene regulation. An oncogenic super-enhancer formed through somatic mutation of a noncoding intergenic element. *Science*. 2014. **346**(6215): p. 1373-7.

164. Chapuy, B., M.R. McKeown, C.Y. Lin, S. Monti, M.G. Roemer, J. Qi, P.B. Rahl, H.H. Sun, K.T. Yeda, J.G. Doench, E. Reichert, A.L. Kung, S.J. Rodig, R.A. Young, M.A. Shipp, and J.E. Bradner Discovery and characterization of super-enhancer-associated dependencies in diffuse large B cell lymphoma. *Cancer Cell*. 2013. **24**(6): p. 777-90.

165. Zhang, T., X. Song, Z. Zhang, Q. Mao, W. Xia, L. Xu, F. Jiang, and G. Dong Aberrant super-enhancer landscape reveals core transcriptional regulatory circuitry in lung adenocarcinoma. *Oncogenesis*. 2020. **9**(10): p. 92.

166. Sarkisian, M.R. and S.L. Semple-Rowland Emerging Roles of Primary Cilia in Glioma. *Front Cell Neurosci*. 2019. **13**: p. 55.

167. Hoang-Minh, L.B., M. Dutra-Clarke, J.J. Breunig, and M.R. Sarkisian Glioma cell proliferation is enhanced in the presence of tumor-derived cilia vesicles. *Cilia*. 2018. **7**(1): p. 6.

168. Seo, S., L.M. Baye, N.P. Schulz, J.S. Beck, Q. Zhang, D.C. Slusarski, and V.C. Sheffield BBS6, BBS10, and BBS12 form a complex with CCT/TRiC family chaperonins and mediate BBSome assembly. *Proc Natl Acad Sci U S A*. 2010. **107**(4): p. 1488-93.

169. Xu, G., S. Bu, X. Wang, H. Zhang, and H. Ge Suppression of CCT3 inhibits the proliferation and migration in breast cancer cells. *Cancer Cell International*. 2020. **20**(1): p. 218.

170. Wattanathamsan, O., R. Thararattanobon, R. Rodsiri, P. Chanvorachote, C. Vinayanuwattikun, and V. Pongrakhananon Tubulin acetylation enhances lung cancer resistance to paclitaxel-induced cell death through Mcl-1 stabilization. *Cell Death Discovery*. 2021. **7**(1): p. 67.

171. Boggs, A.E., M.I. Vitolo, R.A. Whipple, M.S. Charpentier, O.G. Goloubeva, O.B. Ioffe, K.C. Tuttle, J. Slovic, Y. Lu, G.B. Mills, and S.S. Martin α-Tubulin acetylation elevated in metastatic and basal-like breast cancer cells promotes microtentacle formation, adhesion, and invasive migration. *Cancer Res*. 2015. **75**(1): p. 203-15.

172. Oh, S., E. You, P. Ko, J. Jeong, S. Keum, and S. Rhee Genetic disruption of tubulin acetyltransferase, αTAT1, inhibits proliferation and invasion of colon cancer cells through decreases in Wnt1/β-catenin signaling. *Biochem Biophys Res Commun*. 2017. **482**(1): p. 8-14.

173. Shorstova, T., W.D. Foulkes, and M. Witcher Achieving clinical success with BET inhibitors as anti-cancer agents. *British Journal of Cancer*. 2021. **124**(9): p. 1478-1490.